TARGET TYPES AND PLACEMENT FOR TERRESTRIAL AND MOBILE MAPPING

by

Scott M Peterson

A Dissertation

Submitted to the Faculty of Purdue University

In Partial Fulfillment of the Requirements for the degree of

Doctor of Philosophy

Lyles School of Civil Engineering

West Lafayette, Indiana

December 2018

THE PURDUE UNIVERSITY GRADUATE SCHOOL
STATEMENT OF COMMITTEE APPROVAL

Dr. Steven Johnson, Chair

Department Geomatics Engineering

Dr. James Bethel

Department of Geomatics Engineering

Dr. Hubo Cai

Department of Construction Engineering and Management

Dr. Jason Ackerson

Department of Agronomy

Approved by:

Dr. Dulcy Abraham

Head of the Graduate Program

ACKNOWLEDGMENTS

I am grateful to my family and friends for their support in sacrificing their time, talents and energies to assist me in completing this dissertation.

I thank my committee for their guidance and direction. My advisors Dr. Steven Johnson, Dr. James Bethel, Dr. Hubo Cai, and Dr. Jason Ackerson who have provided the educational foundation necessary to complete such a project.

I love my savior, Jesus Christ, and am grateful for the love and inspiration with which I have been blessed to finish this dissertation.

TABLE OF CONTENTS

LIST OF TABLES

LIST OF FIGURES

ABSTRACT

Author: Peterson, Scott, M. PhD
Institution: Purdue University
Degree Received: December 2018
Title: Target Types and Placement for Terrestrial and Mobile Mapping
Committee Chair: Steven Johnson

The use of digital three-dimensional (3D) data has increased over the last two decades as private and public firms have begun to realize its utility. Mobile Terrestrial Laser Scanning (MTLS) or Mobile Mapping Systems (MMS), which utilizes LiDAR (Light Detection and Ranging) data collection from a moving platform along with advances in positioning systems—e.g., Global Navigation Satellite Systems (GNSS), Inertial Navigation Systems (INS), and Distance Measurement Instruments (DMIs)—have paved the way for efficient, abundant, and accurate 3D data collection. Validation and control targets are vital to ensure relative and/or absolute accuracy for MTLS projects. The focus of this dissertation is to evaluate several types of targets and the positional spacing of said targets for MTLS.

A mostly planar two-dimensional (2D) targeting system (painted target on ground) is commonly used to constrain, register, and validate the 3D point clouds from MTLS. In this dissertation, 3D objects—a sphere and a cube—were evaluated with varied angles of incidence and point densities as more appropriate alternatives to constrain and validate the 3D MTLS point clouds. Next, a planar circular 2D target—with the use of the raw intensity of the LiDAR pulse as another measured dimension—was evaluated as a proof of concept to also constrain and validate 3D LiDAR data. A third and final component of this dissertation explored analyses of INS data to determine the positional spacing of control and validation targets in MTLS projects to provide maximum accuracy for all data points.

1. INTRODUCTION

1.1 Background

Laser scanning has been around since the mid-1990s and is highly accurate on positioning, which can be less than a centimeter [1]. In recent years, LiDAR (Light Detection and Ranging) technology has vastly improved and with the advent of MTLS (Mobile Terrestrial Laser Scanning), high density LiDAR data can be acquired over larger areas in less time and with a high degree of accuracy. LiDAR requires measurements from a known position, known orientation, and a known coordinate system to create a registered 3D point cloud. MTLS utilizes a laser scanner on a terrestrial moving platform using similar principles as Airborne LiDAR but on the ground [1]. LiDAR alone on a moving platform cannot produce a registered point cloud. MTLS integrates LiDAR for measurements, GNSS (Global Navigation Satellite Systems) for positioning, INS (Inertial Navigation System) for positioning and orientation, and DMI (Distance Measurement Instrument) for distance traveled. With precise calibration and integration of all the MTLS components, Cartesian coordinates can be produced and registered into a complete 3D point cloud. Each component of MTLS produces errors—systematic and random—leading to uncertainty of the accuracy of the registered point cloud. Poreba and Goulette [2] explained that validation can be assessed in terms of resolution, accuracy, and repeatability of the captured data. Targets are used in MTLS projects to validate, constrain and register the collected data. Barber et al. [3] explained that engineers require validation of the point cloud data to confidently make the right decisions and create accurate and precise designs. In this dissertation, different target types will be evaluated and a procedure for proper spacing of said target will be discussed to allow for a more accurate representation of the features found in the 3D point clouds.

1.1.1 LiDAR

LiDAR is found in airborne, terrestrial, and MTLS applications. LiDAR is an active method of remotely sensing objects [4]. Puente et al. [1] explained that LiDAR is for measurement of range and angle and can be time-of-flight based or phase shift; phase shift is more accurate, however more limited in range (<75m) while time of flight has a

greater range [4]. Relative positions of objects are calculated from LiDAR sensors by measuring the distance and angle to the object. In terrestrial scanning, the position and

$$\rho = \frac{c}{n}\frac{\tau}{2} \qquad \text{equation (1-1)}$$

orientation of the scanner is typically known (exceptions are resections) by the use of vendor supplied targets and known control points. Measured points are all referenced together in a Cartesian coordinate system based on the control points as reference. Most airborne, terrestrial, and MTLS systems employ a time of flight sensors for positioning of objects according to equation 1-1,

where, ρ = distance, c = speed of light, n = index of refraction of medium, and τ = round trip time delay [4]. The density of data returned is a function of the pulse repetition rate and the rate of horizontal rotation of the scanning sensor, which produces collection rates from 50kHz up to 1000kHz. With terrestrial scanning, all measurements are registered together based on each setup of the scanner. In airborne and MTLS applications, each individual data point has its own Cartesian coordinate system derived from the integration of the IMU, GNSS, and DMI further explained in sections 1.3 – 1.5. Registration of all airborne and MTLS data sets requires millions of coordinate system transformations to be able to create one final product.

The intensity is a measurement of the returned energy from the returned pulse. Intensity values can be used to distinguish between objects [4,5] with different reflective properties. Control targets often employ different areas of intensity, from which commercially developed software can extract the controlling positional information. Intensity values are affected by range, angle of incidence, atmospheric conditions, and the physical properties of the objects being scanned [4].

1.1.2 **Inertial Measurement Unit in MTLS**

The INS (Inertial Navigation System) provides instant positions for the MTLS (Mobile Terrestrial Laser Scanning) system. The INS contains an inertial sensor, the IMU (Inertial Measurement Unit), which is a self-contained system that measures linear and angular motion using a triad of gyroscopes and a triad of accelerometers. Puente et al. [6] explained these gyroscopes and accelerometers provide instantaneous velocity and

attitude of a vehicle. Without the assistance of other measuring devices such as GNSS or a DMI, the IMU measures the roll rate, pitch rate, yaw rate, and the x acceleration, y acceleration, and z acceleration, respectively, resulting in the INS producing positional and attitude measurements. Typical IMUs utilized in MTLS measure in a range of 100 to 2,000 Hz [4,7]. The IMU determines the orientation of the scanner sensor as the scanner sensor makes each individual measurement for the resultant 3D point cloud. MTLS applications rely heavily upon interpolated measured data. The observed measured data are a function of the IMU. If an MTLS has a scan sensor with a 600kHZ pulse rate and an IMU with a 200Hz measurement rate, then the XYZ positional coordinates of 3,000 data points will be interpolated values due to the limits of the IMU. Due to the interpolation of so many data points, the IMU is the driving force of MTLS. While an IMU is highly accurate when initialized at the beginning of a track, over time the errors associated with an IMU (initial alignment errors for roll pitch and yaw angles, gyroscope drift and accelerometer shift), accumulate and degrade the overall positional accuracy of the INS, called drift [1,2,3].

1.1.3 **Distance Measuring Instrument in MTLS**

In MTLS, the DMI (Distance Measuring Instrument) is placed on the wheel of a vehicle to measure the rate and velocity of wheel rotation. With knowledge of the circumference of the wheel and tire, distances can be measured [8]. When the DMI fails to register velocity or acceleration, the MTLS will register moments of no movement.

1.1.4 **Global Navigation Satellite Systems in MTLS**

GNSS provides the basic initial positioning information to the MTLS, with known accuracies and precisions in the sub-centimeter range. Poreba and Goulette [2] proved that the quality of 3D data in MTLS depends greatly upon the accuracy of GNSS positioning; however, there are limitations due to the fact GNSS produces the largest positional error. GNSS provides a reference by which the INS can re-calibrate its position. It is virtually impossible to maintain the GNSS signal during a complete project due to multipath errors caused by tunnels, bridges, buildings, and other possible obstructions. The multipath errors create a time which positional accuracy is well above

centimeter tolerances desired for engineering surveys. GNSS systems are used in mobile mapping to aid in the 3D positioning of the vehicle, more specifically the position of the laser scanner sensor at the time of measurement. GNSS sensors will measure anywhere from 1-10 times a second, providing location data for the laser scanner as well as the INS. Some MTLS employ GAMS [9]. GAMS are secondary GNSS receivers mounted to the vehicle. Each receiver has a known position relative to the INS, secondary GNSS unit, and the LiDAR scan sensor. Jointly, the two receivers are used in the heading determination [6].

1.1.5 **Smoothed Best Estimated Trajectory (SBET) in MTLS**

All measured data stems from data received at the LiDAR scanning sensor. The integration of the INS, GNSS, and DMI give the best estimate of the position and orientation of the scanning sensor for each measurement. The desired result of a MTLS project is the final 3D point cloud. SBETs represent the travelled and referenced path of the LiDAR scanning sensor. All measured data received from the INS, GNSS, and DMI is processed taking in positional errors, orientation errors, and predictive modeling errors. This process creates the SBET (smoothed best-estimated trajectory). Commercial software and proprietary software related to the INS used are available to process the MTLS data, commonly known as Kalman filtering [3]. A Kalman filter more specifically is a set of mathematical equations that produces estimations of past, present, and future states, attempting to remove all the noise and other inaccuracies from each measurement [6]. Once an SBET is created, then the positions and attitude of each measurement from the scanner are computed and interpolated to create the final 3D point cloud.

1.1.6 **Targets in MTLS**

In any survey-related project, control points are used to establish absolute/relative coordinate systems and orientation. Targets are placed on the controlling locations to constrain 3D point clouds and to validate the MTLS data. The final 3D registered point cloud data set is dependent upon two things. First, the control established for the project must be established by methods of higher order. Second, a target is placed on, over, or above the controlling location so as to be seen (measured) by the LiDAR scanning

sensor. The measured MTLS data are then registered to fit the controlling locations each target occupies.

1.1.7 **3D Point Cloud Data with MTLS**

The point cloud data are a set of 3D coordinates that as a whole portray surface positions of topographic features. Each 3D point cloud is made up of a few to millions and millions of individual measurements in a Cartesian coordinate system. Due to the nature of the LiDAR sensor, its measured locations are random, unlike a traditional total station that can measure specific locations. As shown in Fig. 1.1, the data points randomly measure topographic features of objects, identifying building corners, building edges, or any other specific geometric vertices that are not measured. Commercial software model all measured data allowing for determination of specific geographic interests.

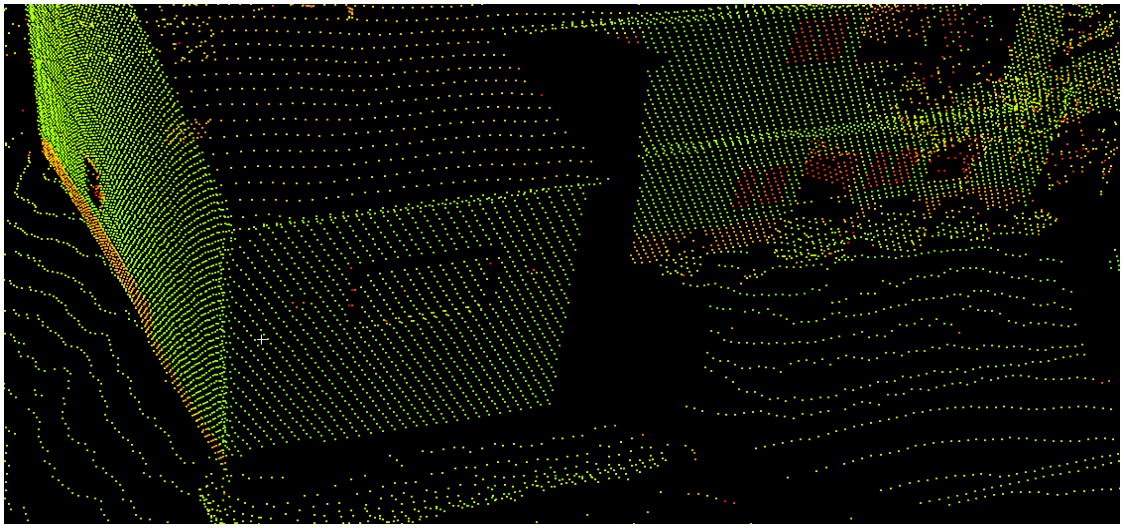

Fig. 1.1 Sample MTLS data of a house

With a high density of data made up of millions and millions of data points, features can be modeled to accurately represent any given scene as shown for a typical approach to an intersection in Fig. 1.2.

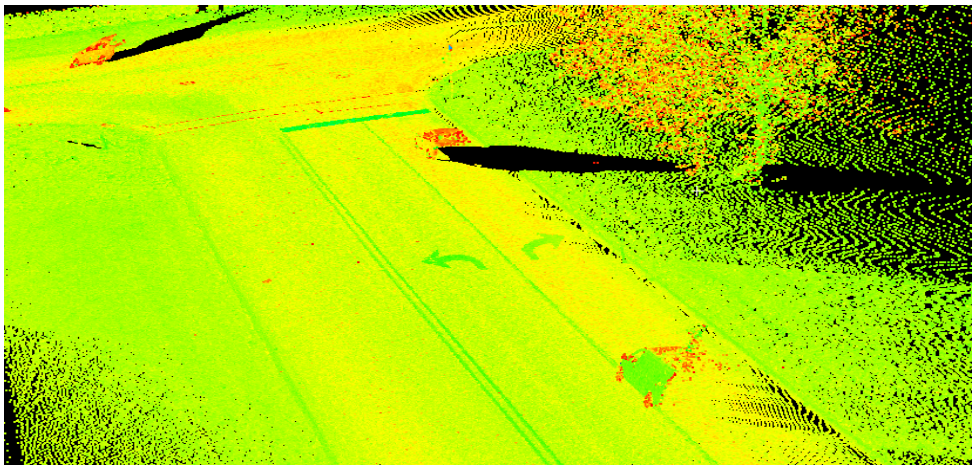

Fig. 1.2 Sample MTLS dataset showing the approach to an intersection highlighting striping on the street and curb and gutter

A LiDAR sensor on any given MTLS measures at different rates as discussed in Section 1.1.1. Table 1.1 shows a typical datasheet for the Trimble MX8 with the different configurations possible. The pulsing rate of the sensor remains consistent while the scan speed (revolutions per second) can be varied to achieve a higher or lower density of data points.

Table 1.1 Sample Datasheet from the Trimble MX8 System Which Uses Velodyne LiDAR Sensors

	VQ®-250 Configuration	VQ®-450 Configuration
Accuracy	10 mm[1]	8 mm[1]
Precision	5 mm[2]	5 mm[2]
Maximum effective measurement rate	600,000 points/second (2 x 300,000 points/second)	1,100,000 points/second (2 x 550,000 points/second)
Line scan speed	up to 200 lines/second (2 x 100 lines/second)	up to 400 lines/second (2 x 200 lines/second)
Echo signal intensity	high resolution 16 bit intensity	high resolution 16 bit intensity
Range	up to 500 m @ 100 KHz (natural targets ρ ≥ 80%)	up to 800 m @ 150 KHz (natural targets ρ ≥ 80%)

1.2 Statement of the Problem

Several methods exist to validate and constrain a 3D MTLS point cloud. Control and validation targets are placed throughout a project over known positions for absolute accuracy or over random points for relative accuracy. While research agrees on the need for control and validation targets, there is not a consensus for the positional location of the targets (proximity to the scanner sensor), the spacing of the targets, nor the type of target [4,10,11,12].

1.3 Motivation

Certainly, researchers continue to improve upon IMUs, DMIs, and both GNSS and laser scanner sensors, but the motivation driving this research is the need to know how to adapt and accommodate data collection styles and proper validation of the data using existing technology. The public and private sectors rely heavily upon the data provided by manufacturers and researchers working on their behalf. For example, the Georgia Department of Transportation refers the user back to the equipment manufacturer for assistance [13]. However, little guidance to actual, real world scenarios is given, leaving end users to their own devices to best complete projects. Several departments of transportation from multiple states have created standards for the use of MTLS that

dictate target placement and target types, and various methods to achieve desired engineering accuracies. Novice users blindly follow set instructions, with failed attempts to understand every detail of each component and how they work. The Indiana Department of Transportation (INDOT) commissioned a project to develop performance-based standards due to the constant changes and advances in technology [14]. As the public and private sector drive and push for performance-based standards, one of two scenarios is necessary: first, the end user becomes proficient at research, or second, the end user is provided guidance on how to understand causes and effects of closed form technology. The National Cooperative Highway Research Program (NCHRP) [4] suggested its research be used for a wide audience who may or may not be familiar with LiDAR.

Control targets are necessary to realize accurate 3D point clouds. Validation targets are necessary to provide quality control and assure accuracy of 3D point clouds. While current research is concentrated on eliminating errors in all components of MTLS, little work has been done on suggestions for better targeting. Research has investigated the impact of angle of incidence measured on each observed object [4], but it has not addressed its impact on the control and validation targets. Target types are driven by abilities of commercial software to identify and extract the positional information of the target, as well as what manufacturers suggest [4].

Several state department of transportation agencies [10,13,15,16] have tried to address proper application of MTLS. The state manuals require a high degree of user understanding, but provide little guidance; this combination serves as a point of frustration for users collecting and processing MTLS data.

In this dissertation, a proof of concept of a new target is explored, utilizing the absolute measured intensity to assist in locating the controlling position of a control or validation target. To date, no other research has performed or developed an experiment similar to this new target. In addition, no research has detailed the positional spacing of control and validation targets. This research explores the ability to examine the SBET, using only the INS data, to provide insight as to the performance of the INS and develop guidance for the positional spacing of control and validation targets. Specifications for spacing of targets are currently provided by several state departments of transportation,

mostly mimicking one another [10,15]. Since the GNSS provides the largest positional error [2], and is often in an autonomous state, reliance on the INS is mission critical, especially in urban scenarios. Much research has been performed in ideal situations, assuming all integrated MTLS systems are active and providing valuable data. There has been no research that shows worst case scenarios when the system relies wholly upon the IMU.

1.4 Goals and Objectives

Because MTLS is a newer and developing technology, little guidance and direction is available on its use and quality control for engineering projects. This research examines the use of 3D objects—spheres and cubes—to properly control and validate 3D point clouds derived by MTLS over conventional uses of planar targets painted on the ground. A method to determine the proper spacing of targets (along and perpendicular to the travelled path) is presented in this research. Proper application of the type of target and spacing of the targets will result in a more accurate 3D point cloud, as well as providing a higher degree of confidence in the 3D point cloud data. General users will have sufficient knowledge to properly plan and execute a MTLS project.

Due to the need of highly accurate control and validation targets properly spaced throughout an MTLS project, a proof of concept of a new MTLS/terrestrial LiDAR target is considered. Research has yet to properly explore the effect of angle of incidence on planar targets on the ground. A vertical 2D planar target that uses raw intensity to aide in the control target's positioning is considered. This new target will be able to help eliminate the need for highly dense scan data and the need to be concerned with angle of incidence while measuring the target.

2. LITERATURE REVIEW

MTLS (Mobile Terrestrial Laser Scanning) is a developing technology. Although the first functioning system was developed and working in the late 1980s to the early 1990s [1], research on how to better integrate multiple systems, then validate and constrain the data, is ongoing [17]. MTLS has been compared to Airborne LiDAR (light detection and ranging) and terrestrial LiDAR. Airborne LiDAR can cover large areas (distance as well and square footage); however, accuracy is lower—on the order of 1-3 m resolutions—and planning requires much more time [18]. Terrestrial LiDAR is highly accurate at short distances and there are fewer time constraints in the planning process; however, it does require increased time to cover large areas. MTLS incorporates techniques of airborne LiDAR in its ability to travel large areas while continuously collecting data, and terrestrial LiDAR uses highly accurate LiDAR sensors to capture immense amount of data at resolutions in the centimeter to decimeter range and short distances. Like any tool, each has its purpose, and there are many advantages and disadvantages with all three methods. However, the key advantage to MTLS is the ability to capture data over large areas, in short amounts of time, and with high resolution [4].

MTLS consists of multiple sensors: INS (Inertial Navigation System) and GNSS (global navigation satellite system), which together are commonly known as a POS (Position and Orientation System); DMIs (distance measurement instrument); and the LiDAR sensor. With the integration of all sensors measuring at different rates, large 3D point clouds with the potential of high resolution data are created from which DEMs (digital elevation models) or DSMs (digital surface models) of any terrain over which the vehicle passes can be created. The INS and GNSS work closely one with another. The INS performs the bulk of the position measuring while the GNSS is constantly providing a check/calibration for the INS for each epoch measured [3,4]. During good GNSS conditions, the GNSS augments the positioning ability of the INS through providing updated positional information [3,4,19]. During poor GNSS conditions, the INS augments the GNSS by providing positional information. The IMU (inertial measurement unit) can measure from 100 to 2,000 Hz [4,20,21], constantly measuring the accelerations of the roll, pitch, and yaw. Those measurements from the IMU translate into

precise orientation and position of the LiDAR sensor further allowing a distance and angle measurement to any object. INSs have a distinct disadvantage: due to positioning based on previous measurements that in turn were based on other previous measurements, INS positions degrade over time [1,2,3,4]. In the short term, an INS is very accurate, but over time, it will consistently drift due to errors contained in each of the preceding measurements. As mentioned above, GNSS assists the INS with each measured epoch providing a new positioning point for the INS. After measurements by the IMU, GNSS, and DMI, a SBET (Smoothed Best estimated Trajectory) is created by using a series of Kalman filtering [3]. Post-processing to integrate the Kalman filter data, the IMU data, the GNSS data, the DMI data, and all other measured data produces a final trajectory of the MTLS. The LiDAR sensor has now positional and orientation values from which a geo-referenced 3D point cloud is created.

Control targets are used in MTLS projects to constrain and validate the 3D data. Validation is a large part of any mobile mapping project [3,4]. The Federal Geographic Data Committee (FGDC) created the National Standard for Spatial Data Accuracy (NSSDA) to provide a baseline for validating geospatial data. The NSSDA outlines a method utilizing a minimum of 20 GCPs (ground control points) that were surveyed to a higher order of accuracy from which subsequent survey data could be compared to standards that either validates measured data or determine inaccuracies [22]. The NSSDA method of validating data has been common in MTLS applications, however the standards as they apply to MTLS are outdated.

While there is some research providing guidelines on control and validation target positioning, there is not a consensus with respect to the placement and frequency of the placement. Ussyshkin [12] has suggested a placement every 50-80m. Caltrans and Florida DOT (Department of Transportation) [10,15] has suggested every 500 feet (~150m) for validation and every 1500 feet (~450m) for control. Hiremagalur [11] has simply suggested redundancy as a best practice. Control targets are also suggested to be spatially distributed throughout the project. Recent research has created a DCC (data collection category) denoting the accuracy and density of a MTLS project defining three accuracy levels: high, medium, and low, with a spacing to be 150-300m, 300-750m, and 750-1500m, respectively [4].

Specific control and validation targets currently used include patterns of checkerboards or chevrons. As explained by NHRCP [4], non-reflective and reflective targets are utilized using the checkerboard or chevron patterns. Research has not addressed the angle of incidence utilizing the painted targets on the ground nor the fact that they require high density of 3D data points to perform the calculations. Bailey [21] addressed the placement of the target by using a fixed checkered pattern EMAT (Elevated Mobile Acquisition Target) for railway right-of-ways, but again this does not address the issue of angle of incidence. In Johnson et al [14], a cube and a sphere are calibrated and tested as validating targets while developing standards for the Indiana Department of Transportation. These results indicate that angle of incidence is not a factor in determining the controlling position of the these types of targets.

Each LiDAR scanner returns a 3D position of a measured location on any given object. That position of the object is non-discriminate. Intensity, the amplitude of the returning signal, is also measured, which helps to identify objects with differing physical characteristics [4]. A lot of research has been performed detailing the characteristics of the return signal, but it has only been used for object distinction, not for positioning applications. The intensity provides ample contrast for controlling targets such as checkered patterns and chevrons, allowing for the proper identification of the controlling position.

As Kaartinen et al [17] explained, further research is necessary under non-ideal conditions. This includes mobile mapping in urban areas where GPS is limited, or where GPS provides positioning at very poor resolutions. Haala et al [23] indicated in their experiments that results came from “good GPS conditions,” but not all conditions are ideal and current research must endeavor to investigate MTLS in substandard settings.

MTLS is an emerging technology with the potential to profoundly change the mobile mapping landscape; thus, there exists a knowledge gap in that few studies have examined the accuracy of mobile terrestrial LiDAR using independent data [18].

3. NEW LIDAR TARGET

3.1 Target Acquisition Techniques

Mobile mapping commonly implements the use of 2-D targets as validation or as control to constrain the acquired 3-D point cloud. Common targets are squares, rectangles, plus signs, and chevron signs painted on the road surface. Through the use of image matching algorithms from the acquired 3-D point cloud, the 2-D targets can be utilized as control or validation. The use of 2-D targets, however, is limited based upon the density of data on the target. Developed algorithms and data processing using the controlling targets are quite straightforward and based on commercial software [4,24]. Two main variables affect density of the point cloud: 1) distance from the scanner sensor, which also impacts horizontal and vertical angle of incidence, and 2) speed of the vehicle. As shown in Fig. 3.1 and Fig. 3.2, Trimble MX8 data show that the density is based upon speed of the vehicle. At 15 mph, the high volume of spatial data defines the shape of the '+' target; however, at 60 mph, the lower volume of spatial data cannot accurately define the '+' shape. Fig. 3.3 shows eight controlling '+' targets, four controlling square targets, and four controlling rectangle targets, spaced 5m apart at ranges of 0-20m from the LiDAR sensor. The '+' shape at 15m and 20m distant targets cannot be determined. 2-D ground targets must be closer to the scanning path to be of value as controlling targets. In most experiments, there is a requirement to use very dense point clouds to extract reference target positional data [4,17]. However, high volume target data are not always possible due to speed and distance from the LiDAR sensor.

Terrestrial scanners use targets as shown in Fig. 3.4. They are utilized and processed as 2D targets, with the controlling centers calculated by data processing algorithms. Terrestrial targets are not utilized in mobile mapping due to the inability to always produce high enough volume data on the target for image matching needs. While image matching is extremely powerful, it does require more data to accurately extract the control location. Through commercial software, a Leica P20 terrestrial laser scanner will identify the controlling center of its corresponding target within 3mm at 50m from the laser scanner [25].

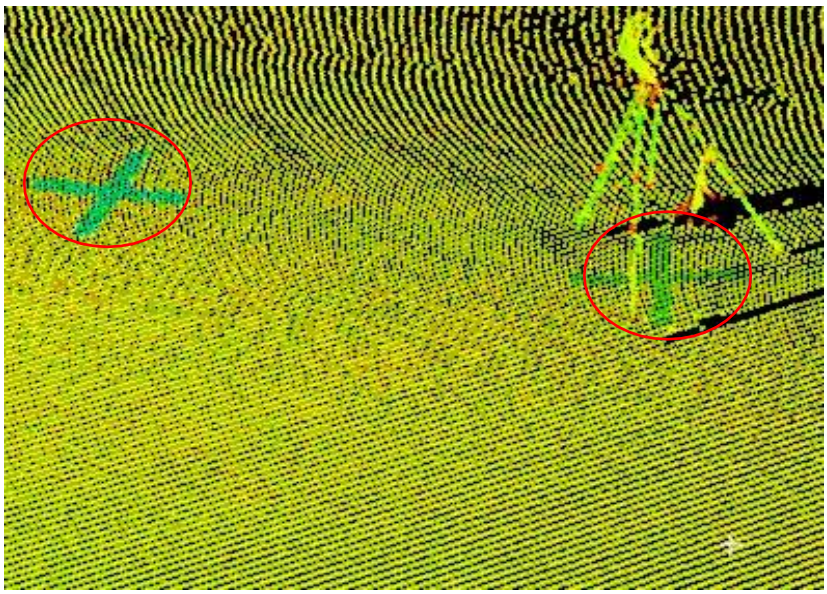

Fig. 3.1 Observed point cloud at 15mph; red circles show the visible targets on the pavement

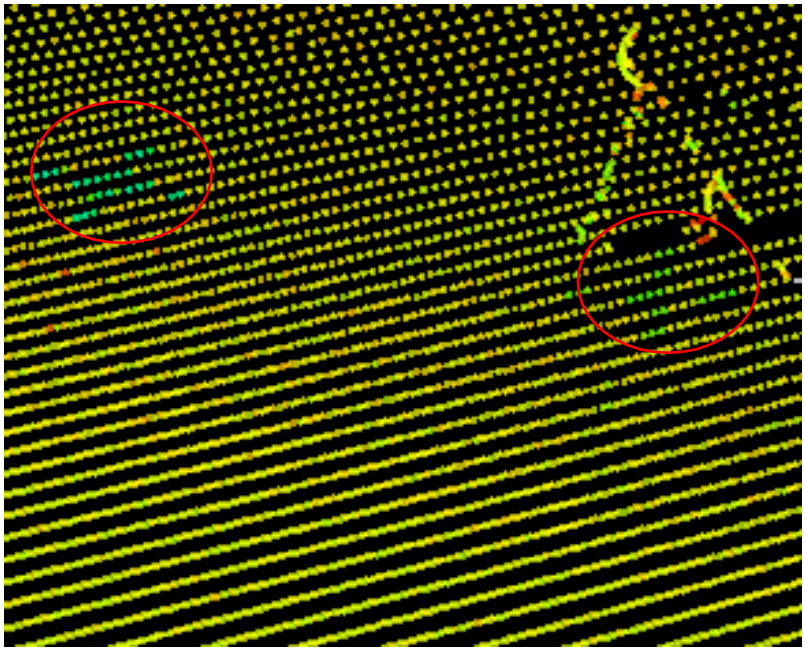

Fig. 3.2 Observed point cloud at 60 mph; red circles show the visible targets on the pavement

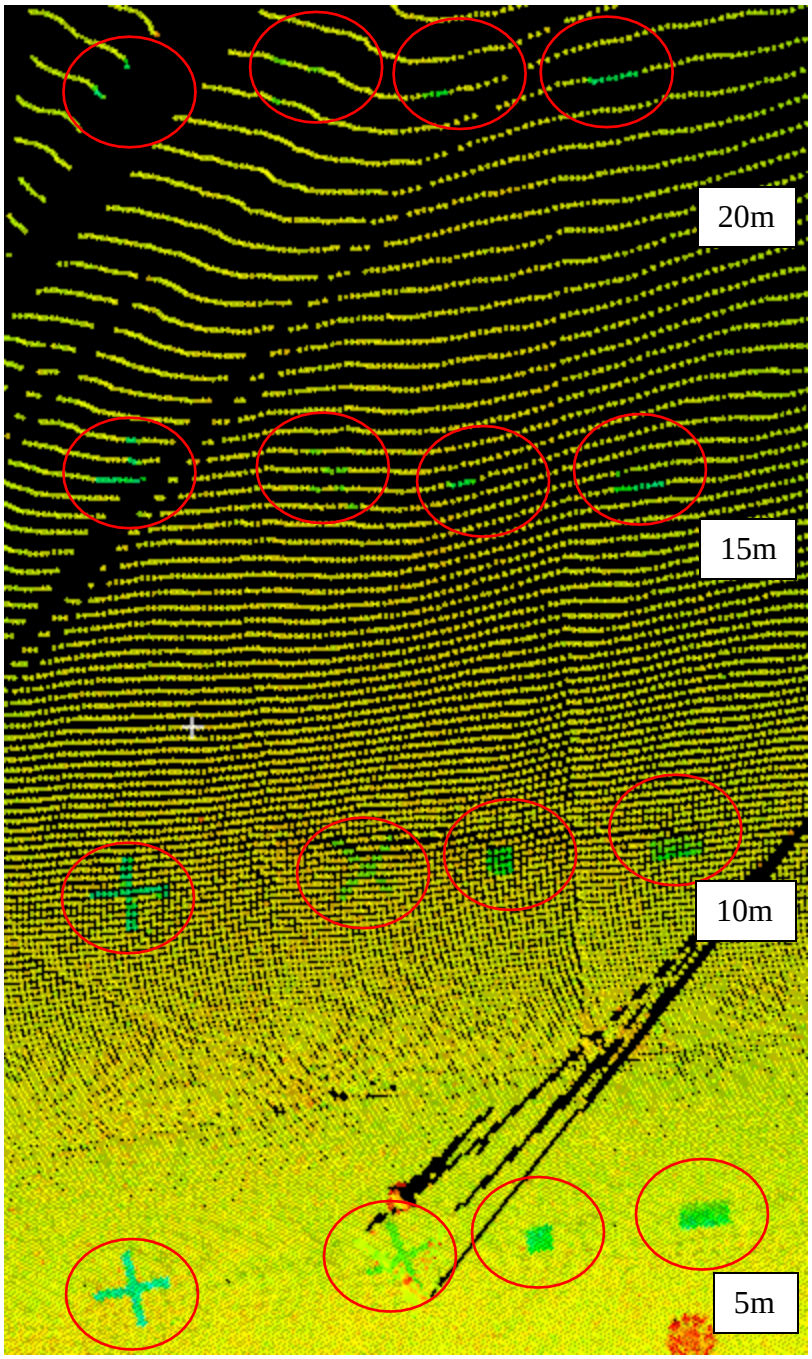

Fig. 3.3 Observed scan data at 15mph showing 0 to 20m offsets in the control targets on the ground

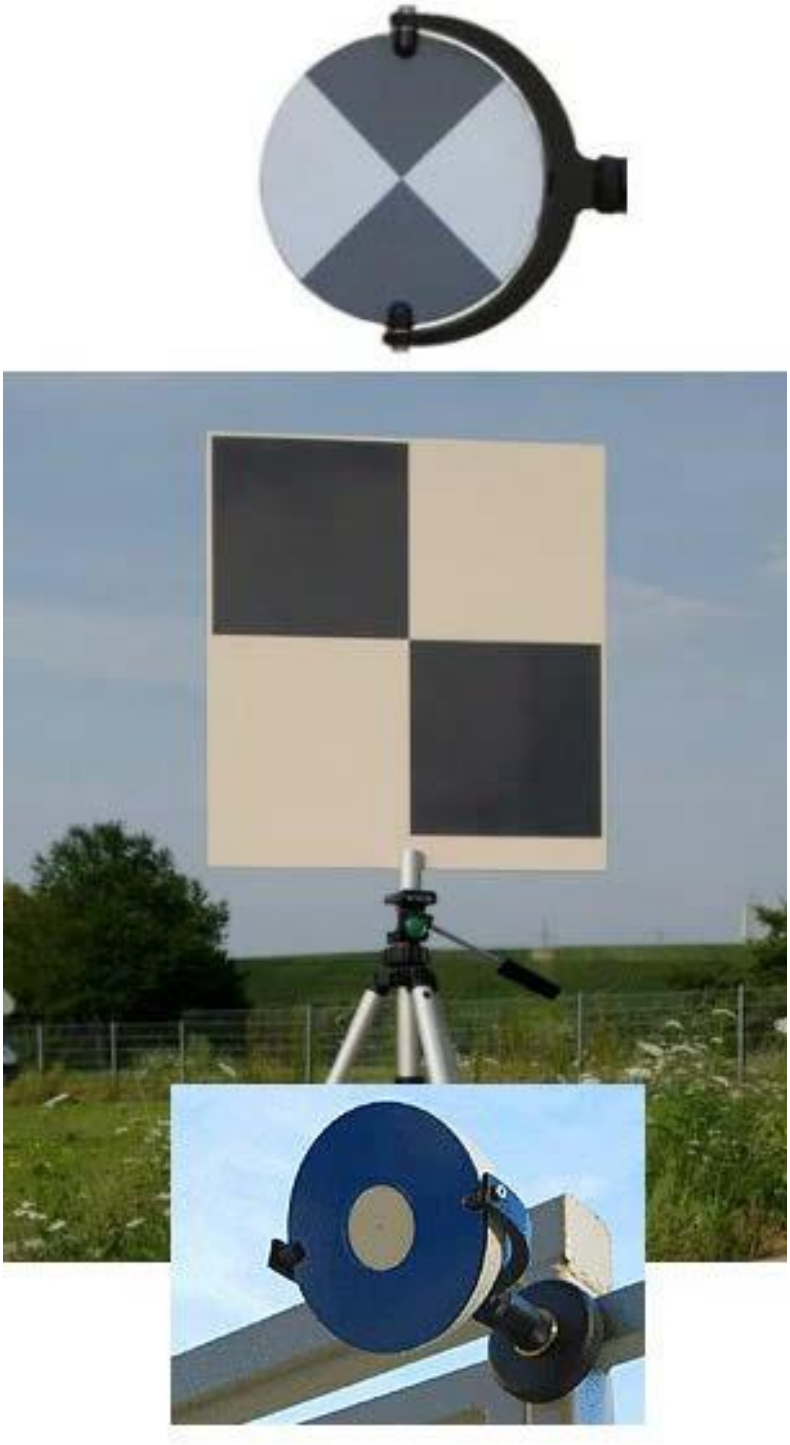

Fig. 3.4 Typical control targets used with terrestrial LiDAR

3-D targets typically require less dense data. For example, with proper geometric spacing of the point data, a sphere would only require four known measured values on its surface to determine the radius and center location through a least squares solution, beginning with the definition of a sphere in equation 3-1 with the center x_O, y_O, and z_O as the unknowns and a known calibrated radius r.

$$(x-x_0)^2+(y-y_0)^2+(z-z_0)^2=r^2 \qquad \text{equation (3-1)}$$

In laser scanning, a single measurement not only measures x, y, and z coordinates, it also measures intensity on the return signal. Intensity relates to reflectance values obtained through other remote sensing applications. Simply, intensity is the measured amount of returned energy from a given signal. Intensity is affected by color and other physical characteristics of the object. Both contribute to the amount of energy absorbed at the surface location. As shown in Fig. 3.5, targets are created with highly reflective surfaces with contrasting low reflective surfaces for easy identification by the commercial software. In the case shown in Fig. 3.5, blue represents high intensity (absorption of less energy) while orange represents a lower intensity (absorption of more energy).

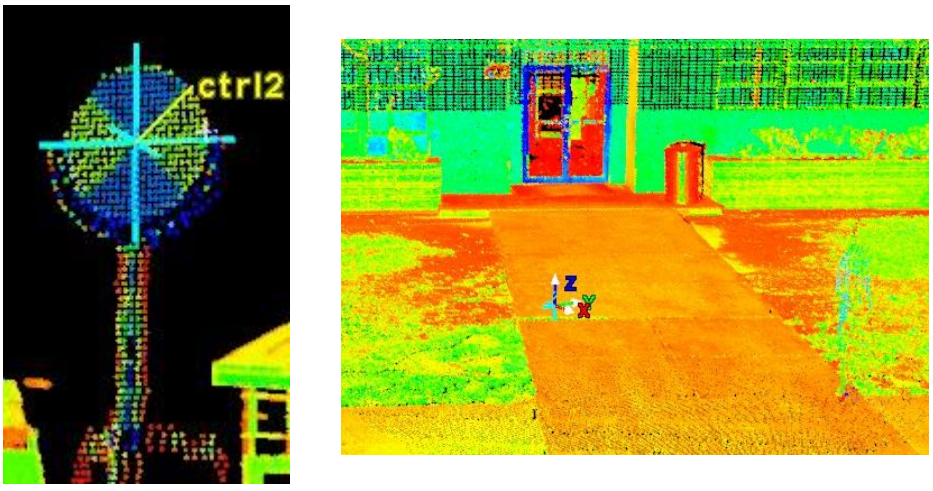

Fig. 3.5 Typical scan data and control targets; coloring represents the intensity of each collected data point

Functional surfaces are surfaces that provide two dimensions of data with a third dimension derived from pictorial information. A contour map as shown in Fig. 3.6 is an

example of a functional surface, providing horizontal data (longitude and latitude) and derived elevation data from the drawn contour lines.

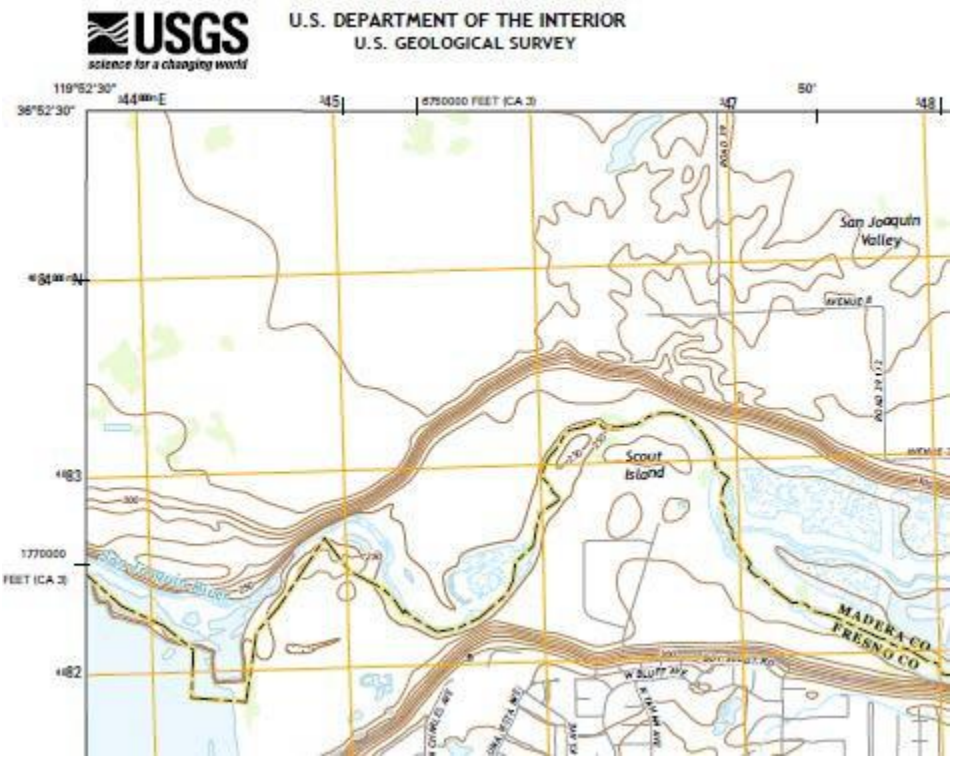

Fig. 3.6 USGS topoquad map

As shown in Figs. 3.1 through 3.5, high volume target measurements are made in a plane (a 2D surface on road or manufactured target) to control a 3D spatial environment; 1 3D component and measured intensity are not utilized in spatial computations for the controlling center of the target.

3.2 Principles of New LiDAR Target

Intensity measured on a circular planar target with a radial color gradient can provide a third dimension of spatial measurement not acquired on previous 2-D targets mentioned in the previous subsection (3.1). A circle has the following equation (3-2):

$$(x-x_0)^2+(y-y_0)^2=r^2 \qquad \text{equation (3-2)}$$

with the center x_O, y_O, and radius r. If the radius of the circle is known, then given two measured points along the circumference of the circle, the center can be determined (Fig. 3.7).

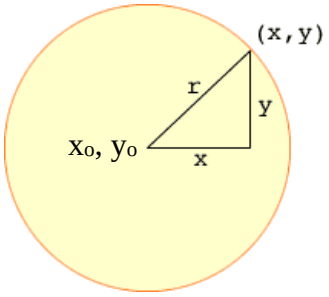

Fig. 3.7 Components of a circle

A variant of the circle's equation can be implemented to allow the use of the measured intensity. A laser scanner measures an object indiscriminately, resulting in a failure to measure a point on the circumference of a planar circular target. The collection of the data on the target will be orderly in its point spacing, but random in the measured location on the target. Indiscriminate measuring produces unknowns with respect to the center of the target as well as the radius of said target, rendering the circle equation useless. Since intensity is affected by color, a colored radial gradient is employed on the circular target. The intensity and radial gradient will have a direct relationship to compute the radius of each measured data point on the circle. Each measurement on this planar target will now give two dimensions of spatial data on the target, with a known radius for each point. Equation 3-2 of a circle can now be used through at least three measurements on the target as shown in Fig. 3.8 and Fig. 3.9, using a least squares method to solve for the two remaining unknowns x_O, y_O. Three circles, each with a known radius and a 2-D measurement on the circumference of each circle, allow for a simultaneous solution of the center of the target. This becomes a basic three-point to n-points resection problem.

3.3 Process of Target Creation and Calibration

A 6-inch diameter target was created and printed with a gradient of color as shown in Fig. 3.8. As discussed earlier, each measurement contains intensity data. The color gradient creates a relationship between the intensity from the outside of the target to the center. The intensity is then utilized to determine the radius of each measured point to the center of the target. Described below is the process for determining the solution of the controlling center.

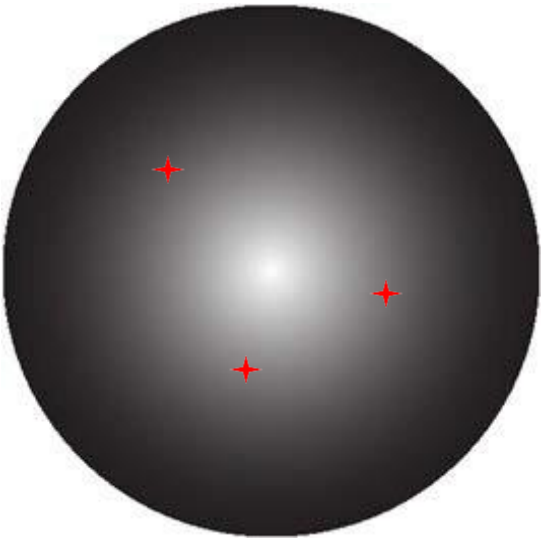

Fig. 3.8 Control target

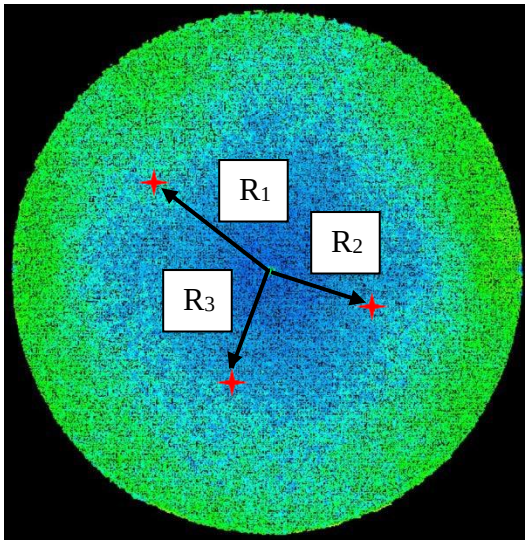

Fig. 3.9 Scanned control target showing three randomly picked data points

1. A Leica P20 scanner was first set up over a control point then given the coordinates X = 1000.000m, Y = 1000.000m, and Z (Elevation) = 100.000m. The scanner was set up with an instrument height of 1.769m. A regular 6-inch target used by the Leica P20 scanner was set up 5.000m away in the Y direction. The control location of the ground at the target's location was measured to be X = 1000.000m, Y = 1004.998m, and Z (Elevation) = 100.013m, with a target height of 1.769m. With orientation set, the test target was scanned, and the center was determined to have coordinate values of X = 1000.000m, Y = 1004.998, and Z (Elevation)=101.779m. Due to the planar characteristics of the target, the y coordinates remained the same from each measurement, and the planar coordinates of X,Z were used for the remainder of the tests (Fig. 3.10).

Fig. 3.10 Orientation of scanner for experiment

2. A very dense scan of the radial gradient target was performed using the Leica P20 Scanstation scanner. The center of the target was created to have a lower intensity reading to ensure that we could find the center of the target based upon the intensity readings. The center of the target was also known from an initial setup and calibration of the orientation of the scanner as described in step 1.

3. With a known center, and the printed target placed in the same location, the XZ positions of each measurement were used to determine the radius of each measurement on the target. In total, 6,072 measured points were used to calibrate the target (Fig. 3.11).

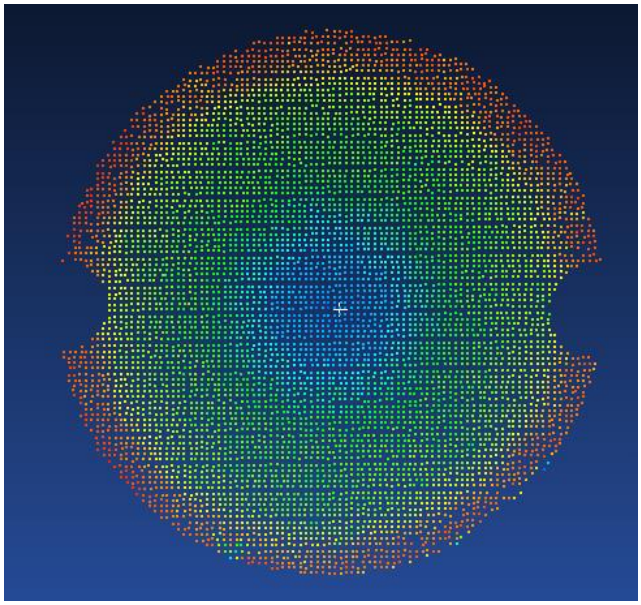

Fig. 3.11 Scanned target showing center by intensity

4. Fig. 3.12 shows the relationship of the radii of each measured point with respect to its measure intensity. A 5^{th}-degree polynomial was created to best fit the resultant data from the printed target. An R^2 value of .9318 was reported. The lower R^2 value is a direct result of the noise seen in the measured data. This noise is the result of the printing mechanism, not being able to print the designed gradient with enough accuracy.
5. Now, given any observed data point, the planar coordinates of the target and the intensity can be used to solve for the controlling center of a planar target. A simple least squares routine was created by doing a resection. There are two unknowns, X center and Z center. Equations 3-3 and 3-4 show the computations.

$$X = (A^T A)^{-1} \times (A^T L) \qquad (3\text{-}3)$$

$$A=\begin{bmatrix} \frac{\partial f_1}{\partial x_0} & \frac{\partial f_1}{\partial y_0} \\ \frac{\partial f_2}{\partial x_0} & \frac{\partial f_2}{\partial y_0} \\ \frac{\partial f_3}{\partial x_0} & \frac{\partial f_3}{\partial y_0} \\ \frac{\partial f_4}{\partial x_0} & \frac{\partial f_4}{\partial y_0} \end{bmatrix} \qquad X=\begin{bmatrix} \Delta x \\ \Delta y \end{bmatrix} \qquad L=\begin{matrix} f_1(x_0, y_0) \\ f_2(x_0, y_0) \\ f_3(x_0, y_0) \\ f_4(x_0, y_0) \end{matrix}$$

$$(x_o, y_o) = r_i^2 - (x_i - x_o)^2 - (y_i - y_o)^2 = 0 \qquad i = 1, 2, 3 \ldots n \tag{3-4}$$

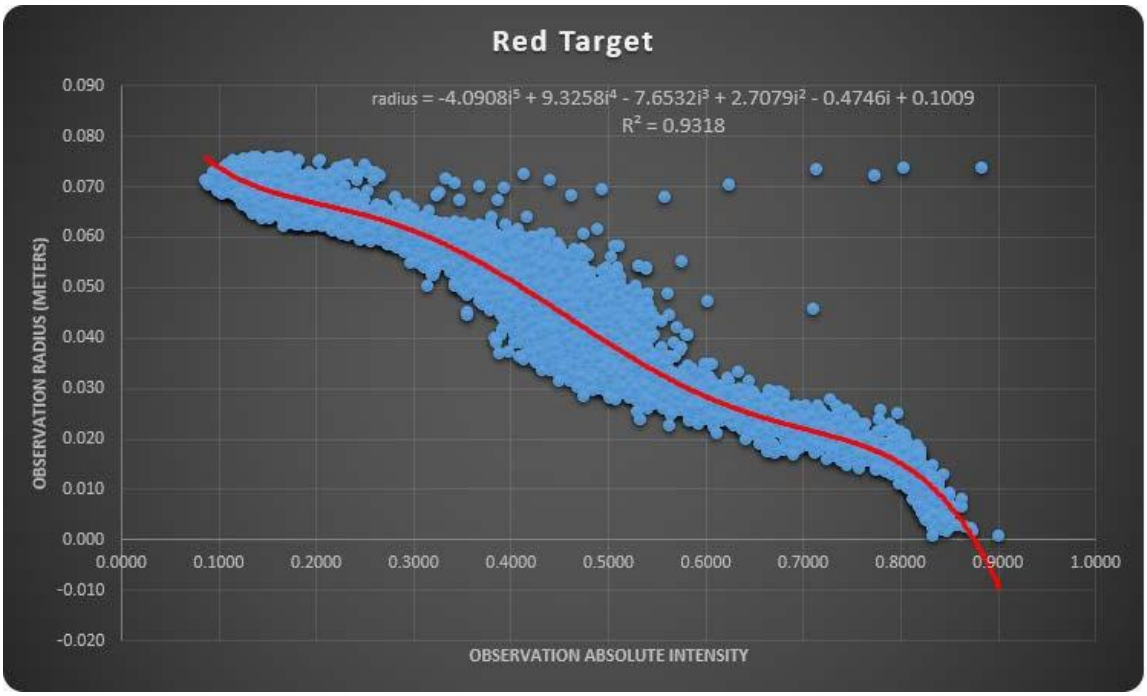

Fig. 3.12 Best fit equation to determine radius of a measured point

Tests were done with a minimal number of data points to test the ability of the function as shown in Fig. 3.13. Three data sets were created to test and validate the resultant formula.

1. Data Set 1. The known coordinates of the center of the target previously measured are X true center = 1000.000m, Z true center = 101.799m. Based on the randomly chosen points (full results found in sec. 3.4, Table 3.2) X measured center = 1000.003m, Y measured center = 101.781m,

with a standard deviation of ±0.0022m in both X and Z. Some results as shown in Tables 3.2 – 3.4 did not converge and produced data values outside of the three standard deviation limit; thus, they were considered to be blunders. Those sets of observations were rejected and not used in the final calculation. Fig 3.13 shows a sample of randomly chosen points selected for the test.

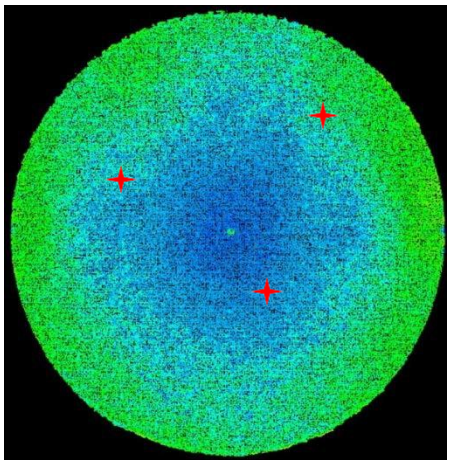

Fig. 3.13 Data Set 1 randomly chosen points method

2. Data Set 2. Linearly picked data points were used to evaluate the performance of the derived equation as shown in Fig. 3.14. Results are X measured center = 1000.003m ± 0.0070m and Z measured center = 101.776m ± 0.0075m. (Full results are shown in sec. 3.4, Table 3.3.) Again a few blunders were detected in the data sets and were not used in the final calculation.

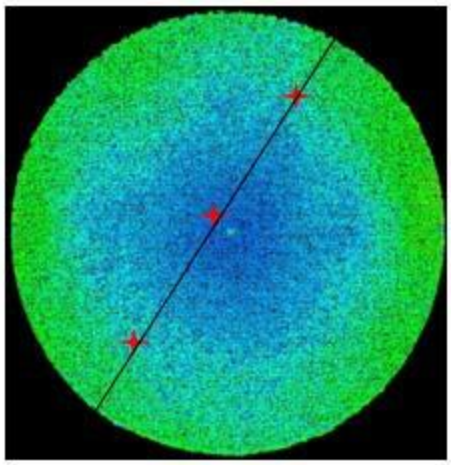

Fig. 3.14 Data set 2, 1 linearly random chosen points method

3. Data Set 3. The Leica P20 Scanstation scans in vertical patterns sweeping horizontally. Not all scanners follow the same pattern due to the manner of the setup. More than likely, more linear lines will be measured on the target. This test shows the results of at least two linear lines measured on the target as shown in Fig 3.15.

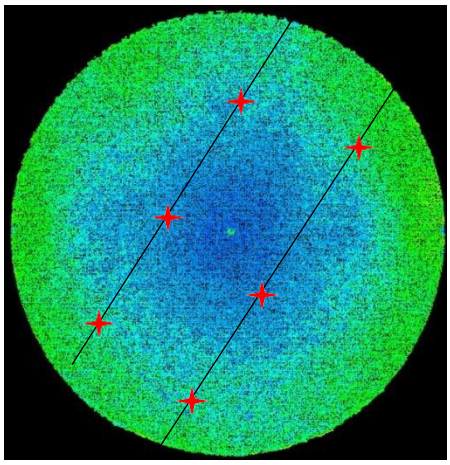

Fig. 3.15 Data Set 3, 2 linearly random chosen points method

4. Summarized results of the three data sets are shown in Table 3.1.

Table 3.1 Results from Data sets 1, 2 and 3 (Units in Meters)

		Known Center	
		X	Z
		1000.000	101.779
Data Set 1	Average	1000.003	101.781
	STD	0.0022	0.0022
Data Set 2	Average	1000.003	101.776
	STD	0.0070	0.0075
Data Set 3	Average	1000.003	101.780
	STD	0.0027	0.0018

3.4 Table Results from Data Sets 1, 2, and 3

Table 3.2 Data Set 1, Randomly Picked from Observed Data (No Regularity of Chosen Points)

	Target Center X = 1000.000m and Z = 101.779m							
		Randomly chosen data points						**Euclidean Distance (m)**
		Observed X(m)	**Observed Z(m)**	**Observed Intensity**	**Calculated Radius (m)**	**Center X(m)**	**Center Y(m)**	
Set 1	Point #1	999.979	101.752	0.5126	0.0374	999.9987	101.7846	0.0057
	Point #2	1000.017	101.773	0.7419	0.0199			
	Point #3	999.993	101.838	0.3836	0.0533			
Set 2* NC	Point #1	1000.056	101.752	0.3155	0.0600	1000.0126	101.7962	0.0213
	Point #2	1000.007	101.774	0.8457	0.0079			
	Point #3	999.973	101.826	0.4427	0.0461			
Set 3	Point #1	999.960	101.740	0.3534	0.0565	1000.0010	101.7789	0.0010
	Point #2	999.990	101.793	0.7577	0.0189			
	Point #3	1000.025	101.782	0.6376	0.0256			
Set 4	Point #1	1000.039	101.732	0.3128	0.0602	1000.0062	101.7823	0.0070
	Point #2	999.946	101.785	0.3091	0.0605			
	Point #3	1000.012	101.790	0.8002	0.0152			
Set 5	Point #1	1000.028	101.843	0.1563	0.0688	1000.0025	101.7791	0.0025
	Point #2	999.993	101.783	0.8159	0.0132			
	Point #3	1000.053	101.746	0.3099	0.0604			
Set 6	Point #1	999.956	101.727	0.1397	0.0699	1000.0017	101.7793	0.0017
	Point #2	999.981	101.846	0.1372	0.0701			
	Point #3	1000.064	101.795	0.2437	0.0647			

Table 3.2 (cont.)

	Target Center X = 1000.000m and Z = 101.779m							
		Randomly chosen data points						Euclidean Distance (m)
		Observed X(m)	Observed Z(m)	Observed Intensity	Calculated Radius (m)	Center X(m)	Center Y(m)	
Set 7	Point #1	999.998	101.737	0.4391	0.0466	1000.0046	101.7831	0.0062
	Point #2	1000.007	101.776	0.8632	0.0037			
	Point #3	999.984	101.796	0.6605	0.0242			
Set 8	Point #1	1000.053	101.735	0.1382	0.0700	1000.0020	101.7830	0.0045
	Point #2	999.981	101.756	0.5387	0.0344			
	Point #3	1000.006	101.795	0.8068	0.0144			
Set 9	Point #1	999.937	101.796	0.1614	0.0685	1000.0029	101.7784	0.0030
	Point #2	1000.006	101.709	0.1380	0.0700			
	Point #3	1000.035	101.837	0.1829	0.0674			
Set 10 NC	Point #1	1000.000	101.763	0.7387	0.0201	1000.0040	101.7814	0.0047
	Point #2	999.995	101.785	0.8317	0.0106			
	Point #3	1000.007	101.787	0.8137	0.0135			
					average	1000.003	101.781	0.004
					STD	± 0.0022	± 0.0022	± 0.0021

NC = non convergence, excluded from final Average and STD
*= one random linear picked data line

Table 3.3 Data Set 2, Randomly Picked from Observed Data – (Linear Relationship)

	Target Center X = 1000.000m and Z = 101.779m							
		Randomly chosen data points -Linear						**Euclidean Distance (m)**
		Observed X(m)	**Observed Z(m)**	**Observed Intensity**	**Calculated Radius (m)**	**Center X(m)**	**Center Y(m)**	
Set 1 NC	Point #1	1000.056	101.752	0.3155	0.0600	1000.0126	101.7962	0.0213
	Point #2	1000.007	101.774	0.8457	0.0079			
	Point #3	999.973	101.826	0.4427	0.0461			
Set 2	Point #1	999.978	101.727	0.389	0.0526	1000.0190	101.7585	
	Point #2	1000.004	101.769	0.8178	0.0128			
	Point #3	1000.031	101.800	0.4552	0.0446			
Set 3	Point #1	999.999	101.713	0.1931	0.0670	1000.0042	101.7791	
	Point #2	1000.031	101.752	0.5231	0.0362			
	Point #3	1000.065	101.804	0.2095	0.0663			
Set 4 NC	Point #1	1000.036	101.738	0.5397	0.0343	1000.0462	101.8049	
	Point #2	1000.000	101.777	0.8432	0.0084			
	Point #3	999.981	101.799	0.6098	0.0276			
Set 5	Point #1	1000.059	101.751	0.2071	0.0664	999.9959	101.7744	
	Point #2	1000.002	101.759	0.6808	0.0231			
	Point #3	999.949	101.766	0.4415	0.0463			
Set 6	Point #1	999.964	101.796	0.4825	0.0411	1000.0011	101.7790	
	Point #2	999.943	101.796	0.3099	0.0604			
	Point #3	999.987	101.796	0.7055	0.0218			

Table 3.3 (cont.)

	Target Center X = 1000.000m and Z = 101.779m							
		Randomly chosen data points -Linear						
		Observed X(m)	**Observed Z(m)**	**Observed Intensity**	**Calculated Radius (m)**	**Center X(m)**	**Center Y(m)**	**Euclidean Distance (m)**
Set 7	Point #1	999.993	101.763	0.7585	0.0189	999.9981	101.7810	
	Point #2	999.998	101.795	0.8129	0.0136			
	Point #3	1000.003	101.829	0.4256	0.0483			
Set 8	Point #1	999.945	101.773	0.3538	0.0564	1000.0009	101.7796	
	Point #2	999.995	101.798	0.7673	0.0182			
	Point #3	1000.042	101.821	0.3326	0.0585			
Set 9	Point #1	1000.062	101.766	0.2755	0.0629	1000.0018	101.7817	
	Point #2	1000.001	101.76	0.7853	0.0167			
	Point #3	999.947	101.752	0.2715	0.0631			
Set 10	Point #1	999.983	101.715	0.2090	0.0663	1000.0057	101.7769	
	Point #2	999.982	101.776	0.7177	0.0212			
	Point #3	999.981	101.827	0.3538	0.0564			
					average	1000.003	101.776	0.006
					STD	± 0.0070	± 0.0075	± 0.0089

NC = Non convergence, excluded from final Average and STD

Table 3.4 Data Set 3, 2 Randomly Picked Linear Lines of Observed Data

		Target Center X = 1000.000m and Z = 101.779m						
		Randomly Chosen data points - 2 Linear Lines						
		Observed X (m()	Observed Z(m)	Observed Intensity	Calculated Radius (m)	Center X(m)	Center Z(m)	Euclidean Distance (m)
Set 1	Pt #1	999.954	101.783	0.4095	0.0502	1000.0050	101.7804	0.0052
	Pt #2	999.985	101.808	0.5399	0.0343			
	Pt #3	1000.013	101.833	0.3834	0.0533			
	Pt #4	999.987	101.744	0.4962	0.0394			
	Pt #5	1000.020	101.773	0.7436	0.0198			
	Pt #6	1000.047	101.798	0.4627	0.0436			
Set 2	Pt #1	999.942	101.757	0.1829	0.0674	1000.0046	101.7805	0.0048
	Pt #2	1000.001	101.759	0.6860	0.0228			
	Pt #3	1000.051	101.759	0.3870	0.0529			
	Pt #4	999.943	101.808	0.1697	0.0681			
	Pt #5	999.998	101.808	0.5846	0.0298			
	Pt #6	1000.048	101.807	0.3993	0.0514			
Set 3	Pt #1	1000.003	101.712	0.1780	0.0677	1000.0010	101.7768	0.0024
	Pt #2	1000.034	101.741	0.4417	0.0462			
	Pt #3	1000.058	101.769	0.3765	0.0540			
	Pt #4	999.979	101.737	0.4510	0.0451			
	Pt #5	1000.007	101.765	0.8186	0.0128			
	Pt #6	1000.039	101.793	0.4156	0.0495			
Set 4	Pt #1	1000.012	101.847	0.1577	0.0688	1000.0047	101.7778	0.0049
	Pt #2	1000.040	101.830	0.2535	0.0642			
	Pt #3	1000.064	101.813	0.1643	0.0684			
	Pt #4	999.946	101.785	0.3091	0.0605			
	Pt #5	999.982	101.757	0.6461	0.0250			
	Pt #6	1000.017	101.737	0.4579	0.0442			
Set 5	Pt #1	999.956	101.822	0.2437	0.0647	1000.0032	101.7814	0.0040
	Pt #2	999.957	101.766	0.4437	0.0460			
	Pt #3	999.959	101.731	0.2020	0.0666			
	Pt #4	999.995	101.838	0.3636	0.0554			
	Pt #5	999.996	101.782	0.8381	0.0094			
	Pt #6	999.998	101.737	0.4391	0.0466			

Table 3.4 (cont.)

		Target Center X = 1000.000m and Z = 101.779m						
		Randomly Chosen data points - 2 Linear Lines						
		Observed X (m()	Observed Z(m)	Observed Intensity	Calculated Radius (m)	Center X(m)	Center Z(m)	Euclidean Distance (m)
Set 6	Pt #1	999.953	101.787	0.3988	0.0515	1000.0015	101.7807	0.0023
	Pt #2	999.999	101.774	0.8315	0.0107			
	Pt #3	1000.044	101.765	0.4332	0.0473			
	Pt #4	999.941	101.751	0.1712	0.0680			
	Pt #5	999.990	101.737	0.4769	0.0418			
	Pt #6	1000.039	101.726	0.1824	0.0675			
Set 7	Pt #1	999.962	101.748	0.3568	0.0562	1000.0054	101.7821	0.0062
	Pt #2	1000.006	101.774	0.8339	0.0102			
	Pt #3	1000.046	101.800	0.4366	0.0469			
	Pt #4	999.939	101.793	0.1717	0.0680			
	Pt #5	999.968	101.818	0.4005	0.0513			
	Pt #6	1000.006	101.851	0.1551	0.0689			
Set 8	Pt #1	999.940	101.813	0.1143	0.0721	1000.0033	101.7802	0.0035
	Pt #2	999.947	101.771	0.3599	0.0558			
	Pt #3	999.956	101.732	0.1768	0.0677			
	Pt #4	999.990	101.832	0.3873	0.0528			
	Pt #5	999.996	101.787	0.8396	0.0092			
	Pt #6	1000.004	101.738	0.4718	0.0424			
Set 9	Pt #1	1000.004	101.847	0.1614	0.0685	999.9966	101.7785	0.0034
	Pt #2	999.995	101.785	0.8317	0.0106			
	Pt #3	999.984	101.721	0.3140	0.0601			
	Pt #4	1000.052	101.825	0.1043	0.0732			
	Pt #5	1000.048	101.761	0.3768	0.0540			
	Pt #6	1000.043	101.727	0.1575	0.0688			
Set 10	Pt #1	999.932	101.795	0.1558	0.0689	1000.0006	101.7818	0.0029
	Pt #2	1000.004	101.798	0.7470	0.0196			
	Pt #3	1000.070	101.799	0.1209	0.0715			
	Pt #4	999.942	101.740	0.1148	0.0721			
	Pt #5	1000.006	101.744	0.4899	0.0402			
	Pt #6	1000.061	101.748	0.1746	0.0678			
					Average	1000.003	101.780	0.004
					STD	0.0027	0.0018	0.0013

3.5 Varied Distances and Angles of Incidence

Table 3.1 supports the hypothesis that absolute intensity can be utilized to help identify

the controlling center of a circular target. Following the same steps as shown in Sections 3.3, two more targets (see fig. 3.16 below) were created to test the impact of angle of

Fig. 3.16 Black and Red Gradient Targets

incidence and distance in relation to the LiDAR scanner. Fig. 3.17 shows the results of the best fit equation representing the radius with respect of the intensity value of the gradient. Each target was set up and tested at distances of 5m, 10m, 15m, and 20m. At each distance, the angle of incidence was also varied per test with angles of 0°, 15°, 30°, and 45°. In total, 16 tests were run per target to test their performace of calculating the controlling center of the target. While testing the impact of distance and angle of incidence, 3 randomly chosen points spread around the cetner of the target were chosen following the pattern as shown in Fig. 3.3. Fig. 3.18 graphically displays the results from the test of angle of incidence and distance.

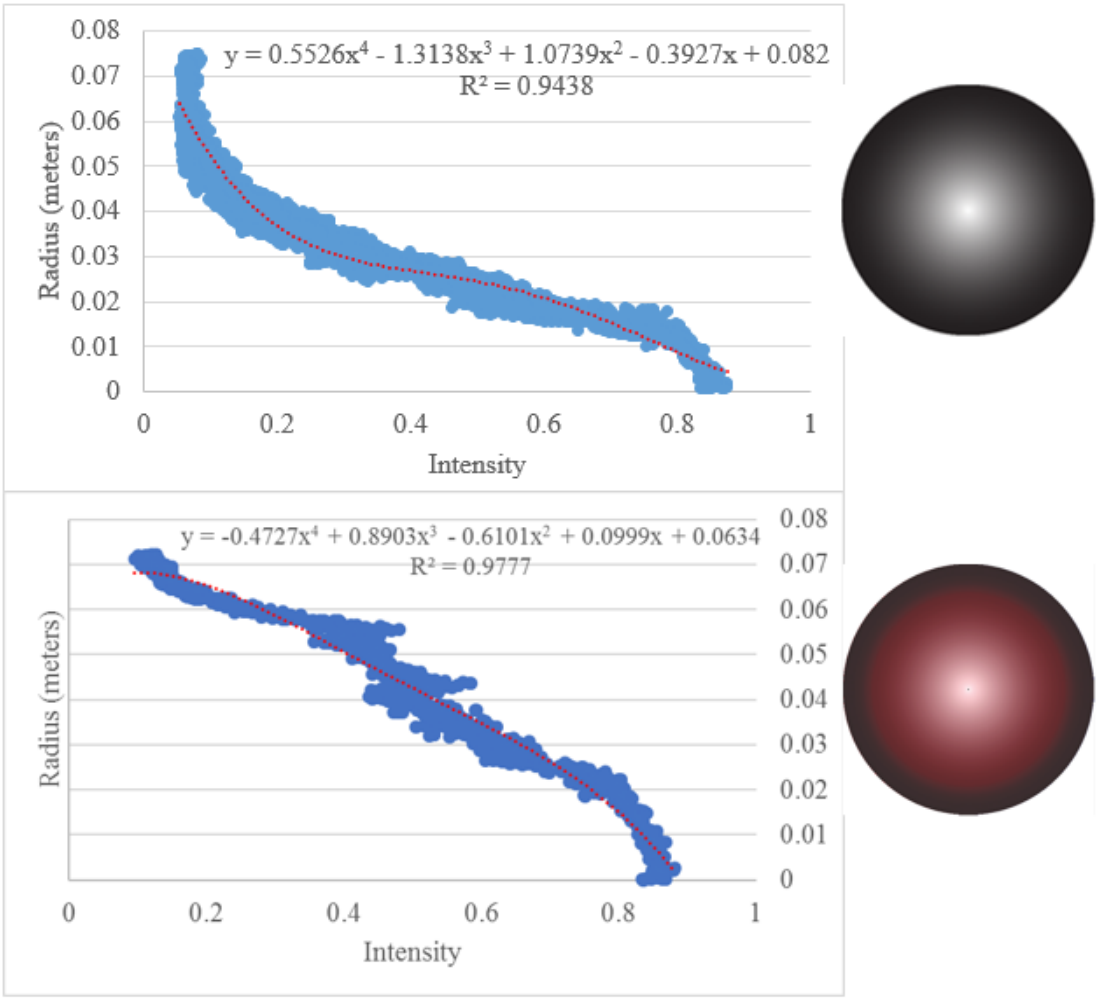

Fig. 3.17 Intensity vs Radius graph and best fit equation for the black and red target

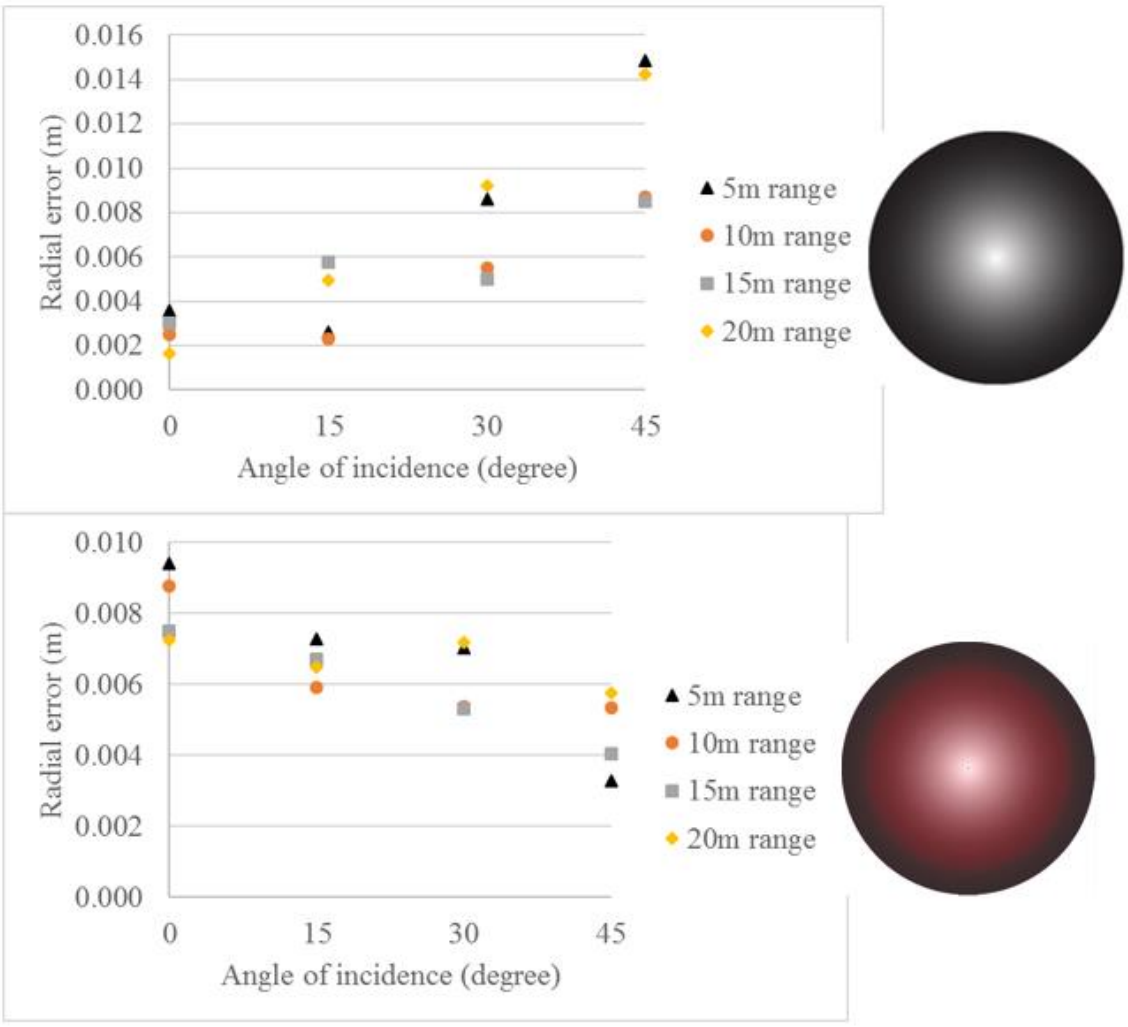

Fig. 3.18 Results of Angle of Incidence and Distance for the Black and Red Gradient Target

3.6 Discussion

As shown in Section 3.4, each data set resulted in less than a centimeter in distance away from the center of the target, the largest being 6mm.

1. Each data set tested will not be typical of real-world applications. These tests were performed merely to show minimums required given certain scenarios. As shown in data set 2, although tests suggest a good performance of the model, a single linear data set with a few data points represent poor geometry, straining the performance ability of the least squares solution. Data set 3 will best represent traditional datasets due to the linear nature of the collection patterns of LiDAR

data. Results support the hypothesis that a circular radially gradient target can perform will aide MTLS or terrestrial scanners where low density of points exist.

2. As shown in Fig. 3.12, there is significant amount of noise present in all the measurements. Outliers are present as well. This is due to the printing function of the gradient on the target. The printing here was done on a laser-jet, consumer-grade printer. This produced some banding in the printing creating abrupt changes in the gradient which lead to inaccurate calibrations of the radius with respect to intensity.

As shown in Section 3.5, angle of incidence and distance does have an impact of the performance of the calibrated targets.

1. Both the black and the red target performed well when tested for angle of incidence and distance. All results were sub centimeter, except two data sets performed on the black target with an angle of incidence of 45° and corresponding distances of 5m and 20m.
2. With the black target, error increases as angle of incidence increases on the target. However, the red target displayed the opposite results, whereas angle of incidence increased, the error got smaller. Further research will be required to either confirm the same results from the two targets, or to support either the black target's pattern of error or the red target's pattern of error. Further research can determine the relationship between color gradient, angle on incidence, and distance from the laser scanner. Regardless of the pattern of error, 87.5% of the experiments performed to sub-centimeter accuracy in identifying the controlling center of the control target.

As seen throughout the chapter, this experiment was not designed to address every possible concern, only to prove that the concept is feasible. More research is necessary to be able to have a functioning target for use in the industry that is a highly accurate and precise targeting method for control and validation points for terrestrial and mobile scanning.

Despite the difficulties with the printing of the target and its calibration, the technique was a success. With the limitations presented, a sub centimeter distance and standard deviation in the planar coordinates was achieved.

4. SBET AND CONTROL TARGETS

4.1 Control and Validation Target Placement – Current Methods

Research continues to find ways to improve all aspects of MTLS systems. Control and validation targets are a common tool to constrain and validate the 3D data. As discussed in the literature review, knowledge gaps exist beyond the MTLS components in the area of target placement. Ussyshkin [12] has suggested a placement of targets every 50-80m. Caltrans and the Florida DOT (Department of Transportation) [10,15] have suggested every 500 feet (~150m) for validation and every 1500 feet (~450m) for control. Hiremagalur [11] has suggested redundancy as a best practice. Control targets are also suggested to be spatially distributed throughout the project [4]. Recent research create a DCC (data collection category) denoting the accuracy and density of a MTLS project defining 3 Accuracy levels: high, medium, and low; with a spacing to be 150-300m, 300-750m, and 750-1500m, respectively. Another gap in research is testing systems in non-ideal situations.

Mobile mapping units consist of two positioning systems: GNSS (Global Navigation Satellite Systems), IMUs (inertial measurement units). In good GNSS conditions, the IMU is augmented and updated by the GNSS. While there is poor GNSS coverage, the IMU acts independently to control positioning of the LiDAR sensor data [4].

4.2 SBET (Smoothed Best Estimated Trajectory)

A LiDAR sensor is placed on a vehicle in a known position relative to all other MTLS components; certain boresights are calculated to know specifically where the scanner sensor is in relation to the GNSS sensor, the IMU, and the DMI. Through commercial software packages, all MTLS data is integrated to produce a SBET (smoothed best estimated trajectory). A SBET is a best-estimated path of the laser scanner sensor derived from GNSS, IMU, and DMI data. The term “best estimate” is frequently used because there are errors in each measurement of each sensor, i.e., positioning from GNSS, orientation from the IMU, and distance from the DMI. Several

factors are taken into account when calculating the “best-estimate” path. The driving force behind the mobile mapping system is the IMU. Due to drift error, an IMU requires the assistance of the GNSS. Without GNSS, each measurement from the IMU is based on the previous measurement and calculated position. Errors compound, producing a drift away from the actual position. GNSS sensors measure between 1 to 10 times a second. Each measurement provides an updated position to help reset the IMU and reset the drift error. Due to many factors such as multipath errors and obstacles blocking satellite signals, GNSS sensors can lose lock and positioning capabilities. With a known SBET, the LiDAR scanner data can be processed and eventually tested for overall completeness and accuracy through control and validation targets.

4.3 Non-ideal Environment

Most experiments testing the accuracy of mobile mapping systems are conducted in an ideal environment, meaning open areas that contain good GNSS lock for proper corrections to be given to the IMU. Rural environments with few vertical obstructions, are excellent testing grounds for MTLS technologies. Urban areas, however, are much more challenging due in large part to the presence of trees, buildings, tunnels, bridges, and bad satellite configurations that block or interrupt the GNSS signal, all of which combine to produce GNSS outages. As described in section 4.3, without corrections, the IMU will drift, leading to a poor calculation of an SBET. In urban areas, an IMU is often the sole positioning system due to the above-mentioned issues with GNSS.

4.4 Target Placement

Control targets are placed to assist and constrain the LiDAR data. As discussed in Section 4.1, control and validation targets are a necessity until technology advances to a point where GNSS corrections are not needed. Target placement is project-dependent; requiring good forethought and planning. A good understanding of the performance capabilities of the INS and GNSS systems is required to properly plan the placement of the targets. Target placement should be based on knowing when the IMU will drift too far out of an acceptable range.

4.5 Efficiency of IMU

As previously mentioned, the importance of an IMU to an SBET is heightened in non-ideal environments (sec. 4.4). A non-ideal situation is defined here as one in which GNSS and DMI are not used to calculate the SBET, which simulates loss of GNSS lock. With the data processing software Applanix [7], measurement features can be manually adjusted to simulate GPS loss of lock, and failed corrections can be given to the IMU. SBET comparisons of given time intervals with good GNSS lock and simulated loss of lock during the same time interval were calculated to analyze the performance of the IMU during those non-ideal situations. The experiment is detailed and outlined below.

1. A full survey with a Trimble MX-8 was conducted that included movements at varying speeds, periods of no movement, periods of good GNSS lock, and periods of loss of GNSS lock. This simulated an urban environment where loss of GNSS is a common occurrence.
2. After the run was complete, all measured data from the GNSS sensor, the IMU, and the DMI were collected and run through Applanix software to compute the SBET. The SBET created here represents a baseline for comparison for all other non-ideal SBET situations.
3. Upon review of the data, nine time stamps of 60-second intervals were created in which GNSS lock was good, with the IMU having received good corrections from the GNSS.
    a. 406300s – 406360s
    b. 407450s – 407510s
    c. 407600s – 407660s
    d. 407980s – 408040s
    e. 407120s – 408180s
    f. 408450s – 408510s
    g. 408600s – 408660s
    h. 408830s – 408890s
    i. 408950s – 409010s
4. Data were then analyzed from each section in two methods: 1. Based on time (Fig. 4.1) and 2. Based on distance traveled (Fig. 4.2).

```
  Event time shift: 0.000000 sec
Photo ID file:
  Photo ID file format: 2 Fields (Time, Photo ID) Format
  Offset between PHOTO ID and EVENT file times: 0.000000 sec
  PHOTO ID time tolerance: 0.300000 sec
Mapping frame datum: WGS84  ; Mapping frame projection : TM;
central meridian = -87.000000 deg;
latitude of the grid origin = 0.000000 deg; grid scale factor = 0.999600:
false easting = 500000.000000 m; false northing = 0.000000 m; |
Boresight values: tx =        0.0000 arc min, ty =        0.0000 arc min, tz =
Lever arm values: lx =        0.0000 m, ly =        0.0000 m, lz =        0.0000 m.
TIME, DISTANCE, EASTING, NORTHING, ELLIPSOID HEIGHT, LATITUDE, LONGITUDE, ELLIPSOID H

 (time in Sec, distance in Meters, position in Meters, lat, long in Degrees, orientat

403858.00000       0.000  593637.161 4094302.728  194.023 36.99020120 -85.94776556
403859.00000       0.000  593637.161 4094302.728  194.023 36.99020120 -85.94776556
403860.00000       0.000  593637.161 4094302.728  194.023 36.99020120 -85.94776556
403861.00000       0.000  593637.161 4094302.728  194.023 36.99020120 -85.94776556
403862.00000       0.000  593637.161 4094302.728  194.023 36.99020120 -85.94776556
403863.00000       0.000  593637.161 4094302.728  194.023 36.99020120 -85.94776556
403864.00000       0.000  593637.161 4094302.728  194.023 36.99020120 -85.94776556
403865.00000       0.000  593637.161 4094302.728  194.023 36.99020120 -85.94776556
403866.00000       0.000  593637.161 4094302.728  194.023 36.99020120 -85.94776556
403867.00000       0.000  593637.161 4094302.728  194.023 36.99020120 -85.94776556
403868.00000       0.000  593637.161 4094302.728  194.023 36.99020120 -85.94776556
403869.00000       0.000  593637.161 4094302.728  194.023 36.99020120 -85.94776556
403870.00000       0.000  593637.161 4094302.728  194.023 36.99020120 -85.94776556
403871.00000       0.000  593637.161 4094302.728  194.023 36.99020120 -85.94776556
403872.00000       0.000  593637.161 4094302.728  194.023 36.99020120 -85.94776556
403873.00000       0.000  593637.161 4094302.728  194.023 36.99020120 -85.94776556
403874.00000       0.000  593637.161 4094302.728  194.023 36.99020120 -85.94776556
403875.00000       0.000  593637.161 4094302.728  194.023 36.99020120 -85.94776556
403876.00000       0.000  593637.161 4094302.728  194.023 36.99020120 -85.94776556
403877.00000       0.000  593637.161 4094302.728  194.023 36.99020120 -85.94776556
403878.00000       0.000  593637.161 4094302.728  194.023 36.99020120 -85.94776556
403879.00000       0.000  593637.161 4094302.728  194.023 36.99020120 -85.94776556
403880.00000       0.000  593637.161 4094302.728  194.023 36.99020120 -85.94776556
403881.00000       0.000  593637.161 4094302.728  194.023 36.99020120 -85.94776556
403882.00000       0.000  593637.161 4094302.728  194.023 36.99020120 -85.94776556
```

Fig. 4.1 Typical output of SBET file, organized by seconds

```
Photo ID file:
  Photo ID file format: 2 Fields (Time, Photo ID) Format
  Offset between PHOTO ID and EVENT file times: 0.000000 sec
  PHOTO ID time tolerance: 0.300000 sec
Mapping frame datum: WGS84  ; Mapping frame projection : TM;
central meridian = -87.000000 deg;
latitude of the grid origin = 0.000000 deg; grid scale factor = 0.999600:
false easting = 500000.000000 m; false northing = 0.000000 m;
Boresight values: tx =        0.0000 arc min, ty =        0.0000 arc min, tz =
Lever arm values: lx =        0.0000 m, ly =        0.0000 m, lz =        0.0000 m.
TIME, DISTANCE, EASTING, NORTHING, ELLIPSOID HEIGHT, LATITUDE, LONGITUDE, ELLIPSOID HI

 (time in Sec, distance in Meters, position in Meters, lat, long in Degrees, orientat

406300.00019       0.000  594944.168 4094189.804  201.358 36.98905234 -85.93309477
406304.55184       1.000  594945.107 4094190.146  201.381 36.98905533 -85.93308419
406305.57410       2.000  594946.047 4094190.485  201.407 36.98905829 -85.93307358
406306.50182       3.000  594946.989 4094190.817  201.431 36.98906119 -85.93306295
406307.29167       4.000  594947.932 4094191.149  201.457 36.98906408 -85.93305231
406307.87530       5.000  594948.877 4094191.474  201.482 36.98906692 -85.93304166
406308.31681       6.000  594949.822 4094191.800  201.507 36.98906977 -85.93303100
406308.67488       7.000  594950.766 4094192.128  201.533 36.98907262 -85.93302035
406308.97920       8.000  594951.709 4094192.457  201.558 36.98907549 -85.93300971
406309.24818       9.000  594952.655 4094192.781  201.587 36.98907832 -85.93299905
406309.49409      10.000  594953.599 4094193.108  201.612 36.98908117 -85.93298840
406309.72248      11.000  594954.543 4094193.436  201.639 36.98908403 -85.93297775
406309.93888      12.000  594955.485 4094193.769  201.666 36.98908694 -85.93296713
406310.14570      13.000  594956.428 4094194.101  201.692 36.98908983 -85.93295649
406310.34667      14.000  594957.371 4094194.430  201.719 36.98909270 -85.93294585
406310.54163      15.000  594958.314 4094194.760  201.744 36.98909559 -85.93293521
406310.72918      16.000  594959.257 4094195.092  201.773 36.98909848 -85.93292458
406310.91057      17.000  594960.201 4094195.420  201.801 36.98910134 -85.93291393
406311.08496      18.000  594961.146 4094195.745  201.834 36.98910417 -85.93290327
406311.25193      19.000  594962.088 4094196.077  201.866 36.98910707 -85.93289264
406311.41227      20.000  594963.029 4094196.414  201.904 36.98911001 -85.93288204
406311.56749      21.000  594963.970 4094196.747  201.944 36.98911292 -85.93287141
406311.71783      22.000  594964.916 4094197.069  201.982 36.98911573 -85.93286075
406311.86453      23.000  594965.860 4094197.397  202.013 36.98911859 -85.93285010
406312.00728      24.000  594966.800 4094197.735  202.047 36.98912154 -85.93283950
406312.14652      25.000  594967.741 4094198.071  202.087 36.98912447 -85.93282889
406312.28301      26.000  594968.684 4094198.401  202.121 36.98912735 -85.93281825
406312.41676      27.000  594969.627 4094198.730  202.157 36.98913022 -85.93280761
406312.54856      28.000  594970.570 4094199.060  202.194 36.98913310 -85.93279697
406312.67911      29.000  594971.510 4094199.397  202.233 36.98913604 -85.93278637
406312.80936      30.000  594972.450 4094199.737  202.272 36.98913901 -85.93277577
406312.94012      31.000  594973.389 4094200.076  202.312 36.98914197 -85.93276517
406313.07156      32.000  594974.329 4094200.416  202.350 36.98914494 -85.93275457
```

Fig. 4.2 Typical output of SBET file organized by distance traveled

5. GNSS outages were then simulated. In the software, GNSS can be disabled. In the 60-second timestamps previously shown, 10-second intervals of GNSS outages were simulated. As the SBET was computed, it computed as though no GNSS lock occurred, and the mobile mapping system was relying completely upon the IMU.
6. Reports were again generated by time and distance.
7. Easting and Northing and elevation coordinates were then extracted from all the files and compared to the original SBET where GNSS lock was good. Fig. 4.3 and Fig. 4.4 demonstrate the typical results of each 10-second interval from the nine time stamps. Fig. 4-3 shows a zoomed-in area displaying the first 20 meters of the difference in the trajectories. If the engineering limit was 0.020m, then a comparison can be made to show how far the vehicle traveled before exceeding the limit:

    - 10s outage – approx. 5m
    - 20s outage – approx. 3m
    - 30s outage – approx. 5m
    - 40s outage – approx. 1.1m
    - 50s outage – approx. 1.3m
    - 60s outage – approx. 2.2m

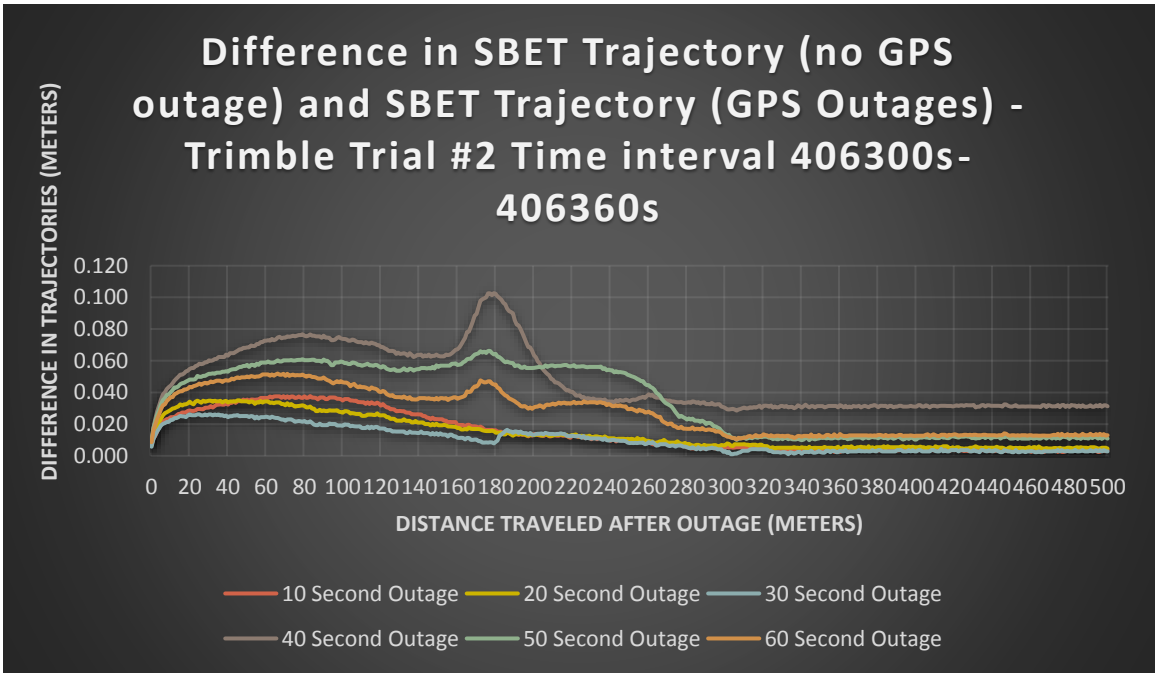

Fig. 4.3 Trial #2, 60s GNSS outage time interval comparison

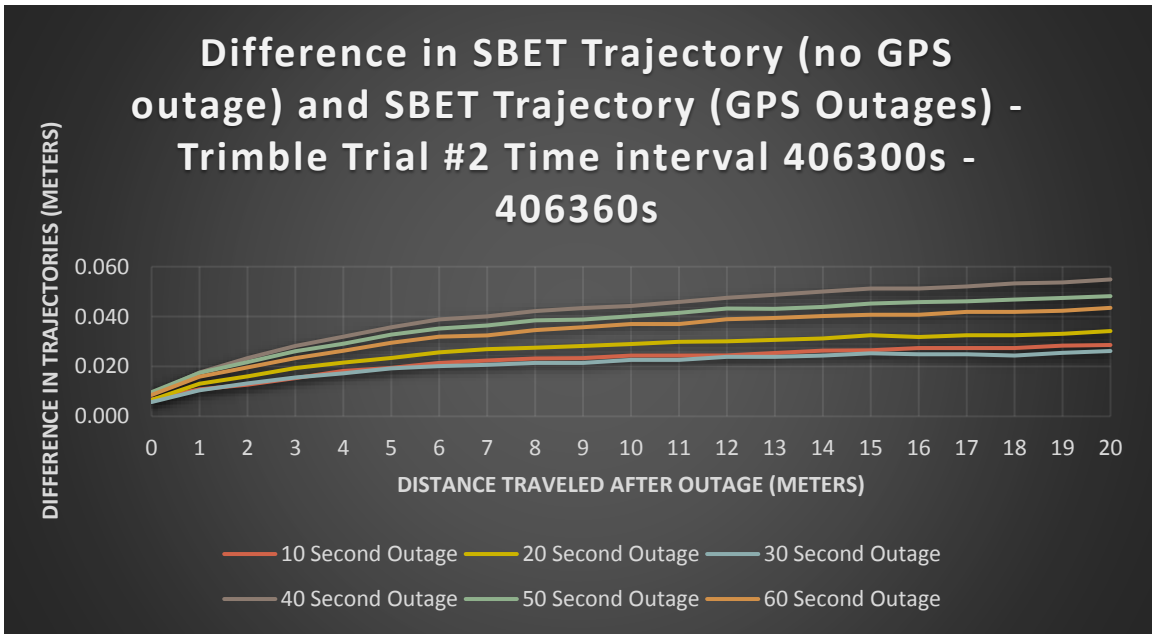

Fig. 4.4 Trial #2, 60s GNSS outage time interval comparison zoomed to first 20m

The difference shown is due to the way the SBET was calculated. As shown in Appendix A, the complete results of each outage varied from one to another. The results show that generally, the longer the outage of GNSS, the shorter distance it takes to go beyond a given engineering threshold. As will be shown later with all samples, this contributes to the idea that the placement of targets should not be constrained by distance, as the distance varies per time length of outage.

Fig. 4.5 shows the same 60s GNSS outage time period as Fig. 4.3 and Fig. 4.4 but in terms of time instead of distance travelled to reach beyond a given 3D threshold. Fig. 4.6 shows a zoomed in portion of the change in SBETs to gain a better perspective how much they change in respect to time instead of distance. The results follow, again given a 0.020m threshold:

- 10 second outage – approx. 7 seconds of travel
- 20 second outage – approx. 6.2 seconds of travel
- 30 second outage – approx. 7 seconds of travel
- 40 second outage – approx. 5 seconds of travel
- 50 second outage – approx. 5.2 seconds of travel
- 60 second outage – approx. 5.5 seconds of travel

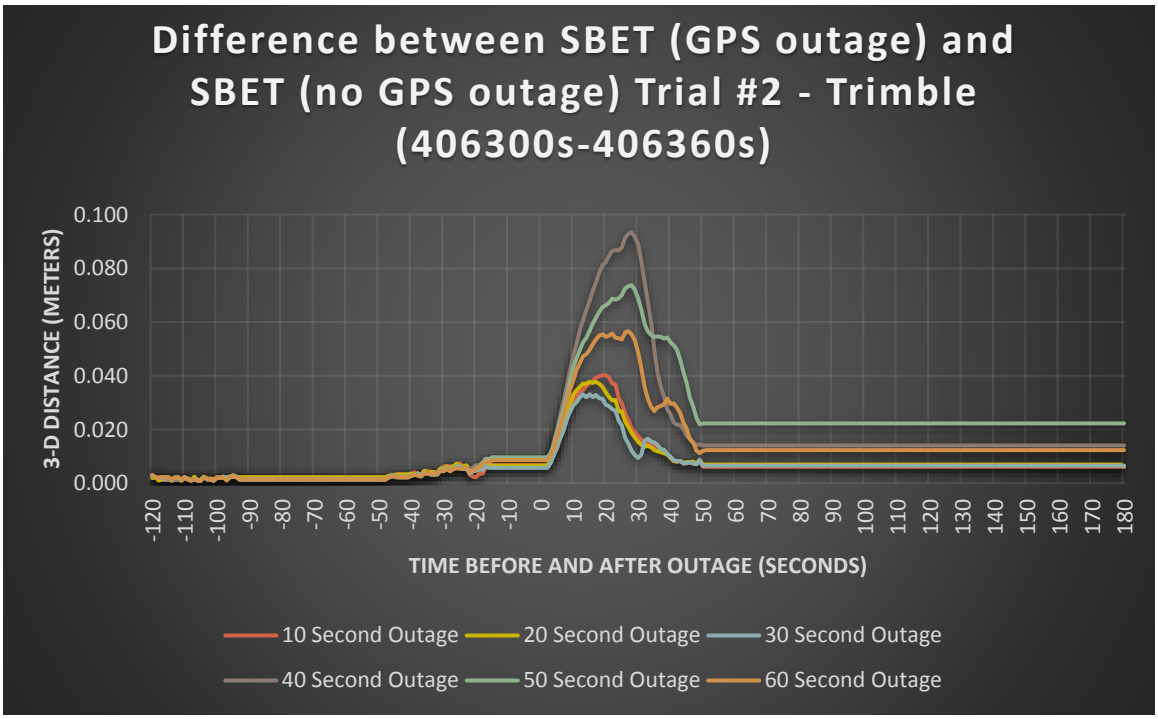

Fig. 4.5 Trial #2, time elapsed to exceed threshold

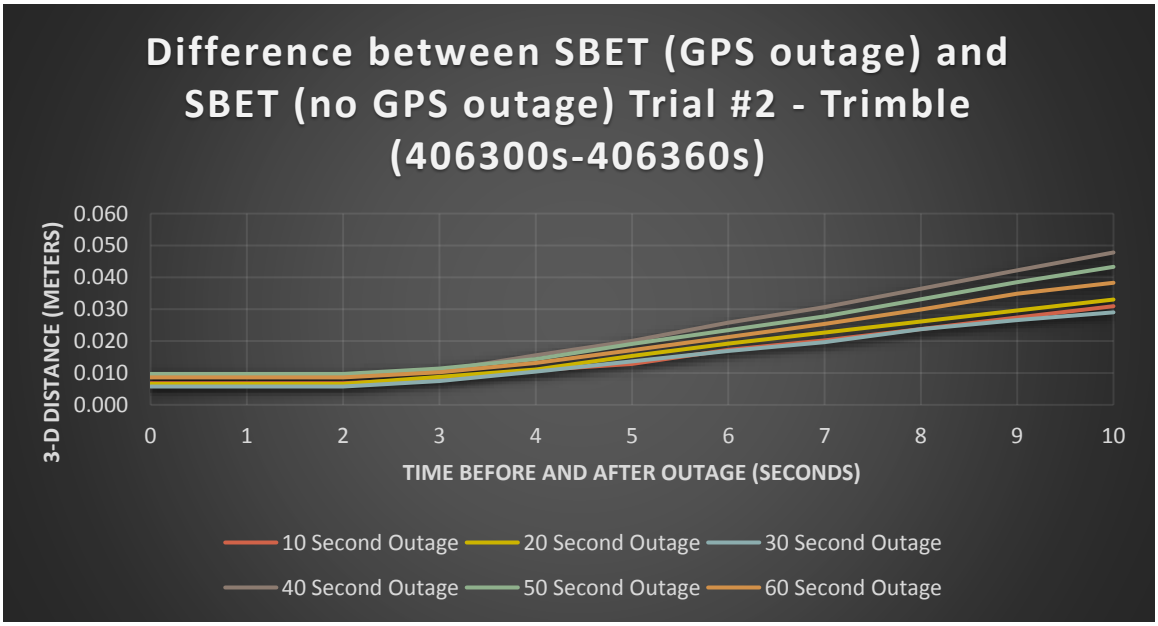

Fig. 4.6 Trial #2, zoomed in time elapsed to exceed threshold

8. A summary of Figs. 4.3-4.6 is provided in Table 4.1 using a threshold of 0.020m. Table 4.1 details the summary of each trial and details how many meters traveled it takes to exceed a certain threshold of 0.020m. If distance was the controlling factor, then all the distances shown in Table 4.1 would be approximately the same distance give or take a few meters. As shown, there is not a correlation between the distances.

Table 4.1 Distance travelled and Time traveled to exceed 0.020m threshold with GNSS outage

		Time (seconds) to exceed 0.020m threshold							
Trial #	Time Interval (sec)	10s	20s	30s	40s	50s	60s	m/s	Avg. mph
1		-	-	-	-	-	-	-	
2	406300-406360	7.00	6.25	7.00	5.00	5.25	5.75	0.9	5
3	407450-407510	7.00	13.00	7.50	6.00	5.50	4.25	5.8	28
4	407600-407660	-	2.50	4.25	6.00	7.00	4.50	13.0	63
5	407980-408040	-	13.75	5.75	3.75	5.50	4.50	12.0	58
6	408120-408180	-	-	-	-	-	-	-	-
7	408450-408510	-	-	8.00	5.75	3.25	2.50	8.6	41
8	408600-408660	-	-	5.25	5.25	5.25	4.00	3.5	17
9	408830-408890	15.00	13.00	6.00	6.00	3.50	5.00	5.1	24
10	408950-409010	6.00	6.25	2.50	3.50	3.00	3.00	4.3	21
	Average	8.75	9.13	5.78	5.16	4.78	4.19		

		Distance (meters) to exceed 0.020m threshold							
Trial #	Time Interval (sec)	10s	20s	30s	40s	50s	60s	m/s	Avg. mph
1		-	-	-	-	-	-	-	-
2	406300-406360	6	4	6	2	2	2	0.9	5
3	407450-407510	10	62	44	35	19	13	5.8	28
4	407600-407660	-	33	64	231	244	55	13.0	63
5	407980-408040	-	204	74	50	73	60	12.0	58
6	408120-408180	-	-	-	-	-	-	-	-
7	408450-408510	-	-	136	415	72	34	8.6	41
8	408600-408660	-	-	29	28	21	19	3.5	17
9	408830-408890	49	-	24	116	29	92	5.1	24
10	408950-409010	22	21	4	12	7	8	4.3	21

9. Final analysis will allow users to the view the difference in SBETs based upon time and not distance so they know where to place control and validation targets. The IMU measures anywhere from 100 to 2,000 Hz, no matter the speed of the vehicle. The drift of the IMU is time dependent, not distance dependent.

4.6 Planning Specifications for Control and Validation Targets

The experiment in Section 4.5 proves that the IMU drift is time-dependent, no matter the speed at which the vehicle is traveling. Understanding the individual performance of each IMU will provide direction and guidance in a planning process; the operator should understand that at 20 mph, and with intermittent lock of GNSS, more targets are necessary to account for the dependency of the IMU during those situations. As outlined by several government agency manuals (e.g., Caltrans and Florida [10,15]) targets were shown to be placed at equal distance intervals. The Caltrans manual even suggests to slow down when scanning the targets to get a more dense set of observations [10]. With an IMU being time-dependent, and the SBET being dependent upon the IMU during non-ideal situations, targets themselves should be placed according to where a correction is necessary. As shown in the beginning of this chapter, state agencies and research dictate placement by distances, regardless of ideal vs non-ideal situations. This process as outlined shows now that such specifications and recommendations are misguided. If an operator loses GNSS lock going 60 mph or 20 mph, the IMU will only function in respect to time, not distance. Recommendations for target placement with respect to distance should be given to govern or guide MTLS surveys. Rather, the goal was to first understand that placement should be time dependent, and second that all users can now have a method to test their own MTLS and determine the limitations of each given system. Combined with proper targets and proper spacing of control targets, a better SBET and 3D data set can be accomplished.

5. SPHERE AND CUBE CALIBRATION

5.1 Sphere Target

As discussed in the literature review, spherical and cube targets are not utilized in typical MTLS applications [4]. Little research shows the use of a sphere in control target applications. Puente et al [26] outlined typical procedures where spheres are used to calibrate the complete MTLS system, not to be used as a controlling target in the registration and validation of the 3D point cloud. As shown in Fig. 5.1, users cannot directly measure to the center of the target, thus the need for calibration. In this research, a nominal 14-inch diameter plastic sphere was used and calibrated. The sphere was sanded to remove all the shiny reflective material. A customized aluminum mounting bracket was constructed to house the sphere, which was then placed on top of a tripod for use. Sections 5.1.1 – 5.1.2 outline the calibration of the sphere and relation to the control/validation point on the ground.

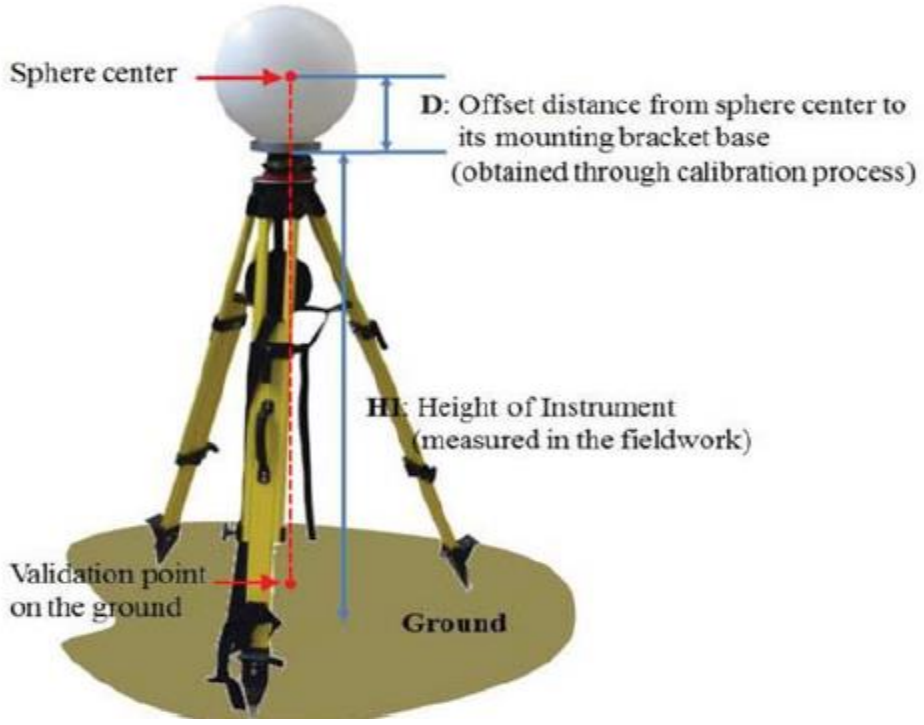

Fig. 5.1 Typical spherical target setup

5.1.1 **Sphere Calibration**

A sphere was placed in the mounting bracket and then together both were placed on a planar and smooth surface. Using a Leica Scanstation II terrestrial scanner, the sphere was scanned from three locations as shown in Fig. 5.2, all in the same coordinate system. Using Leica Cyclone, the three scans were registered together to give a model of the sphere (see Fig. 5.3), consisting of approximately ¾ coverage. As seen in Fig. 5.2, the planar surface is also shown below the sphere. Using Leica's Cyclone software, a best fit surface was created on the table as well as a best fit sphere from the points captured. Subsequent to the sphere creation, the center was also calculated with X,Y, and Z coordinates (see Fig 5.4 for a typical results of the sphere fitting calculation).

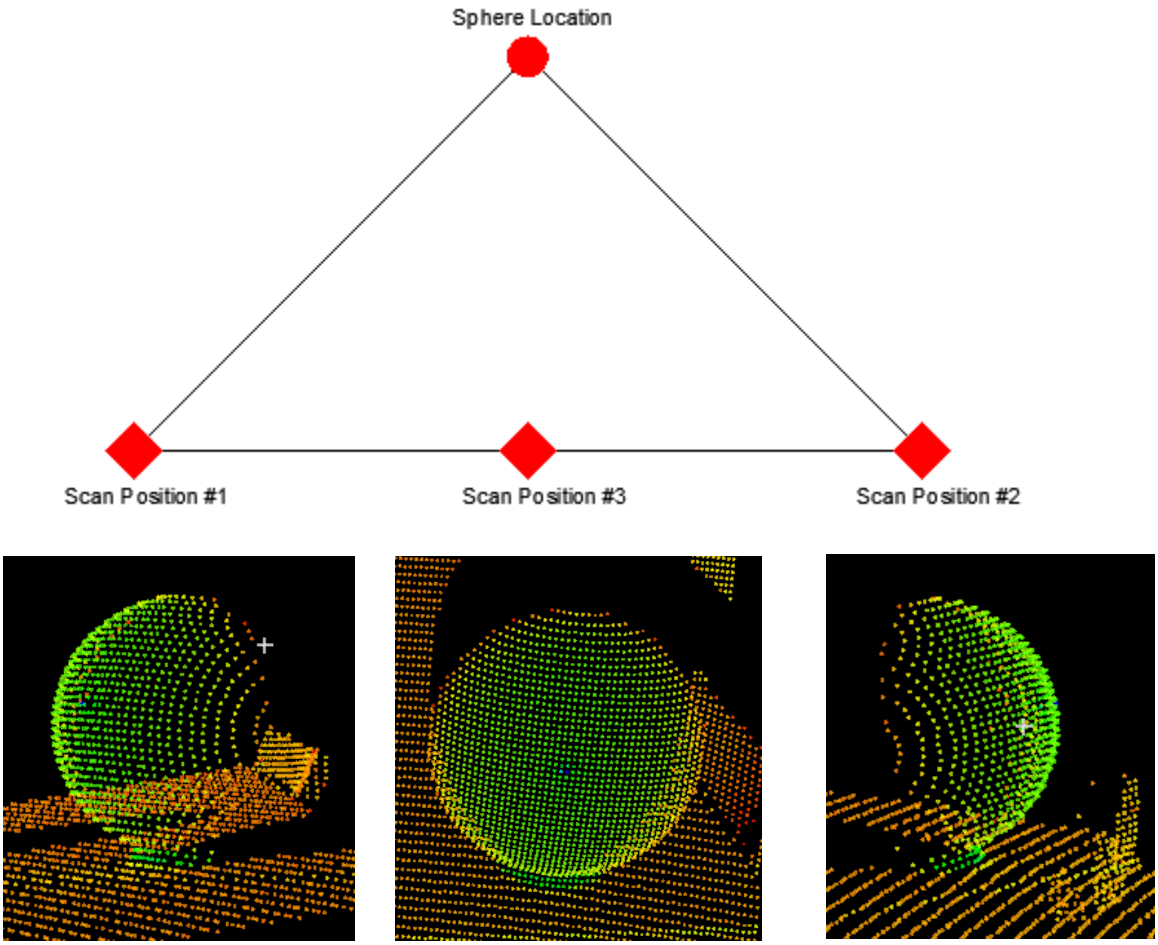

Fig. 5.2 Typical results from the scanner on the sphere

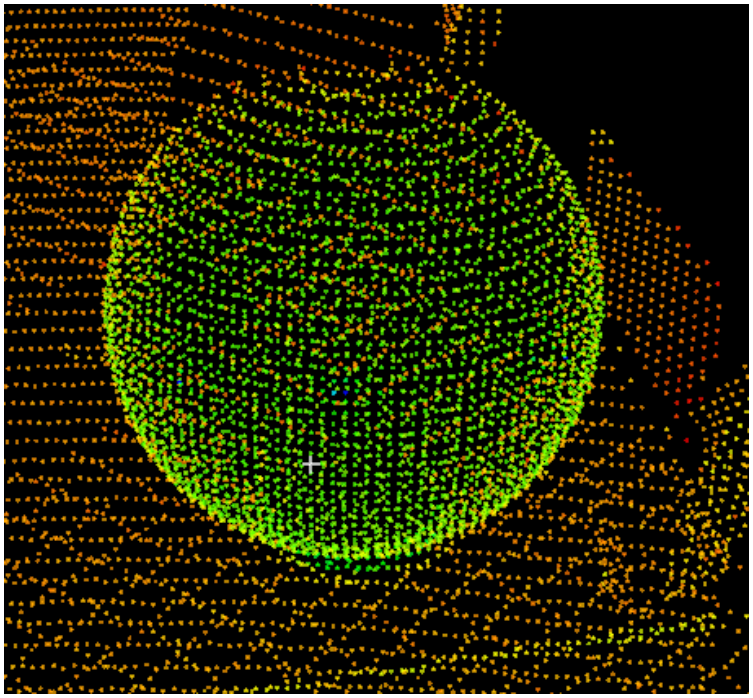

Fig. 5.3 Overall registered data on the sphere

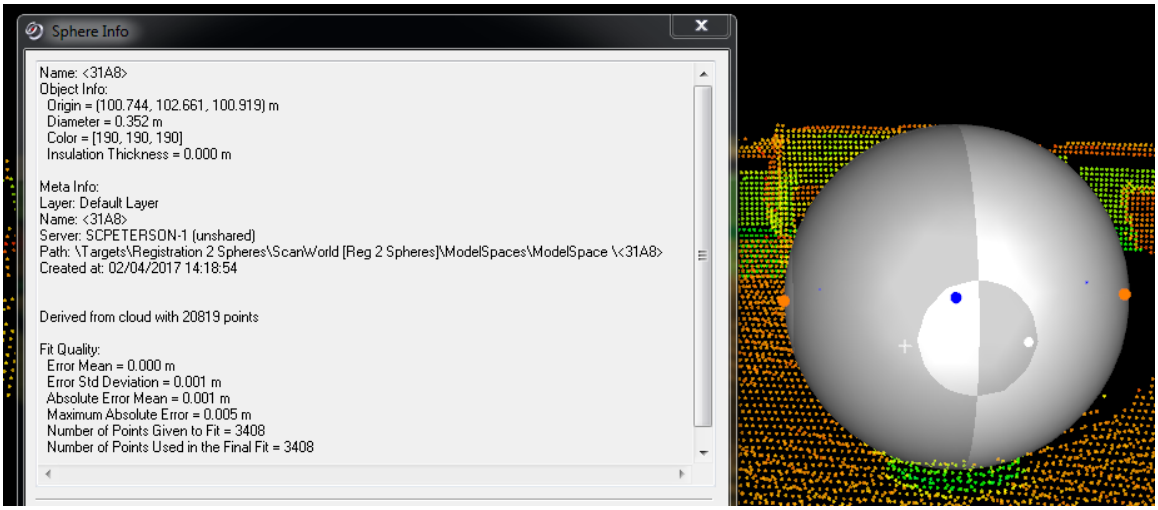

Fig. 5.4 Typical results from calculating the sphere center and size from the scanned data

From the calculations performed in cyclone shown in Fig. 5.4, the sphere has a diameter of 0.352m (radius of 0.176m). The results of the least squares adjustment are given as well the standard deviation of ± 0.001m. From the best fit planar surface as shown in Fig 5.5, a normal vector to the plane is computed with its associated distance. The distance from the control point to the top of the tripod was measured, then added to the calibrated distance from the bottom of the mounting bracket to the center of the sphere. During this research as well as research performed for the Indiana Department of Transportation, eight spheres were calibrated as shown in Table 5.1.

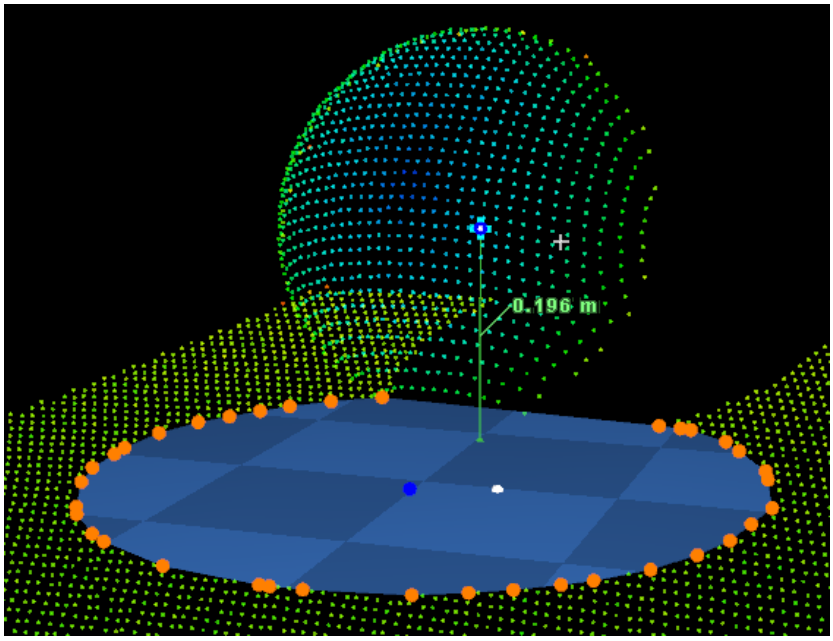

Fig. 5.5 Calculated distance from center of sphere to bottom of mounting bracket

Table 5.1 Johnson et al. [9] Results of Sphere Calibration

Sphere calibration results.

Sphere Target	Setting Environment	Measured Offset Distance (m)	Computed Radius (m)
Sphere 1	Placed on a flat table	0.194	0.177
Sphere 2	Placed on a flat table	0.195	0.177
Sphere 3	Placed on a flat table	0.195	0.177
Sphere 4	Placed on a flat table	0.194	0.177
Sphere 5	Placed on the floor	0.196	0.177
Sphere 6	Placed on the floor	0.193	0.178
Sphere 7	Placed on the floor	0.193	0.178
Sphere 8	Placed on the setup tripod	Unable to recover tripod surface where the sphere was placed on	0.177
		Statistics Computed from 7 Spheres	
Minimum		0.193	0.177
Maximum		0.196	0.178
Average		**0.194**	**0.177**
Standard Deviation		0.001	0.0004

5.1.2 **Test of Cyclone Software**

No details were found as to how the fitment of the sphere was computed mathematically. Further details are required to analyze the fitment of the sphere. A small program was written to verify the fitment of the spheres. Each xyz coordinate measured on the sphere was extracted for each of the three scan locations. Using MATLAB software, each scan was plotted as a visual reference (Fig. 5.6). A least squares program was written to compare the results. The average radius was calculated to be 0.177m (Fig. 5.8), which matches the results from the Leica Cyclone software within 0.001m (Fig. 5.4). After comparison, the cyclone software was used completely for any fitting of the data as necessary for calibrations.

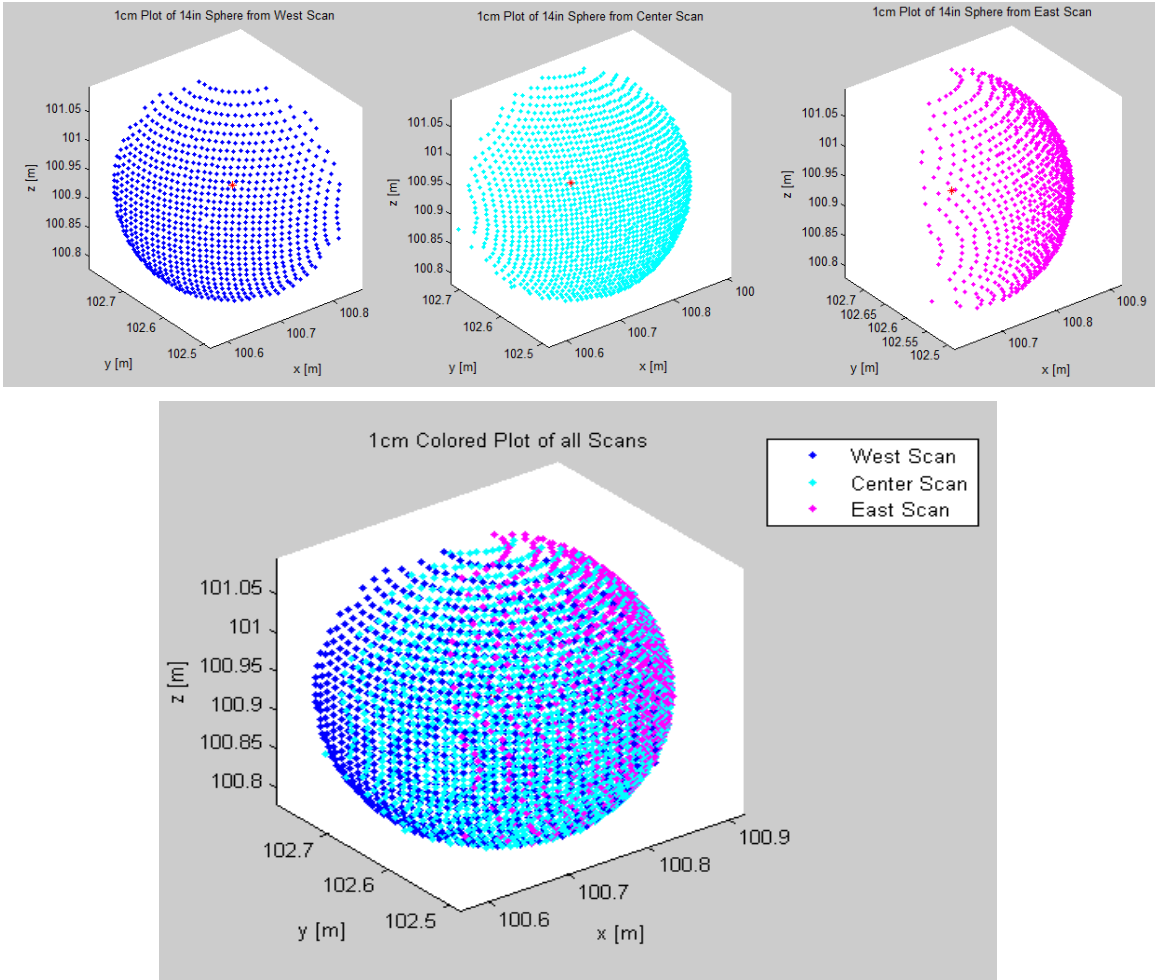

Fig. 5.6 Individual and registered Leica Scanstation II data from three locations

5.1.3 **Angle of Incidence on the Sphere**

As discussed in the literature review, angle of incidence is an area of concern when scanning specific objects to be modeled. Angle of incidence is a major source of error for the LiDAR sensor [4]. As the LiDAR sensor measures objects deviating from the normal of the object, the positioning error increases (see Fig. 5.7).

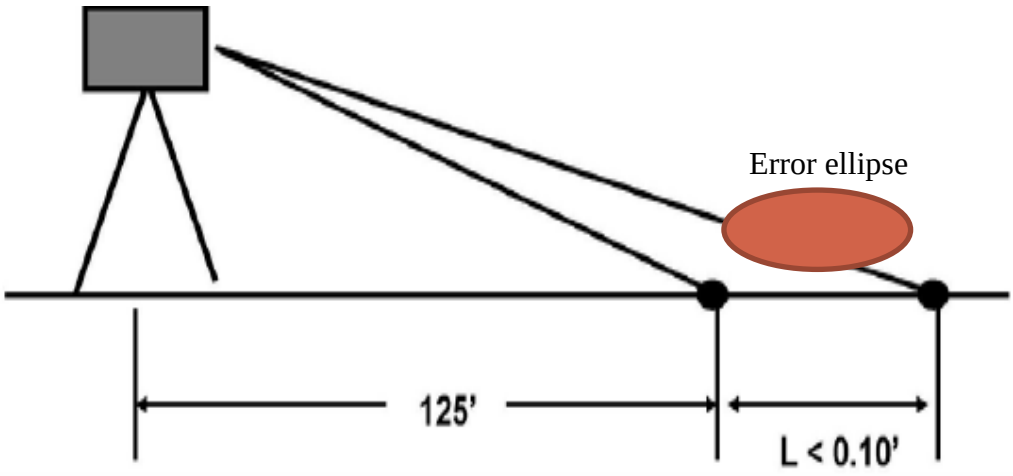

Fig. 5.7 Error due to angle of incidence

As a result of increased positional error, intuitively, one would expect to not be able to use that data in calibration of a desired X,Y, and Z coordinate that will be the controlling location of a target. Fig. 5.8 displays the residuals whether positive or negative, and the magnitude and position of those residuals when creating a best fit object. The larger angles of incidence reside along the outside of the sphere, the portion most deviated from the normal to the object. The expectation is that the highest magnitude residual be along the outside of the edges of the measured sphere. As Fig 5.8 shows, this is not the case. The angle of incidence does not have an impact. All magintudes, positions, and sign of the residuals appear to be randomly distributed. No hidden biases or blunders are detected with the calibration of the sphere.

5.2 Cube Target

Currently, there is a gap in the body of research in that no studies have used a cube as a control or validation target in MTLS. No studies have suggested using one or how to properly calibrate one when used for MTLS. In this research, a 12” cube was

designed and test following similar procedures as outlined in sections 5.1.1 – 5.1.3 for a sphere.

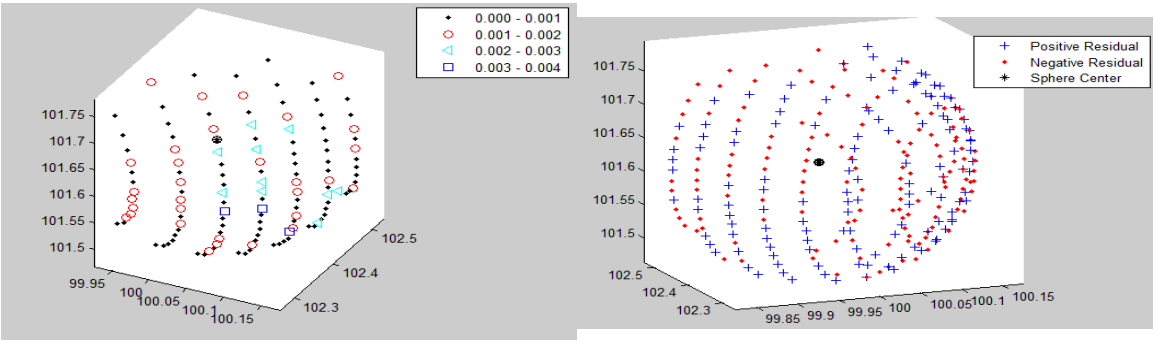


```
Range of Residuals = 0.0035m
High Residual = 0.0035m
Low Residual = 0.0000m
A Priori Sigma = 0.006m
Posteriori Sigma = 0.0012m


Number of Observations = 127
Number of Absolute Value Residuals between 0.000m and 0.001m =  83
Number of Absolute Value Residuals between 0.001m and 0.002m =  31
Number of Absolute Value Residuals between 0.002m and 0.003m =  10
Number of Absolute Value Residuals between 0.003m and 0.004m =   3
```

Fig. 5.8 Distribution of residuals on calibrated sphere

5.2.1 **Calibration of Cube**

A cube has three faces, each of which were scanned, in similar fashion as shown in Fig. 5.2. One position of the cube was chosen to be the controlling location of the target as shown in Fig 5.9. Three faces are required to solve for a single position as seen in Fig. 5.10. Normals from each surface were calculated using Leica Cyclone. Normals were then intersected to provide a controlling center of the cube. An offset was then measured to the base of the cube mounting bracket. Combing all measurements, the height above the control locaiton was calculated.

5.2.2 **Angle of Incidence on Cube**

As with a sphere, angle of incidence initially would be of concern. To scan three faces with MTLS, it must be positioned so that none of the faces would be perpendicualr to the LiDAR sensor. As shown in Fig. 5.7, angle of incidence increases the positional error of the measurement. The error in this instance follows along the plane of each cube

face. Each measurement is a location on the cube surface ± the error on the surface of the cube. To solve the controlling location of the cube, it was surface-fitting, resulting in the ability to ignore the angle of incidence errors as shown in the calibration simulations in Fig. 5.11 and Fig 5.12. The magnitude, position, and sign of the residuals appear without bias or apparent blunders.

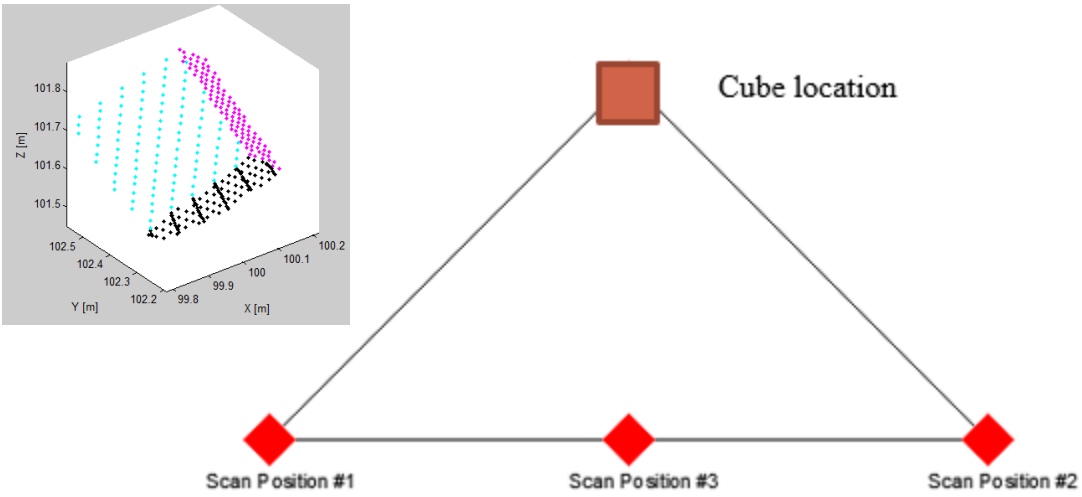

Fig. 5.9 Control setup of a cube

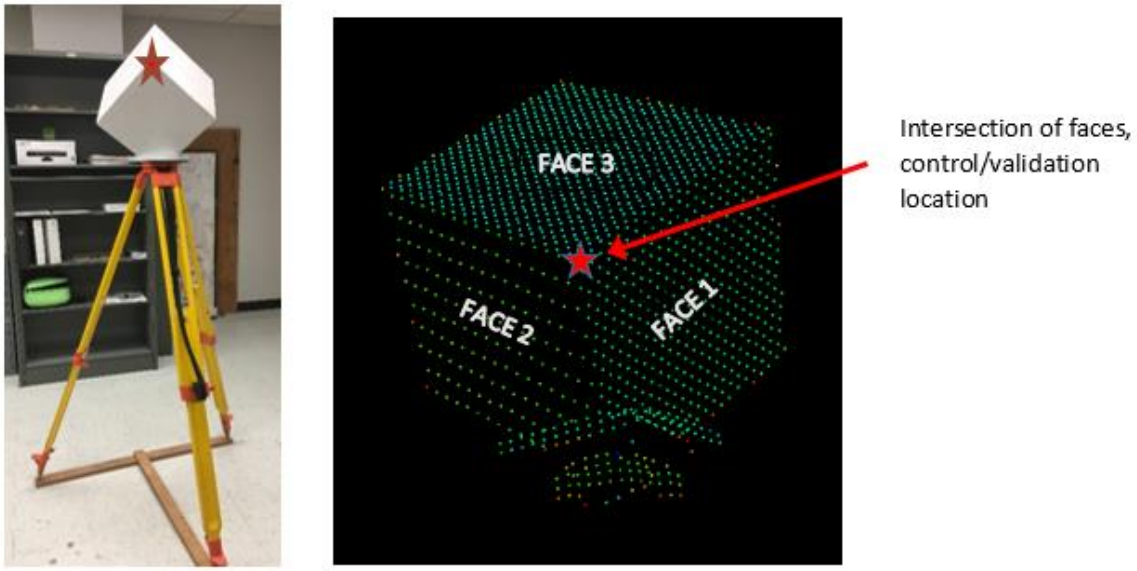

Fig. 5.10 Cube on tripod, and cube with three faces scanned

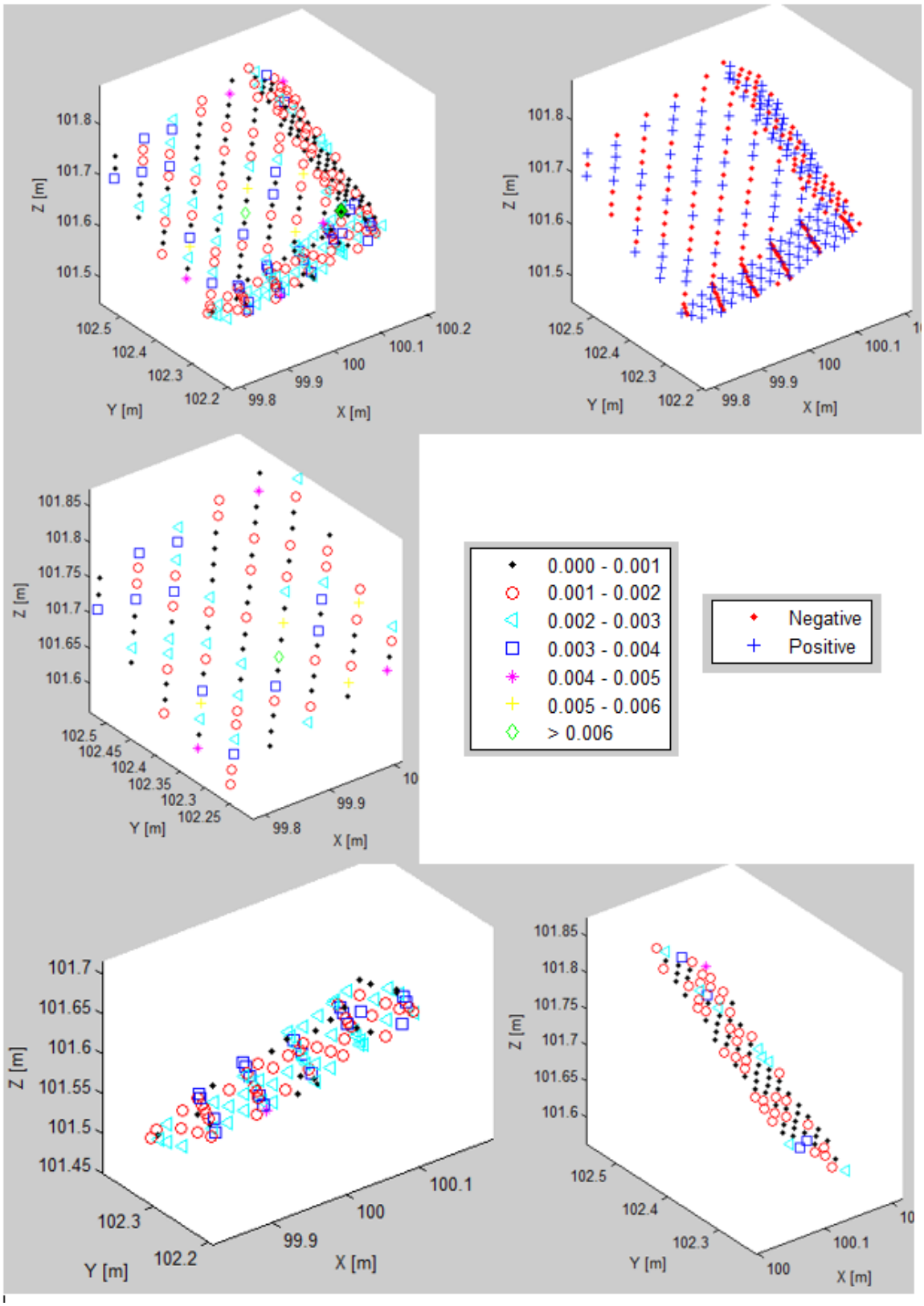

Fig. 5.11 Residual results displaying magnitude of residuals as well as sign of residuals-- 15mph simulation

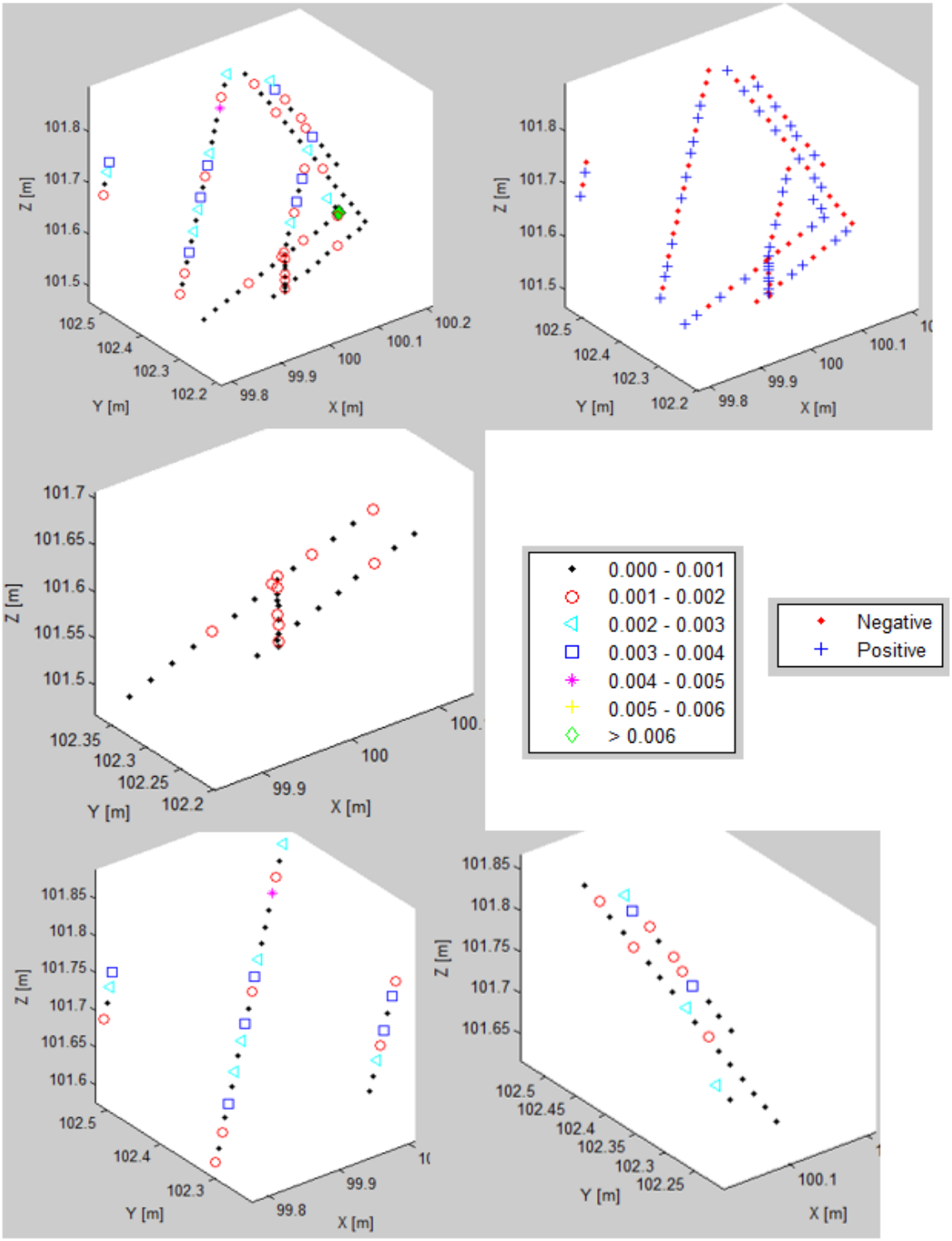

Fig. 5.12 Residual results displaying magnitude of residuals as well as sign of residuals--60 mph simulation

6. PERFORMANCE OF SPHERE TARGET AT VARYING SPEEDS

6.1 Current Employed Targets for MTLS

A common practice for control and validation targets in MTLS projects is painting targets on the ground with varying degrees of reflectance and pattern. These planar targets require high densities of point collection to be properly modeled in least squares matching algorithms [4]. Fig. 6.1 through Fig. 6.6 show the difference of point densities for a 'plus' target as well as a 'square' target. Speed affects the point spacing on each target; faster speeds result in a lower point density across the target while slower speeds result in a higher point density across the target. Fig. 6.7 shows the effect of distance away from the LiDAR sensor in detecting the painted targets.

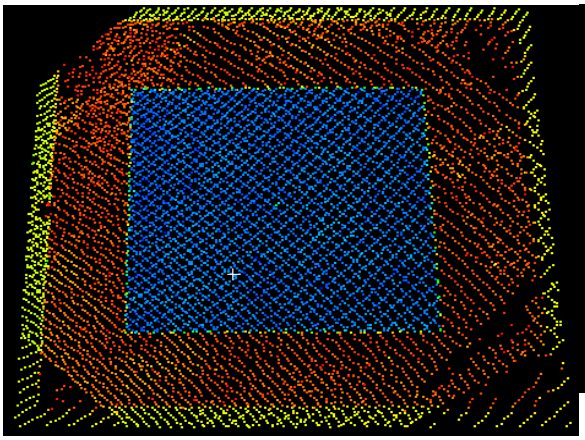

Fig. 6.1 Simulated mobile LiDAR data at 15 mph - square

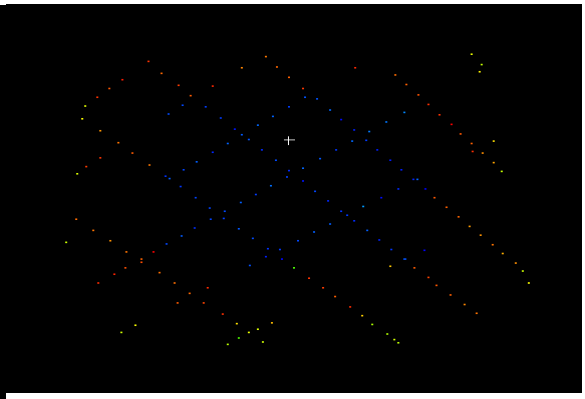

Fig. 6.2 Simulated mobile LiDAR data at 60 mph - square

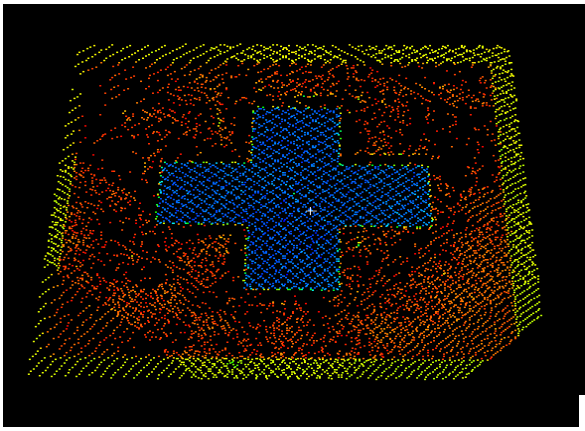

Fig. 6.3 Simulated mobile LiDAR data at 15 mph - plus

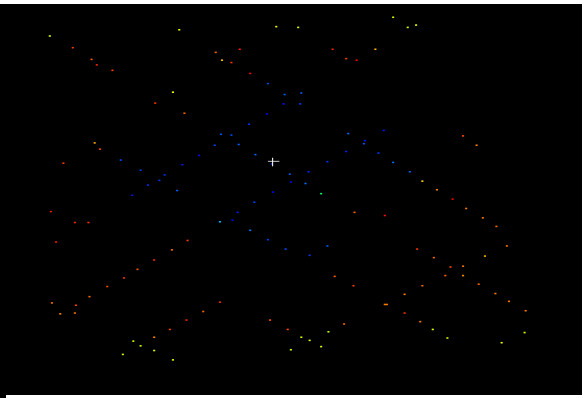

Fig. 6.4 Simulated mobile LiDAR data at 60 mph - plus

Fig. 6.5 Painted plus target on concrete road

Fig. 6.6 Painted square target on concrete road

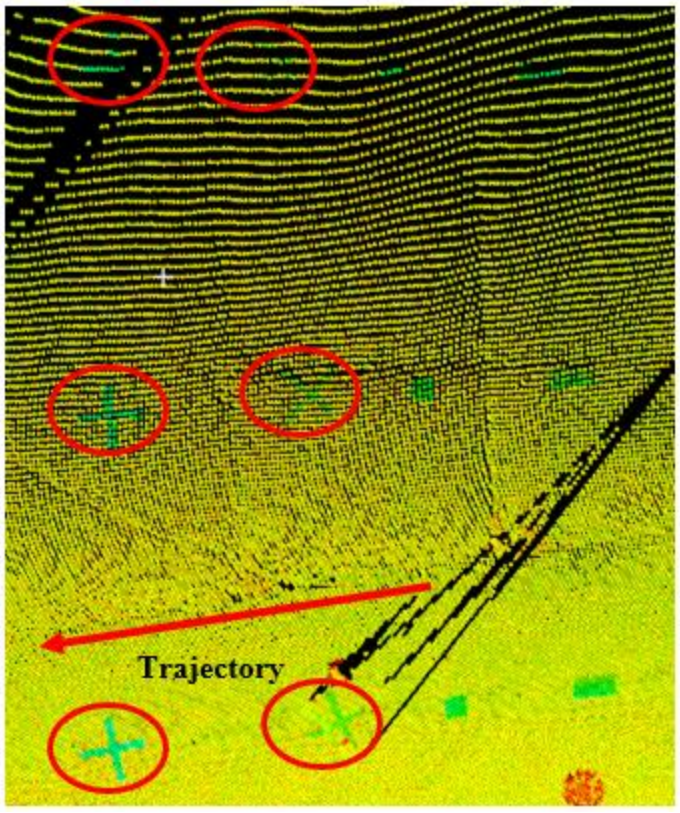

Fig. 6.7 Planar ‘plus’ targets shown at 5m incremental offsets

Fig. 6.8 shows the error ellipse of each measured point. Due to the angle of incidence, it extends longer in the scan direction and less in the trajectory direction on the planar targets. The larger the angle of incidence, the greater the horizontal error present in each measurement. As discussed in the literature review, there is no research to date that discusses the angle of incidence errors with regards to planar targets on the ground. Matching algorithms require good horizontal positioning to accurately determine the controlling center of the control target.

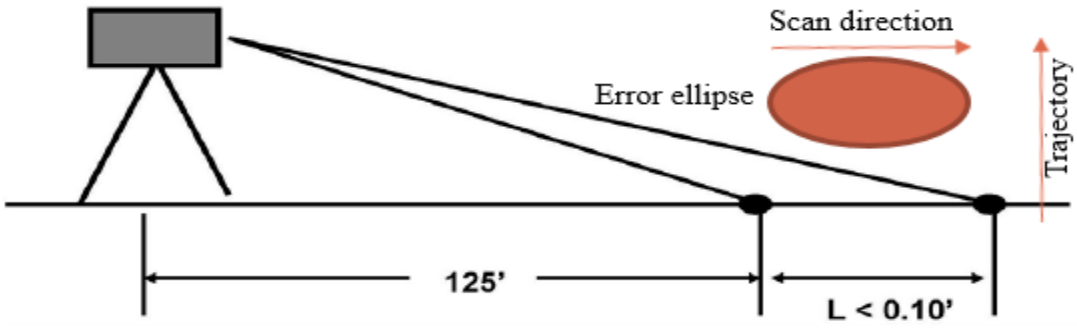

Fig. 6.8 Effect of angle of incidence on a planar target

6.2 Spherical Targets Real World Speed Performance

Johnson et al [14] detailed the use of spherical targets as control and validation points as well as the calibration process necessary to use such targets for control and validation for mobile mapping purposes. Spherical targets are commonly used to calibrate the MTLS systems, but not commonly used as control targets. Chapter 5 discussed the proper method of calibrating a sphere. Using the Trimble MX-8, testing on the spherical target was done at speeds of 15mph, 30mph, 45mph, and 60mph, and at approximate distances of 0m, 5m, 10m, 15m, and 20m away from the scanner sensor. Fig. 6.9 and Fig. 6.10 show a typical scanned scene by MTLS of each run. A Trimble MX-8 has two LiDAR scanning sensors. Each sensor (right and left) was tested separately in this experiment. A pass was made going north and south to scan the target at the given speed and distance away form the LiDAR sensor. Tables 6.1 through 6.4 provide the results from the experiment. The sensor column denotes which sensor was being tested and the N or S represents the direction that the data were collected. In a typical situation, both sensors are calibrated together through bore sighting and pre-calibration methods, but in

the instance that these data were taken, the calibration was not properly aligned, resulting in separate analysis of each sensor individually.

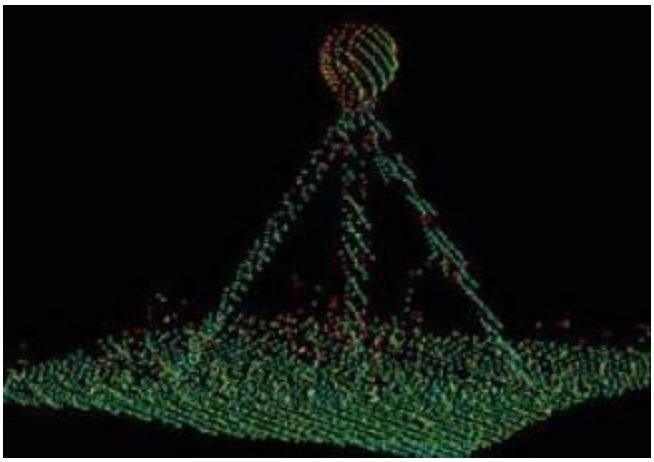

Fig. 6.9 Typical scan of a spherical target

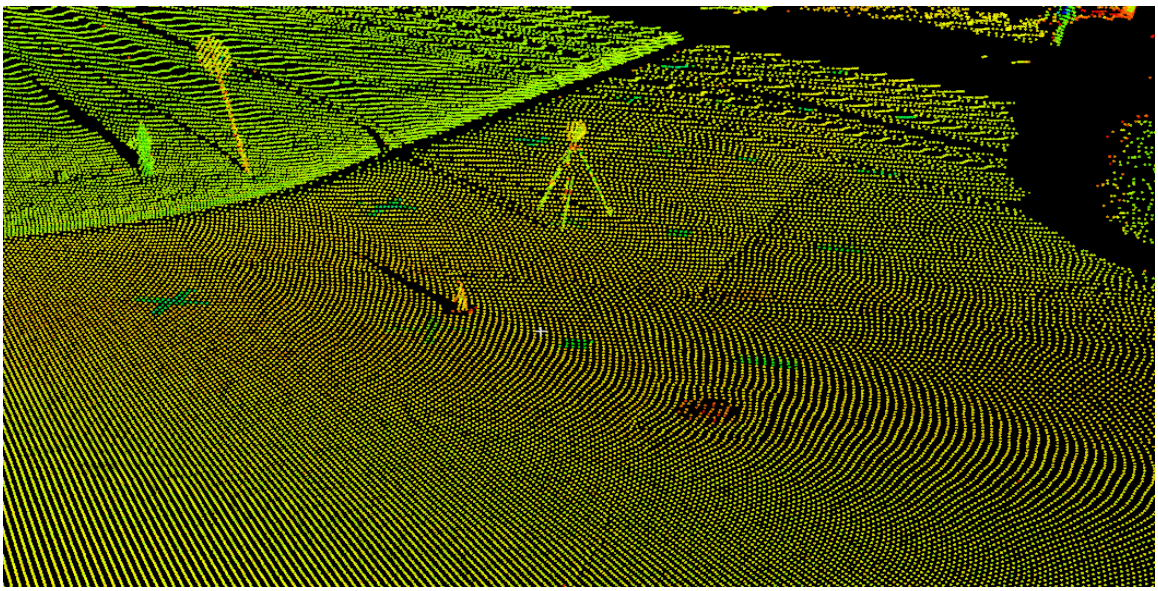

Fig. 6.10 Test run of 15mph with the spherical control target placed approximately 5m from the trajectory and position of the scanner.

As discussed earlier, the calibrated radius was 0.177m. As shown in Table 6.1 through Table 6.4, four different speeds were analyzed at different offset distances from the scanner sensor. The radius was calculated using Leica Cyclone software by taking the scanned data and fitting a sphere to the given data. The columns show calculated radius and the standard deviation for the calculation of the radius. An average radius was

calculated for each speed interval with its corresponding standard deviation. The average calculated radii ranged from 0.174m to 0.186m. The highest standard deviation was calculated at 0.004m. The closest calculated radius to the calibrated one was found at the 0m offsets with the furthest being at the 20m offset. As seen from this experiment, the higher the speed and the further away the control target is from the MTLS trajectory, the less accurate the results are for the calculation of the radii.

Table 6.1 Radii Calculation at 15mph

		0 meter offset		5 meter offset		10 meter offset		15 meter offset		20 meter offset	
Sensor	Speed (mph)	Calculated radius (m)	STD (m)	Calculated radius (m)	STD (m)	Calculated radius (m)	STD (m)	Calculated radius (m)	STD (m)	Calculated radius (m)	STD (m)
Left-S	15	0.177	0.002	0.180	0.002	0.177	0.002	0.180	0.002	0.185	0.002
Left-N	15	0.182	0.002	0.182	0.002	0.182	0.003	0.180	0.003	0.184	0.004
Right-S	15	0.179	0.002	0.183	0.003	0.181	0.003	0.179	0.003	0.182	0.004
Right-N	15	0.182	0.002	0.179	0.002	0.182	0.002	0.179	0.002	0.181	0.004
Average Radius		0.180		0.181		0.181		0.180		0.183	
STD		0.002		0.002		0.002		0.001		0.002	

Table 6.2 Radii Calculation at 30mph

		0 meter offset		5 meter offset		10 meter offset		15 meter offset		20 meter offset	
Sensor	Speed (mph)	Calculated radius (m)	STD (m)	Calculated radius (m)	STD (m)	Calculated radius (m)	STD (m)	Calculated radius (m)	STD (m)	Calculated radius (m)	STD (m)
Left-S	30	0.181	0.002	0.182	0.002	0.181	0.002	0.183	0.001	0.184	0.005
Left-N	30	0.182	0.003	0.183	0.002	0.179	0.003	0.181	0.002	0.184	0.002
Right-S	30	0.180	0.002	0.181	0.003	0.176	0.002	0.178	0.003	0.188	0.002
Right-N	30	0.183	0.003	0.177	0.003	0.183	0.002	0.181	0.002	0.181	0.002
Average Radius		0.182		0.181		0.180		0.181		0.184	
STD		0.001		0.003		0.003		0.002		0.003	

Table 6.3 Radii Calculations at 45mph

		0 meter offset		5 meter offset		10 meter offset		15 meter offset		20 meter offset	
Sensor	Speed (mph)	Calculated radius (m)	STD (m)	Calculated radius (m)	STD (m)	Calculated radius (m)	STD (m)	Calculated radius (m)	STD (m)	Calculated radius (m)	STD (m)
Left-S	45	0.178	0.002	0.180	0.002	0.180	0.003	nnot Calculate		0.191	0.002
Left-N	45	0.181	0.003	0.181	0.002	0.179	0.003	0.181	0.002	0.184	0.002
Right-S	45	0.180	0.003	0.182	0.001	0.181	0.003	0.178	0.002	0.184	0.002
Right-N	45	0.185	0.003	0.180	0.001	0.184	0.002	0.182	0.002	0.183	0.002
Average Radius		0.181		0.181		0.181		0.180		0.186	
STD		0.003		0.001		0.002		0.002		0.004	

Table 6.4 Radii Calculations at 60mph

		0 meter offset		5 meter offset		10 meter offset		15 meter offset		20 meter offset	
Sensor	Speed (mph)	Calculated radius (m)	STD (m)	Calculated radius (m)	STD (m)	Calculated radius (m)	STD (m)	Calculated radius (m)	STD (m)	Calculated radius (m)	STD (m)
Left-S	60	0.180	0.002	0.180	0.002	0.180	0.002	nnot Calculate		0.174	0.001
Left-N	60	0.181	0.002	0.183	0.002	0.180	0.003	0.177	0.004	0.171	0.002
Right-S	60	0.178	0.002	0.182	0.003	0.182	0.003	0.183	0.001	nnot Calculate	
Right-N	60	0.181	0.003	0.178	0.002	0.184	0.002	0.182	0.002	0.178	0.002
Average Radius		0.180		0.181		0.182		0.181		0.174	
STD		0.001		0.002		0.002		0.003		0.004	

6.3 Controlled Simulated Tests on Sphere

Due to cost, time constraints, and poor calibration of the two LiDAR sensors of the Trimble MX-8 from section 6.2, analysis could not be performed to determine the benefit of registering both left and right sensors of the Trimble MX-8 to test against known positions. Based on point spacing obtained from the sample Trimble MX-8 data, simulations using the Leica Scanstation II were run to test the performance ability of calculating the controlling coordinates of the control position itself.

In a lab, a control network was established by using a TOPCON total station. Two scan stations were established to simulate a Trimble MX-8 with two LiDAR sensors. As shown in Fig. 6.11, the Trimble MX-8 has two scanning heads that allow for maximum coverage of objects in the scanning scene. Figure 6.12 shows the planimetric configuration of the control positions that were established in the room with their respective coordinates. From the actual data, sample data spacing was extracted for various speeds to simulate an average 10m offset from the scan sensor. Although the scanner was only approximately 3.45m away from the sphere, the point spacings were adjusted to simulate various speeds for a 10m offset. Four simulated speeds again were tested with certain horizontal and vertical spacings as follows:

- 15 mph Horizontal = 0.043m Vertical = 0.015m
- 30 mph Horizontal = 0.070m Vertical = 0.015m
- 45 mph Horizontal = 0.102m Vertical = 0.015m
- 60 mph Horizontal = 0.140m Vertical = 0.015m

The sphere target was placed on a tripod over the control point five separate times for each of the five simulated speeds. So in total, 25 individual setups of the sphere target were made with differing heights of the target to simulate real world scenarios. Both scanners then made an independent scan of the sphere target. With the scan of the target,

the center of the sphere was determined. An analysis of the calculation of the center of the target was made to assess the ability to resolve the control point below the target given a calibrated height of the sphere and a measured height to the mounting bracket of the sphere target. Simulated results for speeds of 15mph, 30mph, 45mph, and 60mph at a simulated distance of 10m are shown on the following pages (see Figs. 6.13, 6.15, 6.17, 6.19). Because the testing performed was done with a small sample, the data were perturbed with a standard deviation of 0.002m to simulate random noise. Figures 6.14, 6.16, 6.18, 6.20 show the resultant variation of the measured control location with respect to the known position. From the simulated results, each control position was within 0.002m from the calculated positions in X, Y, and Z.

Left Scan Sensor

Right Scan Sensor

Fig. 6.11 Trimble MX-8 Mobile mapping Unit

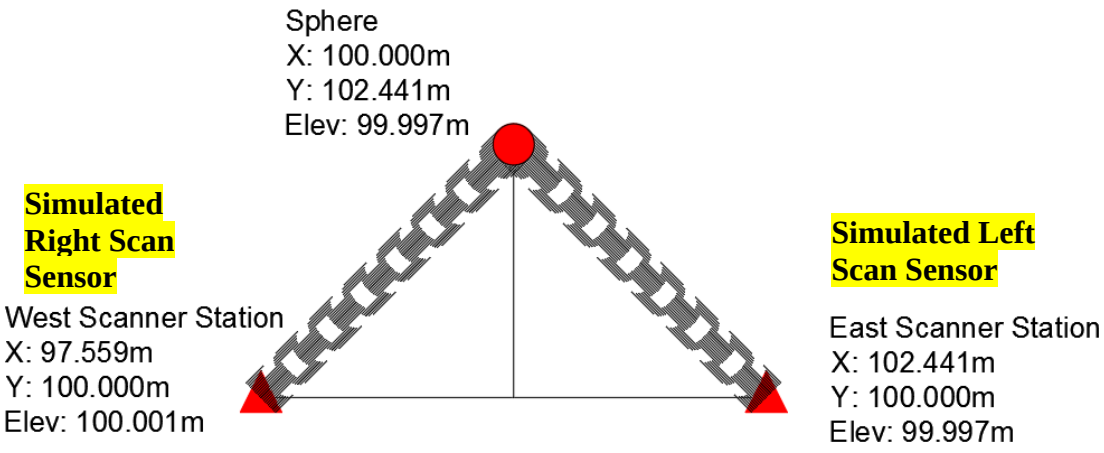

Fig. 6.12 Simulated Trimble MX-8 data

10m offset, 15 mph simulation.

Horizontal spacing = 0.060m, Vertical spacing = 0.018m

LEFT sensor Only

	15 mph - HT = 1.427m, Offset = 0.194m				
Sphere 1	x	y	Calc Z	Control Z	radius
	100.001	102.441	101.619	99.998	0.178
	15 mph - HT = 1.387m, Offset = 0.194m				
Sphere 2	x	y	Calc Z	Control Z	radius
	100.000	102.441	101.578	99.997	0.178
	15 mph - HT = 1.437m, Offset = 0.194m				
Sphere 3	x	y	Calc Z	Control Z	radius
	100.001	102.440	101.629	99.998	0.178
	15 mph - HT = 1.345m, Offset = 0.194m				
Sphere 4	x	y	Calc Z	Control Z	radius
	100.001	102.441	101.536	99.997	0.177
	15 mph - HT = 1.356m, Offset = 0.194m				
Sphere 5	x	y	Calc Z	Control Z	radius
	100.001	102.440	101.547	99.997	0.178
Average	100.001	102.441		99.997	0.178
STD	0.0004	0.0005		0.0005	0.0004

Right sensor Only

	5m - HT = 1.427m, Offset = 0.194m				
Sphere 1	x	y	Calc Z	Control Z	radius
	99.999	102.440	101.618	99.997	0.177
	5m - HT = 1.387m, Offset = 0.194m				
Sphere 2	x	y	Calc Z	Control Z	radius
	99.998	102.440	101.578	99.997	0.177
	5m - HT = 1.437m, Offset = 0.194m				
Sphere 3	x	y	Calc Z	Control Z	radius
	99.999	102.440	101.629	99.998	0.177
	5m - HT = 1.345m, Offset = 0.194m				
Sphere 4	x	y	Calc Z	Control Z	radius
	99.999	102.442	101.535	99.996	0.177
	5m - HT = 1.356m, Offset = 0.194m				
Sphere 5	x	y	Calc Z	Control Z	radius
	100.000	102.440	101.547	99.997	0.176
Average	99.999	102.440		99.997	0.177
STD	0.0007	0.0009		0.0007	0.0004

Both Sensors

	5m - HT = 1.427m, Offset = 0.194m				
Sphere 1	x	y	Calc Z	Control Z	radius
	100.000	102.440	101.619	99.998	0.176
	5m - HT = 1.387m, Offset = 0.194m				
Sphere 2	x	y	Calc Z	Control Z	radius
	99.999	102.439	101.578	99.997	0.176
	5m - HT = 1.437m, Offset = 0.194m				
Sphere 3	x	y	Calc Z	Control Z	radius
	99.999	102.439	101.629	99.998	0.176
	5m - HT = 1.345m, Offset = 0.194m				
Sphere 4	x	y	Calc Z	Control Z	radius
	100.000	102.441	101.536	99.997	0.176
	5m - HT = 1.356m, Offset = 0.194m				
Sphere 5	x	y	Calc Z	Control Z	radius
	100.000	102.440	101.547	99.997	0.176
Average	100.000	102.440		99.997	0.176
STD	0.0005	0.0008		0.0005	0.0000

Sphere
X: 100.000m
Y: 102.441m
Elev: 99.997m

Fig. 6.13 Simulation results of left, right, and both sensors at 15mph

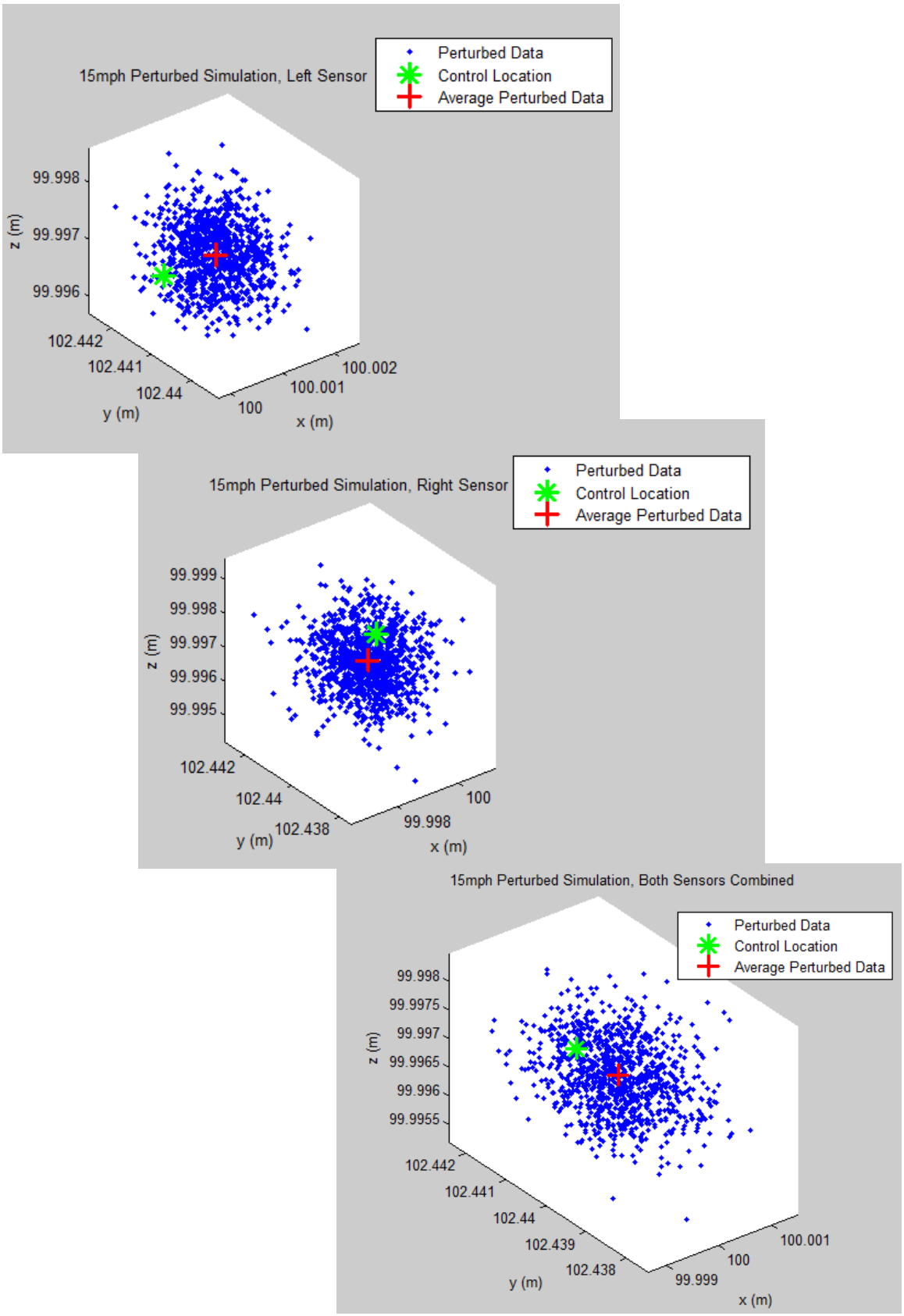

Fig. 6.14 Simulation of perturbed data results of left, right, and both sensors at 15mph

10m offset, 30 mph simulation

Horizontal spacing = 0.090m, Vertical spacing = 0.018m

LEFT sensor Only

	30mph - HT = 1.449m, Offset = 0.194m				
Sphere 1	x	y	Calc Z	Control Z	radius
	100.002	102.441	101.641	99.998	0.178
	30 mph - HT = 1.319m, Offset = 0.194m				
Sphere 2	x	y	Calc Z	Control Z	radius
	100.001	102.440	99.996	99.996	0.177
	30 mph - HT = 1.394m, Offset = 0.194m				
Sphere 3	x	y	Calc Z	Control Z	radius
	100.000	102.440	101.586	99.998	0.177
	30 mph - HT = 1.524m, Offset = 0.194m				
Sphere 4	x	y	Calc Z	Control Z	radius
	100.003	102.443	101.715	99.997	0.177
	30 mph - HT = 1.447m, Offset = 0.194m				
Sphere 5	x	y	Calc Z	Control Z	radius
	100.003	102.443	101.639	99.998	0.178
Average	100.002	102.441		99.997	0.177
STD	0.0013	0.0015		0.0009	0.0005

Right sensor Only

	30mph - HT = 1.449m, Offset = 0.194m				
Sphere 1	x	y	Calc Z	Control Z	radius
	99.999	102.441	101.639	99.996	0.177
	30 mph - HT = 1.319m, Offset = 0.194m				
Sphere 2	x	y	Calc Z	Control Z	radius
	100.000	102.440	101.510	99.997	0.176
	30 mph - HT = 1.394m, Offset = 0.194m				
Sphere 3	x	y	Calc Z	Control Z	radius
	99.999	102.440	101.584	99.996	0.176
	30 mph - HT = 1.524m, Offset = 0.194m				
Sphere 4	x	y	Calc Z	Control Z	radius
	100.003	102.442	101.713	99.995	0.176
	30 mph - HT = 1.447m, Offset = 0.194m				
Sphere 5	x	y	Calc Z	Control Z	radius
	100.000	102.443	101.639	99.998	0.176
Average	100.000	102.441		99.996	0.176
STD	0.0016	0.0013		0.0011	0.0004

Both Sensors

	30mph - HT = 1.449m, Offset = 0.194m				
Sphere 1	x	y	Calc Z	Control Z	radius
	100.000	102.440	101.640	99.997	0.176
	30 mph - HT = 1.319m, Offset = 0.194m				
Sphere 2	x	y	Calc Z	Control Z	radius
	99.999	102.440	101.510	99.997	0.176
	30 mph - HT = 1.394m, Offset = 0.194m				
Sphere 3	x	y	Calc Z	Control Z	radius
	99.999	102.440	101.585	99.997	0.176
	30 mph - HT = 1.524m, Offset = 0.194m				
Sphere 4	x	y	Calc Z	Control Z	radius
	100.002	102.442	101.714	99.996	0.177
	30 mph - HT = 1.447m, Offset = 0.194m				
Sphere 5	x	y	Calc Z	Control Z	radius
	100.001	102.442	101.639	99.998	0.176
Average	100.000	102.441		99.997	0.176
STD	0.0013	0.0011		0.0007	0.0004

Sphere
X: 100.000m
Y: 102.441m
Elev: 99.997m

Fig. 6.15 Simulation results of left, right, and both sensors at 30mph

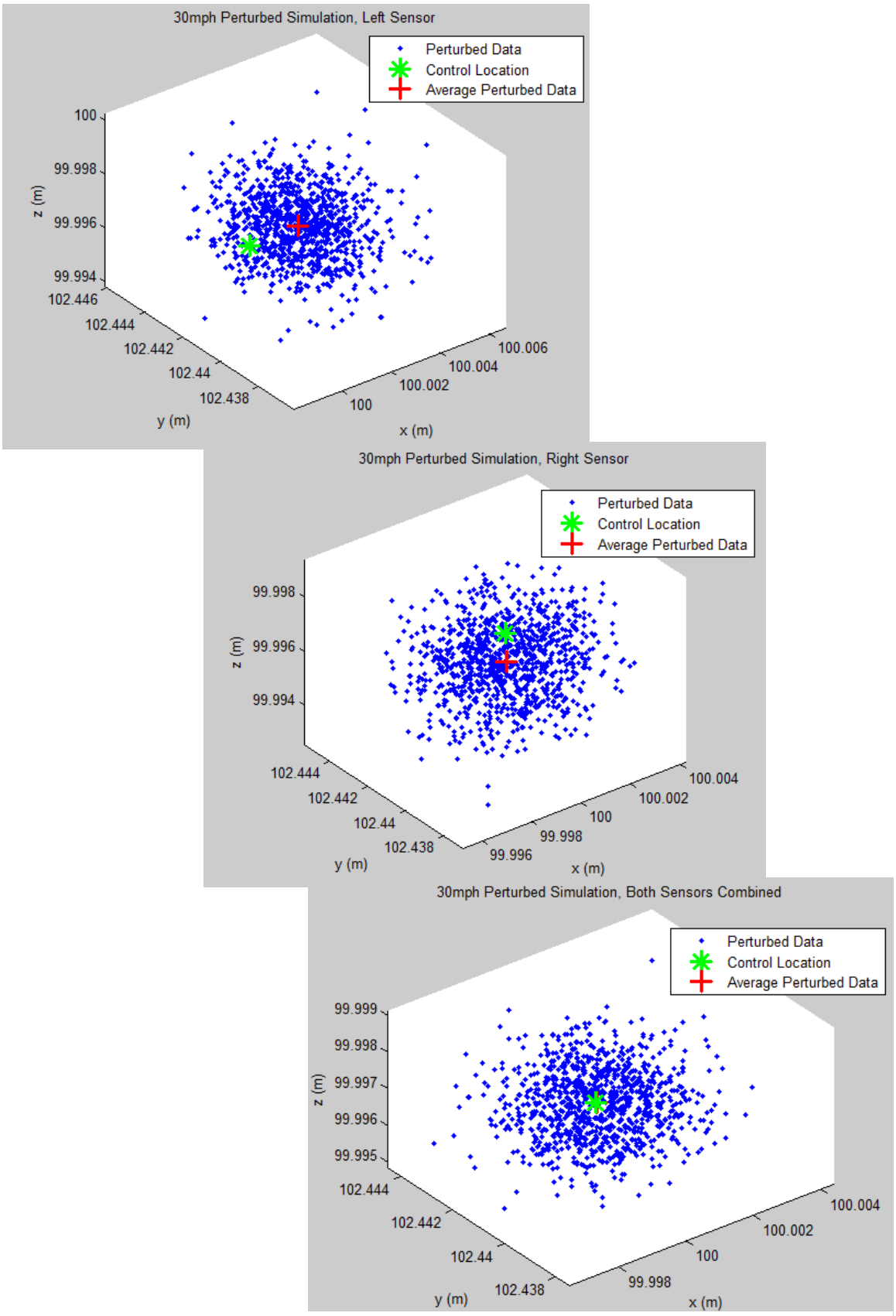

Fig. 6.16 Simulation of perturbed data results of left, right, and both sensors at 30mph

10m offset, 45 mph simulation

Horizontal spacing = 0.130m, Vertical spacing = 0.018m

LEFT sensor Only

	45mph - HT = 1.617m, Offset = 0.194m				
Sphere 1	x	y	Calc Z	Control Z	radius
	100.004	102.441	101.808	99.997	0.177
	45 mph - HT = 1.318m, Offset = 0.194m				
Sphere 2	x	y	Calc Z	Control Z	radius
	100.004	102.443	101.508	99.997	0.178
	45 mph - HT = 1.172m, Offset = 0.194m				
Sphere 3	x	y	Calc Z	Control Z	radius
	99.999	102.439	101.364	99.998	0.176
	45 mph - HT = 1.128m, Offset = 0.194m				
Sphere 4	x	y	Calc Z	Control Z	radius
	100.004	102.441	101.322	100.000	0.178
	45 mph - HT = 1.320m, Offset = 0.194m				
Sphere 5	x	y	Calc Z	Control Z	radius
	100.003	102.441	101.511	99.997	0.178
Average	100.003	102.441		99.998	0.177
STD	0.0022	0.0014		0.0013	0.0009

Right sensor Only

	45mph - HT = 1.617m, Offset = 0.194m				
Sphere 1	x	y	Calc Z	Control Z	radius
	100.001	102.442	101.808	99.997	0.177
	45 mph - HT = 1.318m, Offset = 0.194m				
Sphere 2	x	y	Calc Z	Control Z	radius
	100.001	102.442	101.508	99.996	0.177
	45 mph - HT = 1.172m, Offset = 0.194m				
Sphere 3	x	y	Calc Z	Control Z	radius
	99.999	102.439	101.364	99.998	0.176
	45 mph - HT = 1.128m, Offset = 0.194m				
Sphere 4	x	y	Calc Z	Control Z	radius
	99.998	102.441	101.320	99.998	0.178
	45 mph - HT = 1.320m, Offset = 0.194m				
Sphere 5	x	y	Calc Z	Control Z	radius
	99.999	102.440	101.510	99.996	0.177
Average	100.000	102.441		99.997	0.177
STD	0.0013	0.0013		0.0010	0.0007

Both Sensors

	45mph - HT = 1.617m, Offset = 0.194m				
Sphere 1	x	y	Calc Z	Control Z	radius
	100.002	102.441	101.808	99.997	0.176
	45 mph - HT = 1.318m, Offset = 0.194m				
Sphere 2	x	y	Calc Z	Control Z	radius
	100.002	102.442	101.508	99.996	0.176
	45 mph - HT = 1.172m, Offset = 0.194m				
Sphere 3	x	y	Calc Z	Control Z	radius
	100.000	102.440	101.364	99.998	0.176
	45 mph - HT = 1.128m, Offset = 0.194m				
Sphere 4	x	y	Calc Z	Control Z	radius
	100.001	102.440	101.321	99.999	0.176
	45 mph - HT = 1.320m, Offset = 0.194m				
Sphere 5	x	y	Calc Z	Control Z	radius
	100.000	102.439	101.510	99.996	0.176
Average	100.001	102.440		99.997	0.176
STD	0.0010	0.0011		0.0013	0.0000

Sphere
X: 100.000m
Y: 102.441m
Elev: 99.997m

Fig. 6.17 Simulation results of left, right, and both sensors at 45mph

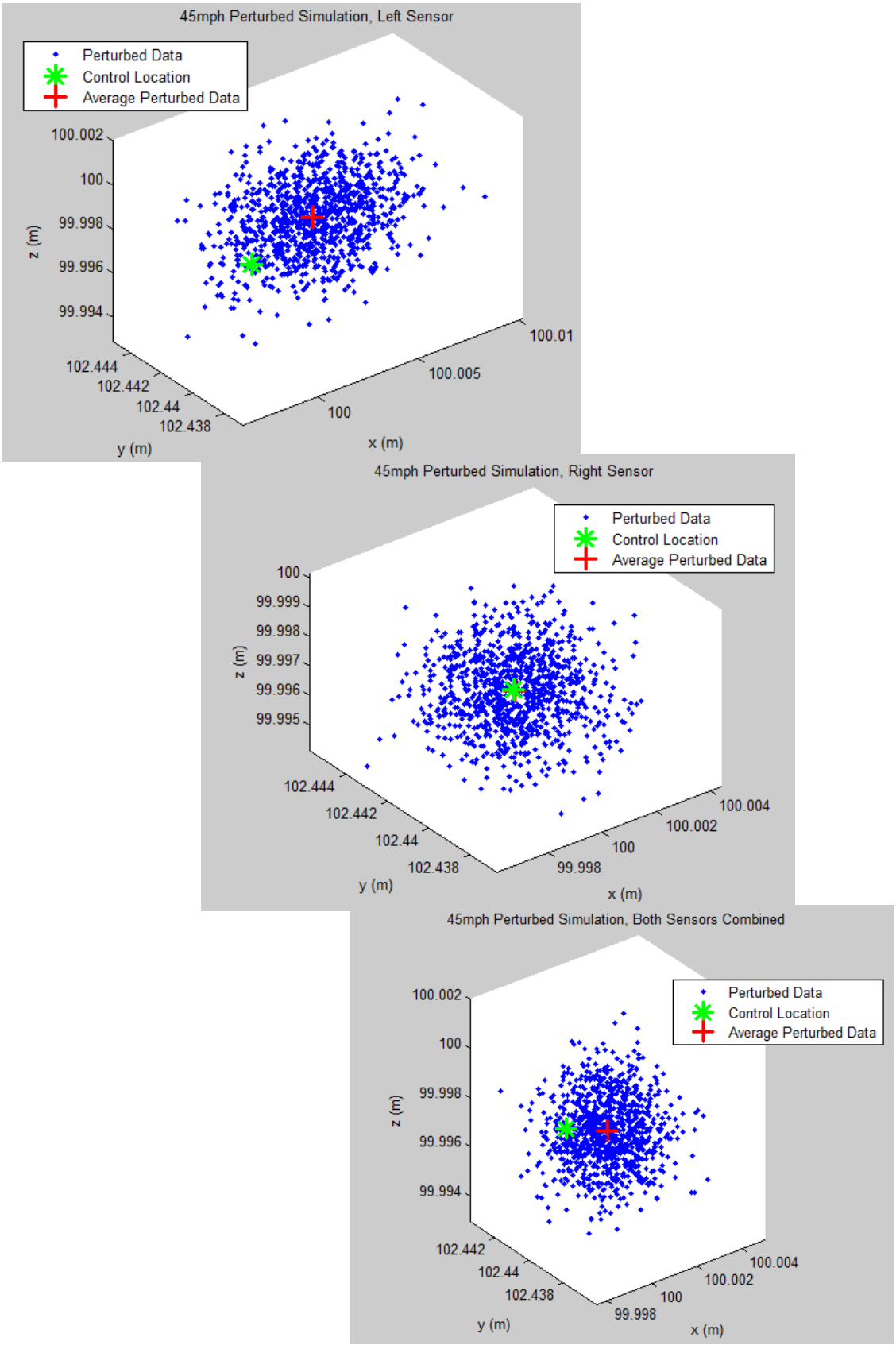

Fig. 6.18 Simulation of perturbed data results of Left, Right, and Both sensors at 45mph

10m offset, 60 mph simulation

Horizontal spacing = 0.160m, Vertical spacing = 0.018m

LEFT sensor Only

	60mph - HT = 1.454m, Offset = 0.194m				
Sphere 1	x	y		z	radius
	100.004	102.442	101.647	99.999	0.178
	60 mph - HT = 1.353m, Offset = 0.194m				
Sphere 2	x	y		z	radius
	100.003	102.442	101.544	99.997	0.177
	60 mph - HT = 1.738m, Offset = 0.194m				
Sphere 3	x	y		z	radius
	100.000	102.442	101.929	99.997	0.177
	60 mph - HT = 1.542m, Offset = 0.194m				
Sphere 4	x	y		z	radius
	100.004	102.443	101.735	99.999	0.178
	60 mph - HT = 1.427m, Offset = 0.194m				
Sphere 5	x	y		z	radius
	100.002	102.446	101.620	99.999	0.178
Average	100.003	102.443		99.998	0.178
STD	0.0017	0.0017		0.0011	0.0005

Right sensor Only

	60mph - HT = 1.454m, Offset = 0.194m				
Sphere 1	x	y		z	radius
	99.998	102.441	101.646	99.998	0.178
	60 mph - HT = 1.353m, Offset = 0.194m				
Sphere 2	x	y		z	radius
	100.004	102.440	101.543	99.996	0.174
	60 mph - HT = 1.738m, Offset = 0.194m				
Sphere 3	x	y		z	radius
	100.000	102.442	101.929	99.997	0.177
	60 mph - HT = 1.542m, Offset = 0.194m				
Sphere 4	x	y		z	radius
	100.000	102.442	101.735	99.999	0.176
	60 mph - HT = 1.427m, Offset = 0.194m				
Sphere 5	x	y		z	radius
	N/A	N/A	101.620	N/A	N/A
Average	100.001	102.441		99.998	0.176
STD	0.0025	0.0010		0.0013	0.0017

Both Sensors

	60mph - HT = 1.454m, Offset = 0.194m				
Sphere 1	x	y		z	radius
	100.001	102.440	101.647	99.999	0.176
	60 mph - HT = 1.353m, Offset = 0.194m				
Sphere 2	x	y		z	radius
	100.001	102.441	101.543	99.996	0.176
	60 mph - HT = 1.738m, Offset = 0.194m				
Sphere 3	x	y		z	radius
	100.002	102.441	101.930	99.998	0.176
	60 mph - HT = 1.542m, Offset = 0.194m				
Sphere 4	x	y		z	radius
	100.001	102.441	101.735	99.999	0.176
	60 mph - HT = 1.427m, Offset = 0.194m				
Sphere 5	x	y		z	radius
	100.001	102.445	101.620	99.999	0.177
Average	100.001	102.442		99.998	0.176
STD	0.0004	0.0019		0.0013	0.0004

Sphere
X: 100.000m
Y: 102.441m
Elev: 99.997m

Fig. 6.19 Simulation results of left, right, and both sensors at 60mph

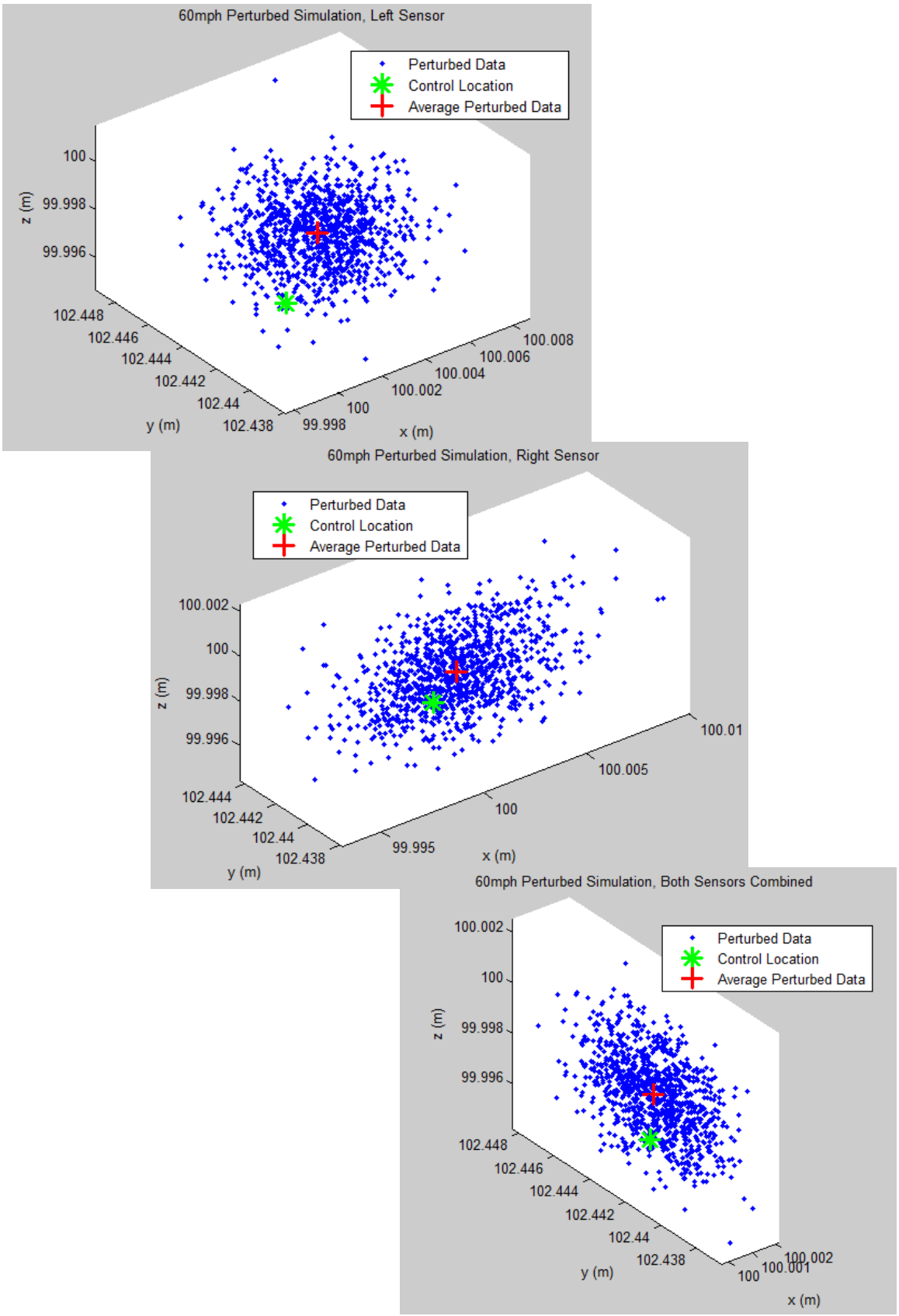

Fig. 6.20 Simulation of perturbed data results of left, right, and both sensors at 60mph

7. DISCUSSION

7.1 3D Targets

To minimize the errors associated with angle of incidence, this research confirms the hypothesis that 3D control and validation targets – spheres and cubes – should be utilized in MTLS projects instead of traditional 2D targets painted on ground surfaces. Simulated data on the sphere and cube, as well as real world tests on the sphere, support the hypothesis that angle of incidence does not affect the calculation of the radii of the sphere, nor the 3D controlling position of the sphere or cube.

In simulated cases, the sphere had a 3D positional error of 0.0014m, 0.0014m, 0.000m, and 0.003m at speeds of 60mph, 45mph, 30mph, and 15mph at a 10m offset distance, respectively, while combining both left and right LiDAR sensors. Simulated tests are somewhat biased as there is no account for orientation errors from the INS, which will eventually propagate into the LiDAR sensor measurements. However, this research provides insight that the sphere is immune from the effects of angle of incidence. The results are not completely conclusive as simulated tests at varying offset distances from the scanner were not performed.

With results from simulations supporting that the angle of incidence does not affect the measurements obtained for controlling parameters of the sphere, real world tests using the Trimble MX-8 on the sphere were performed. After collection of the data, it was found that the two LiDAR sensors were not calibrated together. Each sensor was on its own coordinate system, producing different calculated control point position results. The calibrated radius of the sphere was 0.177m. Each test was run at real world speeds of 15mph, 30mph, 45mph, and 60mph, while measuring at 0m, 5m, 10m, 15m, and 20m offsets. With the misalignment of the two LiDAR sensors, calculation of the radii was sufficient to verify the application of the sphere target. The range of radii calculated from all runs was 0.171m to 0.196m, a difference of 0.025m. Average values had a range of 0.174m to 0.186m, a difference if 0.012m. Results likely would have been better if the radius had been calculated using both left and right sensors. The results are

biased in the direction of the scanner, since the calculation of the radius covered only one-half the sphere, with no overlapping redundant data from the other sensor.

The test on the cube was performed only with simulated results. This test was done to support the fact that angle of incidence does not affect the ability to compute the controlling position of the target. After a least squares adjustment of the data along three of the cubes' surfaces, the residuals showed that the position of the positive and negative residuals were random and not biased. Larger angles of incidence on the target normally would have correlated to larger positional errors. However, since the computation was to identify a surface, any positional measurement error on the surface was negated, each measurement still fell on the surface. Results also showed that the magnitude of the residuals was also random, showing no bias at locations of greater angle of incidence.

Speed is a variable to be considered with MTLS. The faster the vehicle, the lower the point density on the target. Conversely, the slower the vehicle, the higher the point density on the target. Typical targets [4] require higher point densities to allow for the matching algorithms to perform well. By testing varying speeds through simulation and real world tests, results show that regardless of lower densities measured on the targets, controlling radii and centers of the sphere and controlling locations of the cube can still be identified within a centimeter. This will eliminate the need to adjust speed where measurement of targets is necessary during MTLS projects. This will help to achieve safer data collection for the user and the public, as well as assist in the pre-planning process by determining target location.

7.2 New Target

As past research shows, intensity is mainly used for object identification, not for positional data. As described in chapter 3, this research was a proof of concept to test the performance of using intensity as a positional tool, instead of only an identification tool. Results show that the new target concept using raw intensity measurements can be an effective alternative to traditional LiDAR control and validation targets. Results prove that low density scan data along with intensity is effective at constraining 3D point cloud data to sub centimeter accuracies. This use of intensity on a planar target will improve

MTLS accuracy and efficiency as well as terrestrial scanning accuracy by eliminating the need for high point densities on the target.

7.3 Spacing of Control and Validation Targets with MTLS

As research has shown, there is no consensus on what type of target and how often a target is necessary to help constrain and validate LiDAR data. Non-ideal research scenarios have also not been explored. MTLS users can now perform their own tests to determine the actual performance of their MTLS system. Simulating GNSS outages addresses the need to take into account the reliance of the MTLS on the IMU. IMUs measure based on time, 100 Hz to 2000Hz a second, making it time-dependent and not distance-dependent. This research assists in the preplanning process of MTLS projects. Knowing the physical limitations of the IMU, and when to expect GNSS outages, the user will be able to place control and validation targets accordingly by time, and not by a fixed distance along the path of travel nor perpendicular to the path of travel. Suggestions nor guidelines for target placement based on distance should not be considered.

7.4 Recommendations

7.4.1 3D Targets Future Research

Simulated future tests of the 3D targets should be done with terrestrial scanners set up at the actual distances with varying measurement densities so as to not alter the original data, mimicking the various speeds of the vehicle. However, simulated tests should only be done to provide direction and guidance for future tests that can be performed in real MTLS situations. This test needs to be completed again with calibrated sensors on the Trimble MX-8 along with other manufacturers to improve testing procedures and to verify reported results herein. With the results provided, it can be inferred that positional results will correlate the same, making the sphere a recommended choice as a control and validation target.

Further tests on the cube should be performed to completely validate the findings in this research. A carefully constructed cube needs to be constructed, with three faces perfectly perpendicular to one another, thus allowing for the correct calculation of the

control location on the cube, the intersection of the three planes. Given the calculated controlling location, an accurate offset can be calculated as to its position relative to the known position on the ground.

An actual test track with varying manufacturers of MTLS should be considered a further step in the validation of the sphere and cube as recommended targets. Different manufactures have variations of single or multiple scanners sensors with which similar testing will be required as done with the sphere in this research.

7.4.2 **New Target Future Research**

This concept is in its initial stages of testing. Appendix B contains further research addressing different distances and angles of incidence. Future research is needed in several areas before implementation of this target can proceed as outlined:

1. Address whether there is a need for radiometric calibration (this research shows sub centimeter without radiometric corrections)
2. Address better printing techniques to allow for a more uniform radial gradient
3. Although research shows angle of incidence does affect the intensity return, address whether it's a large enough effect to require the need for correction
4. Address varied distances
5. After simulated testing, address verification with an MTLS for real world conditions

7.4.3 **Target Spacing Future Research**

Future research should include performing this test on multiple MTLS manufacturers. This research created simulated GNSS outages by negating certain information used in the SBET calculations. Tests should be conducted with complete GNSS outages by not having the GNSS running at the time of the data collection. A dense network of control monuments should be placed along a path to act as validation points in the comparisons between the SBETs that are created. This step will allow validation as to the distance that can be travelled before losing desired accuracies.

APPENDIX

CHAPTER 4 IMU TESTING GRAPHS – NON-IDEAL SITUATIONS

Trial #1.

Inconsistent data were gathered, therefore it was not used in this discussion.

Trial #2 – Time stamp 406300s – 406360s

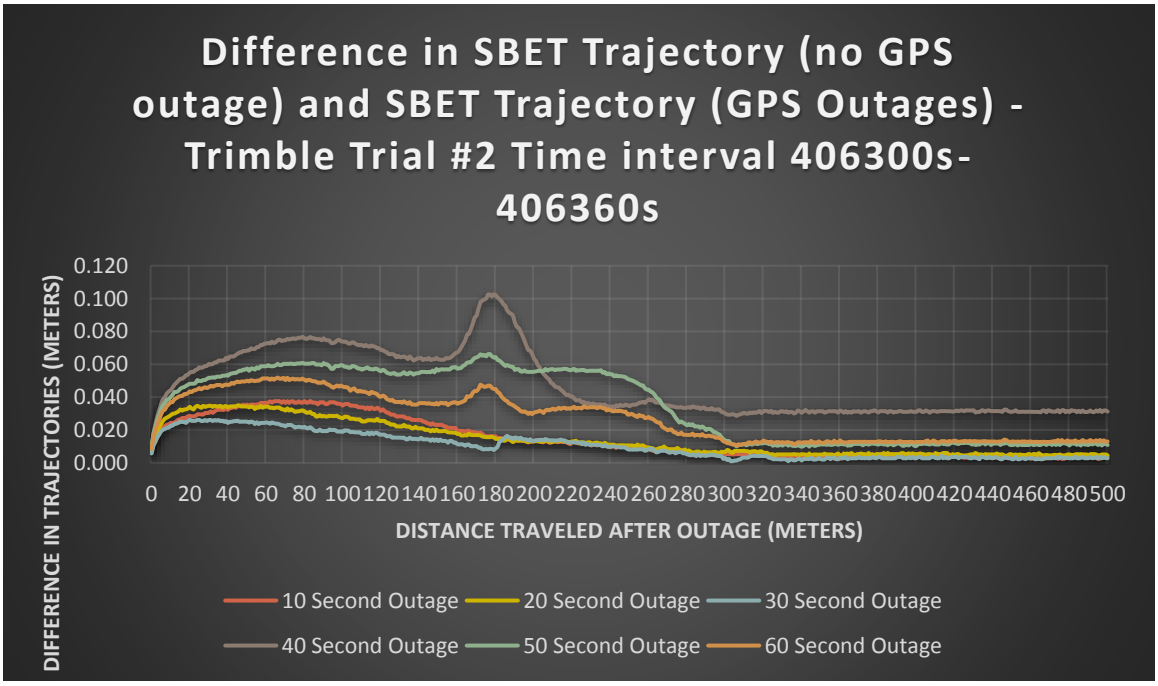

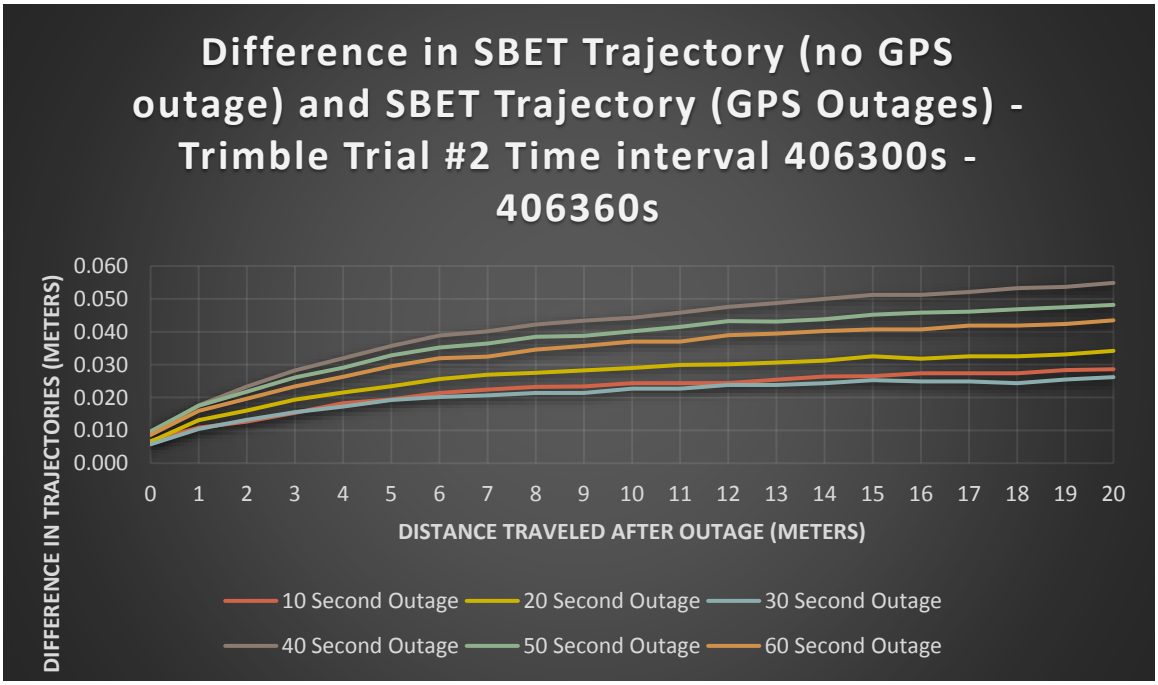

Trial #3 – Time stamp 407450s – 407510s

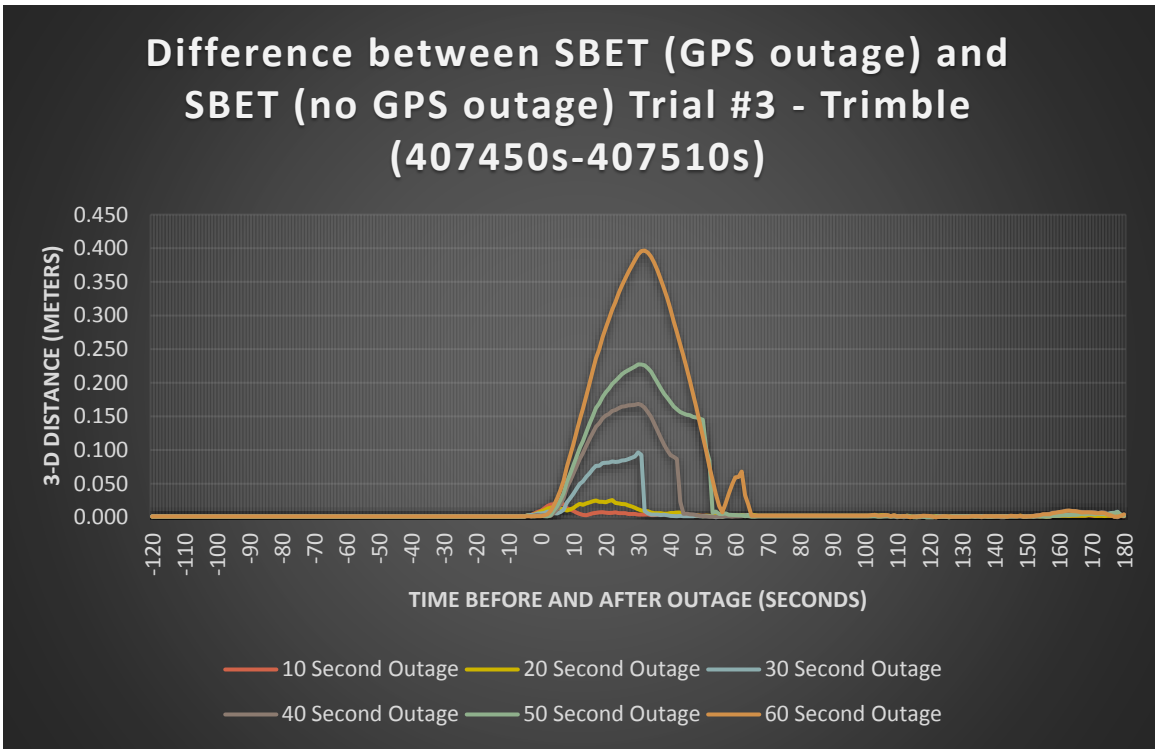

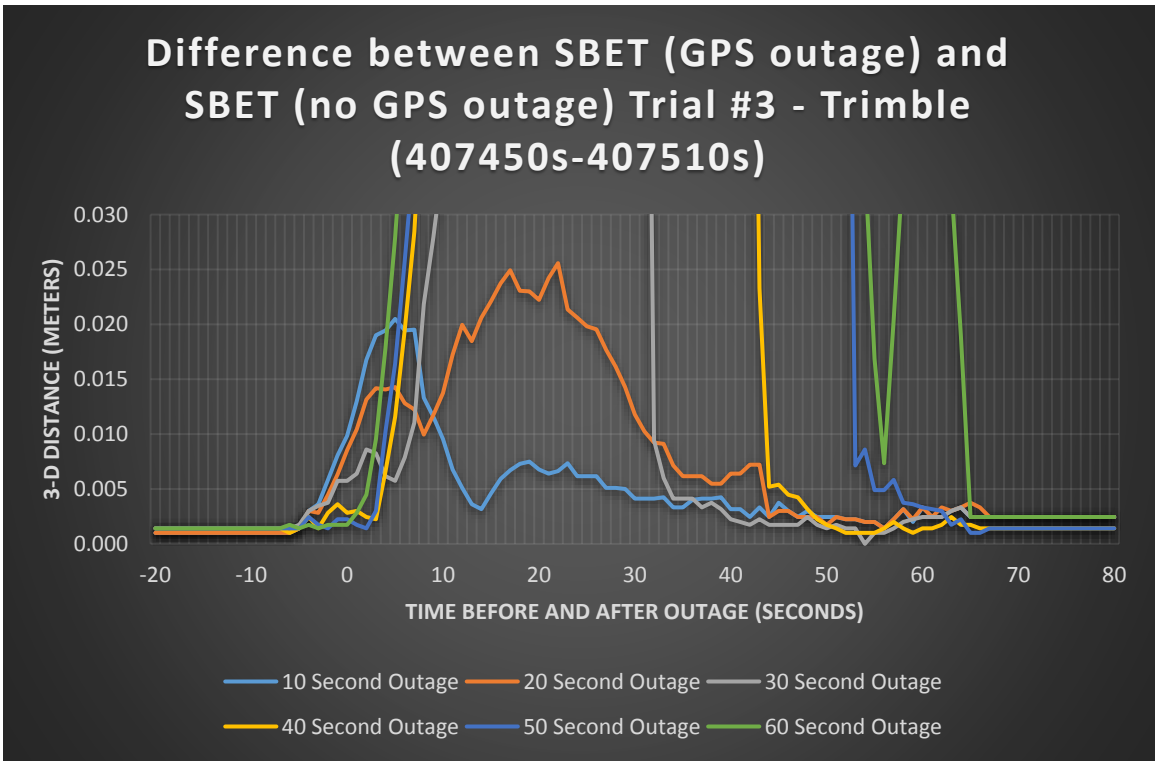

Trial #4– Time stamp 407600s – 407660s

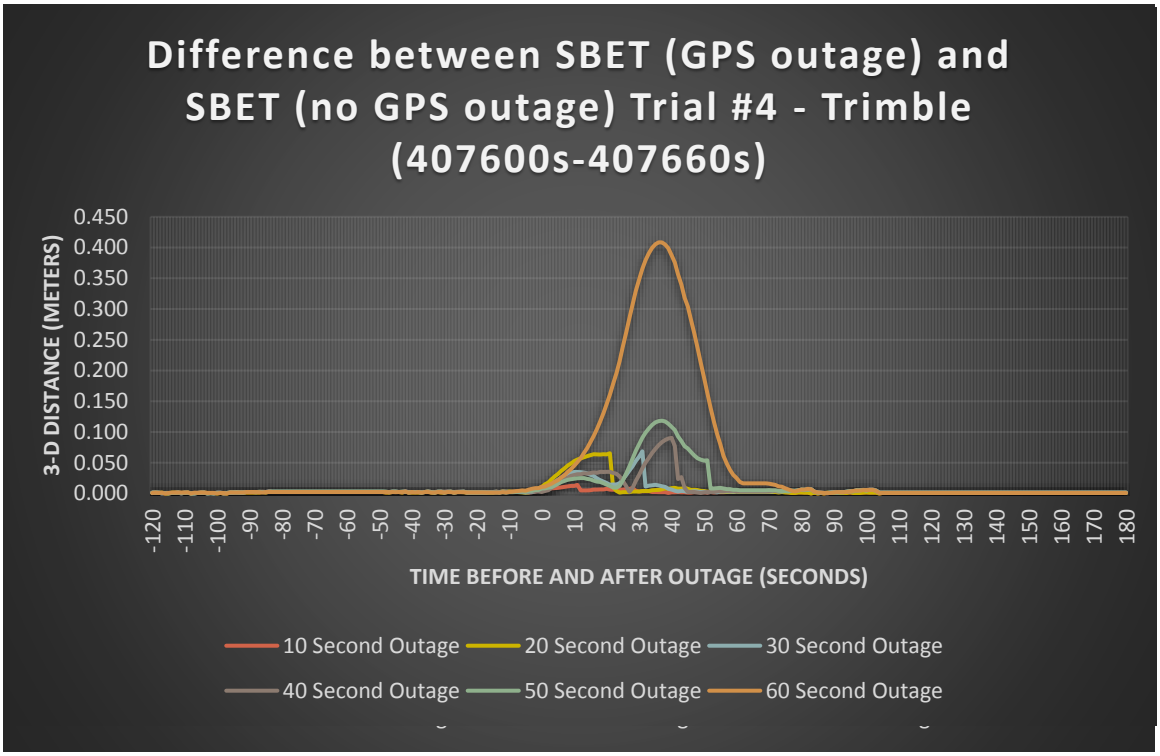

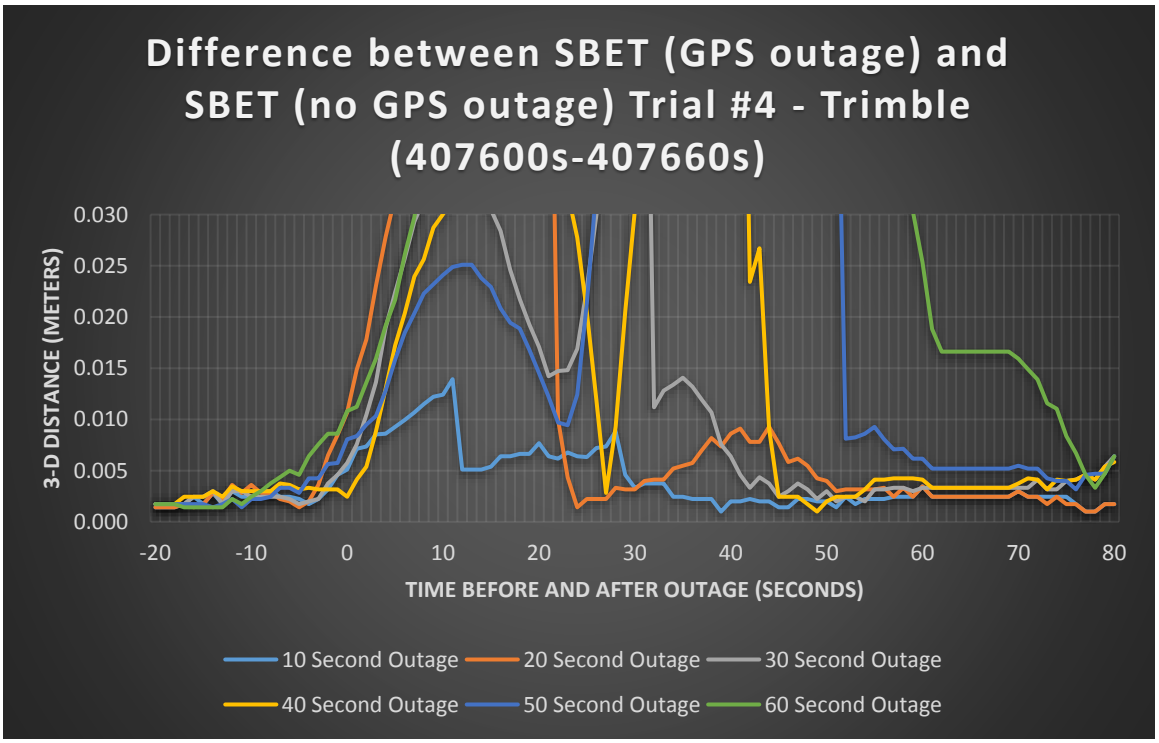

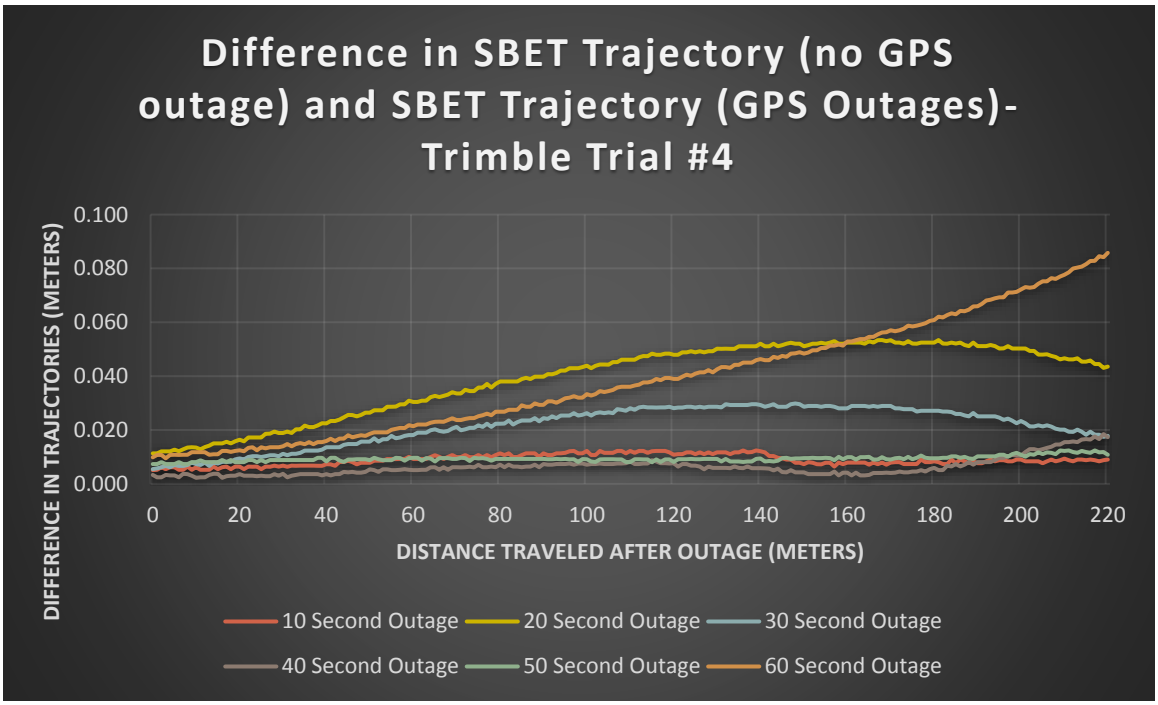
Difference in SBET Trajectory (no GPS outage) and SBET Trajectory (GPS Outages)- Trimble Trial #4
DIFFERENCE IN TRAJECTORIES (METERS)
0.100
0.080
0.060
0.040
0.020
0.000
0 20 40 60 80 100 120 140 160 180 200 220
DISTANCE TRAVELED AFTER OUTAGE (METERS)
10 Second Outage
20 Second Outage
30 Second Outage
40 Second Outage
50 Second Outage
60 Second Outage

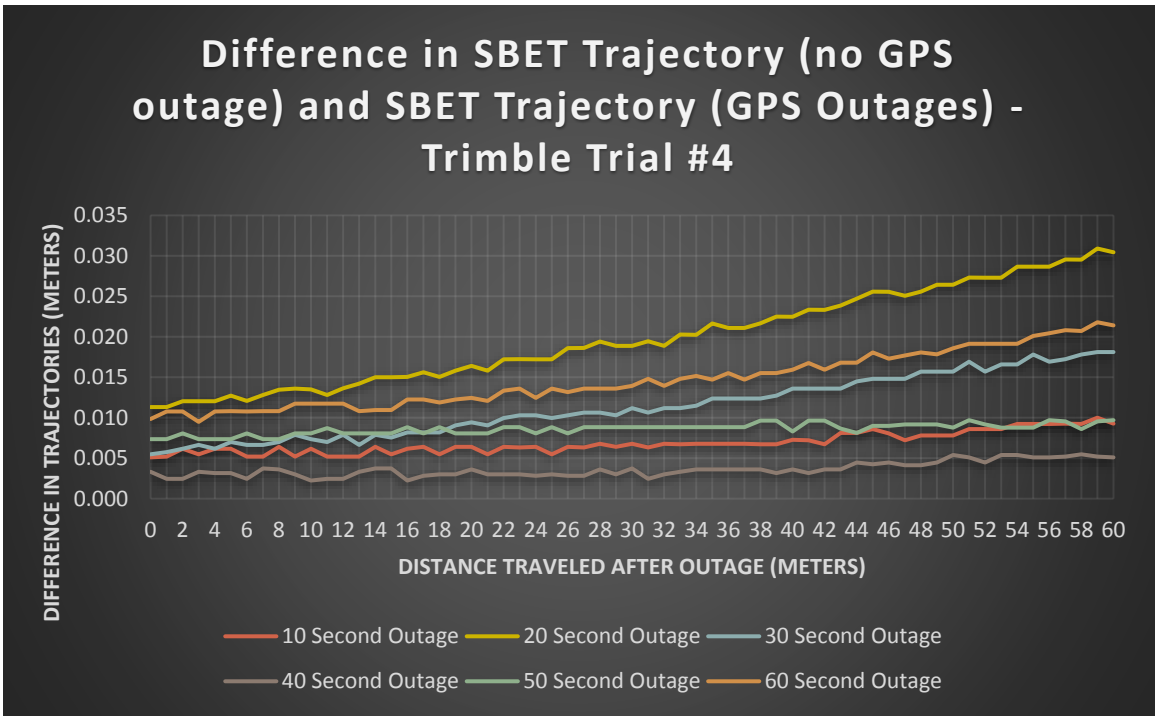
Difference in SBET Trajectory (no GPS outage) and SBET Trajectory (GPS Outages) - Trimble Trial #4
DIFFERENCE IN TRAJECTORIES (METERS)
0.035
0.030
0.025
0.020
0.015
0.010
0.005
0.000
0 2 4 6 8 10 12 14 16 18 20 22 24 26 28 30 32 34 36 38 40 42 44 46 48 50 52 54 56 58 60
DISTANCE TRAVELED AFTER OUTAGE (METERS)
10 Second Outage
20 Second Outage
30 Second Outage
40 Second Outage
50 Second Outage
60 Second Outage

Trial #5– Time stamp 407980s – 408040s

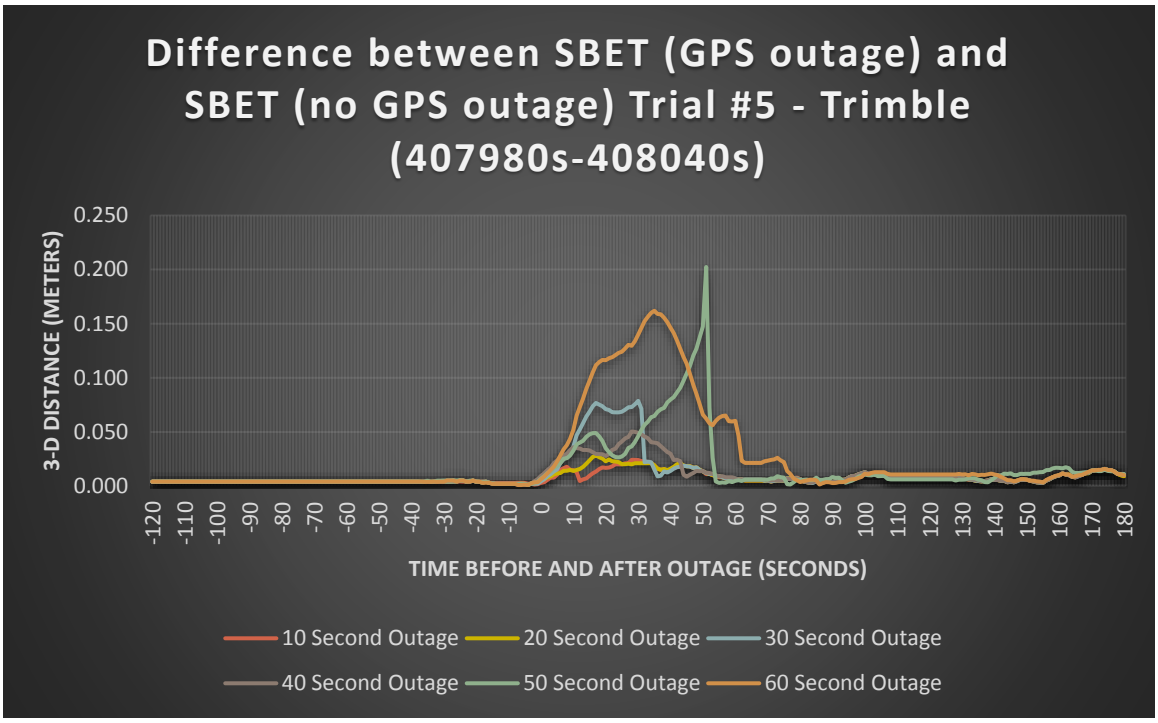

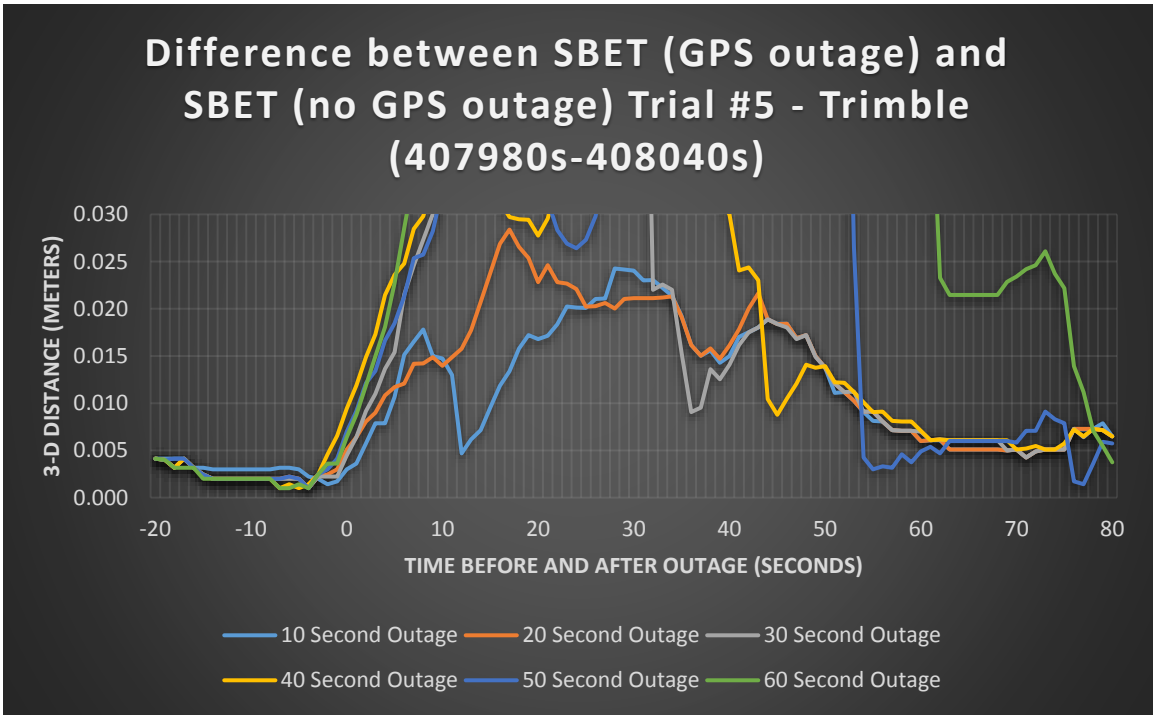

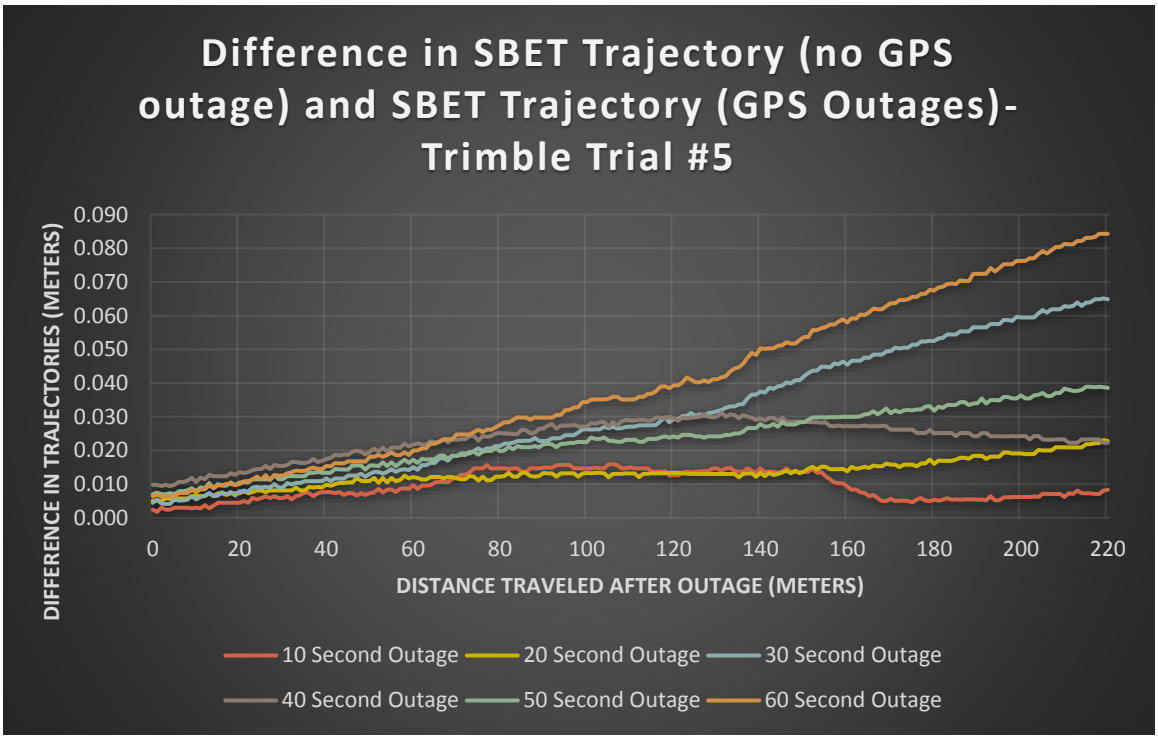
Difference in SBET Trajectory (no GPS outage) and SBET Trajectory (GPS Outages)- Trimble Trial #5
DIFFERENCE IN TRAJECTORIES (METERS)
0.090
0.080
0.070
0.060
0.050
0.040
0.030
0.020
0.010
0.000
0
20
40
60
80
100
120
140
160
180
200
220
DISTANCE TRAVELED AFTER OUTAGE (METERS)
10 Second Outage
20 Second Outage
30 Second Outage
40 Second Outage
50 Second Outage
60 Second Outage

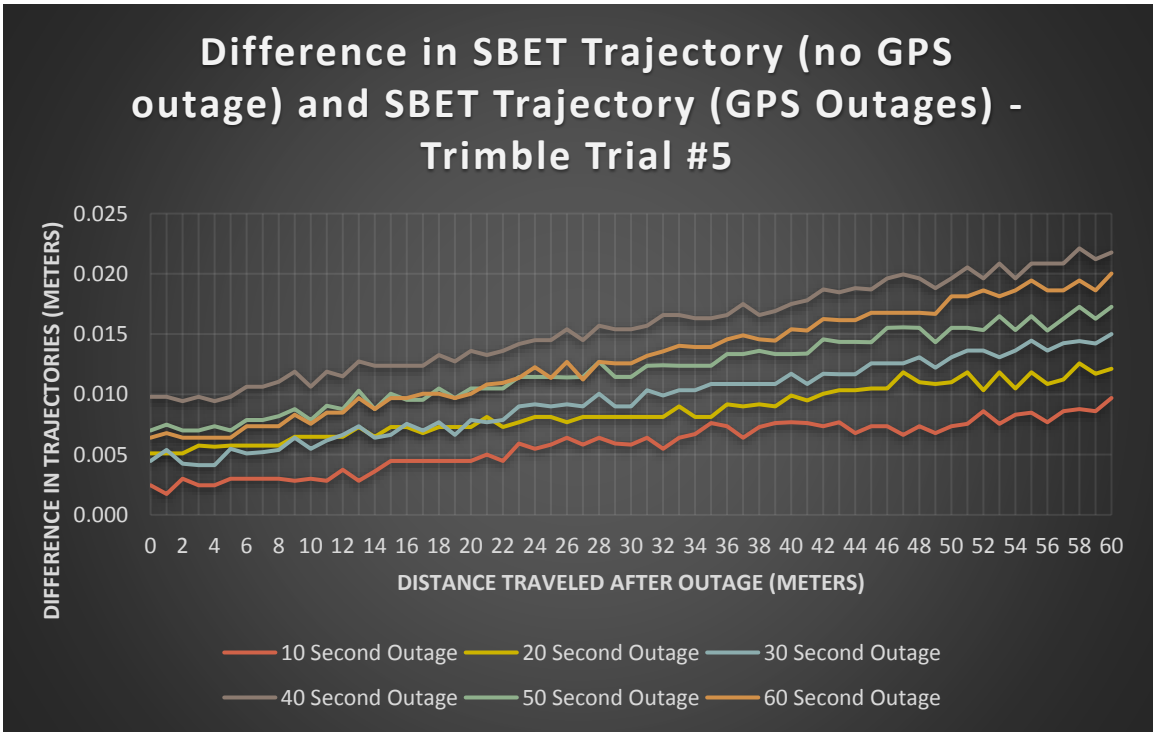
Difference in SBET Trajectory (no GPS outage) and SBET Trajectory (GPS Outages) - Trimble Trial #5
DIFFERENCE IN TRAJECTORIES (METERS)
0.025
0.020
0.015
0.010
0.005
0.000
0 2 4 6 8 10 12 14 16 18 20 22 24 26 28 30 32 34 36 38 40 42 44 46 48 50 52 54 56 58 60
DISTANCE TRAVELED AFTER OUTAGE (METERS)
10 Second Outage
20 Second Outage
30 Second Outage
40 Second Outage
50 Second Outage
60 Second Outage

Trial #6 – Time Stamp 408120s – 408180s

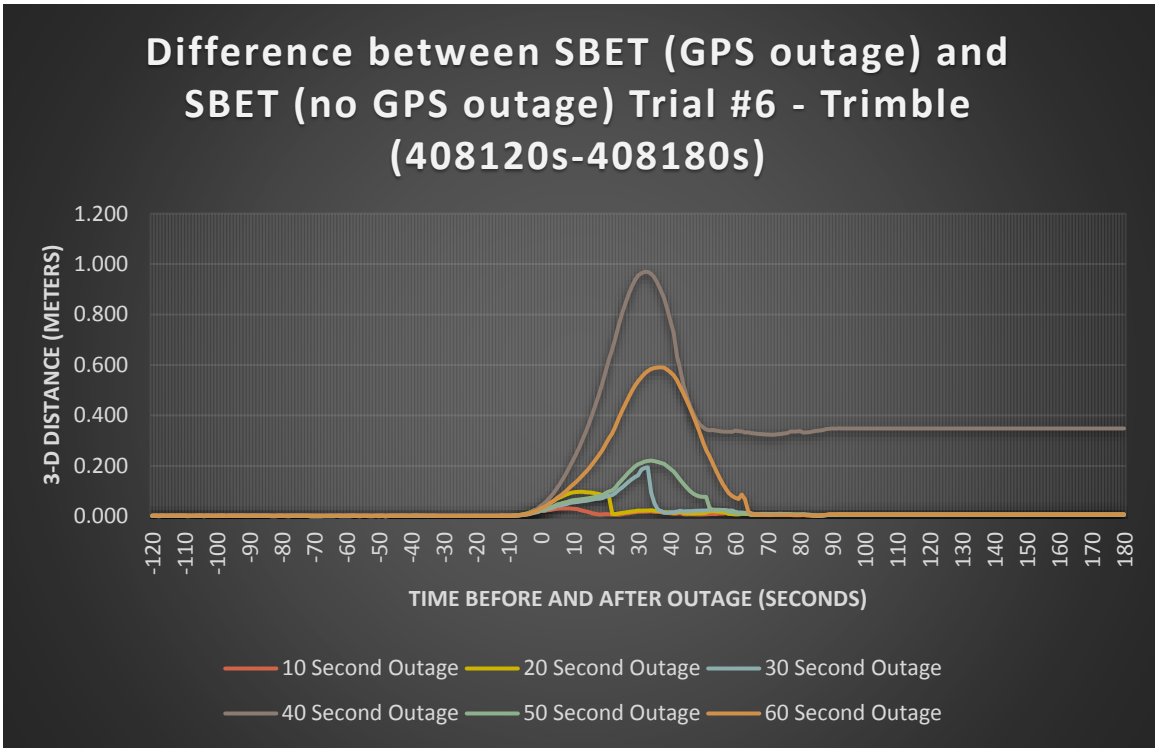

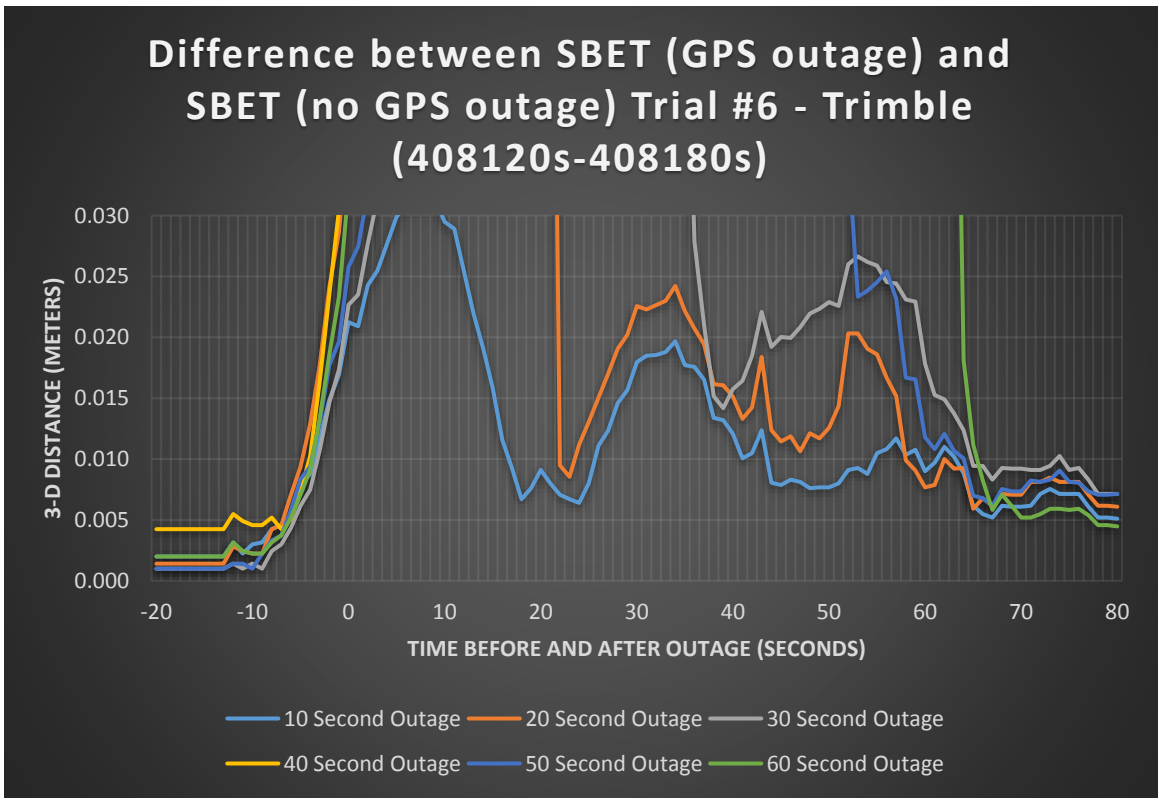

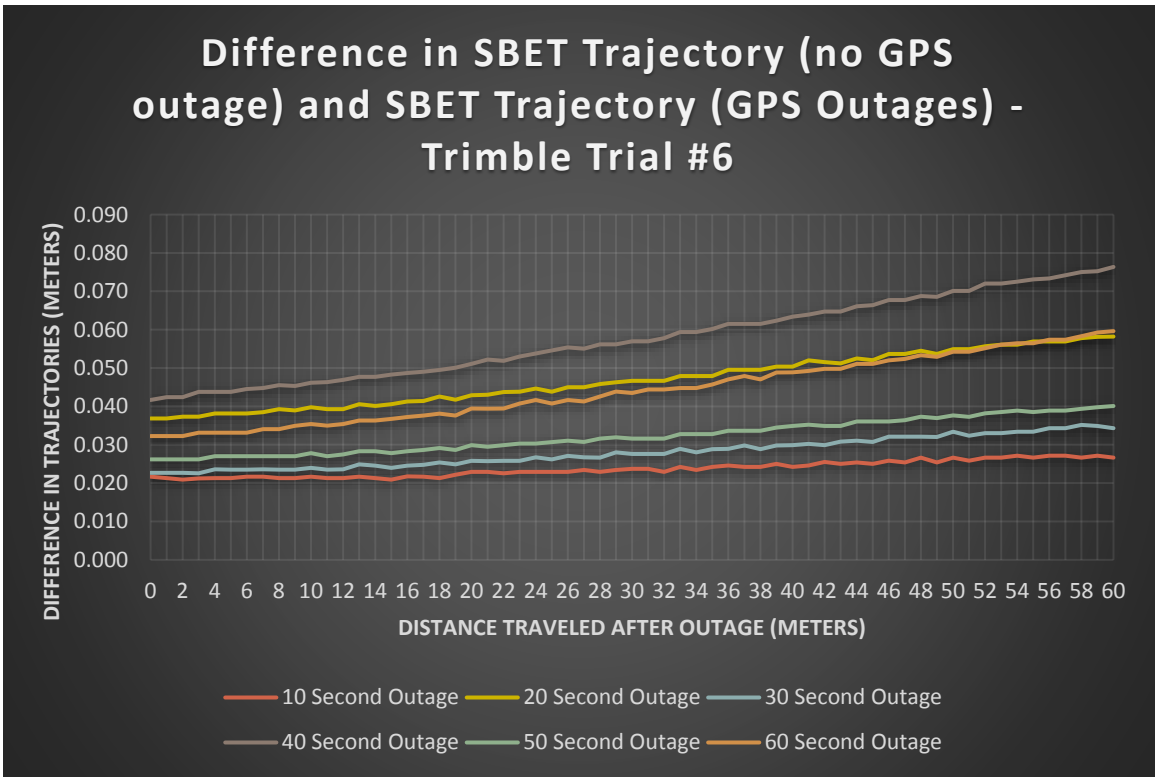
Difference in SBET Trajectory (no GPS outage) and SBET Trajectory (GPS Outages) - Trimble Trial #6
DIFFERENCE IN TRAJECTORIES (METERS)
0.090
0.080
0.070
0.060
0.050
0.040
0.030
0.020
0.010
0.000
0 2 4 6 8 10 12 14 16 18 20 22 24 26 28 30 32 34 36 38 40 42 44 46 48 50 52 54 56 58 60
DISTANCE TRAVELED AFTER OUTAGE (METERS)
10 Second Outage
20 Second Outage
30 Second Outage
40 Second Outage
50 Second Outage
60 Second Outage

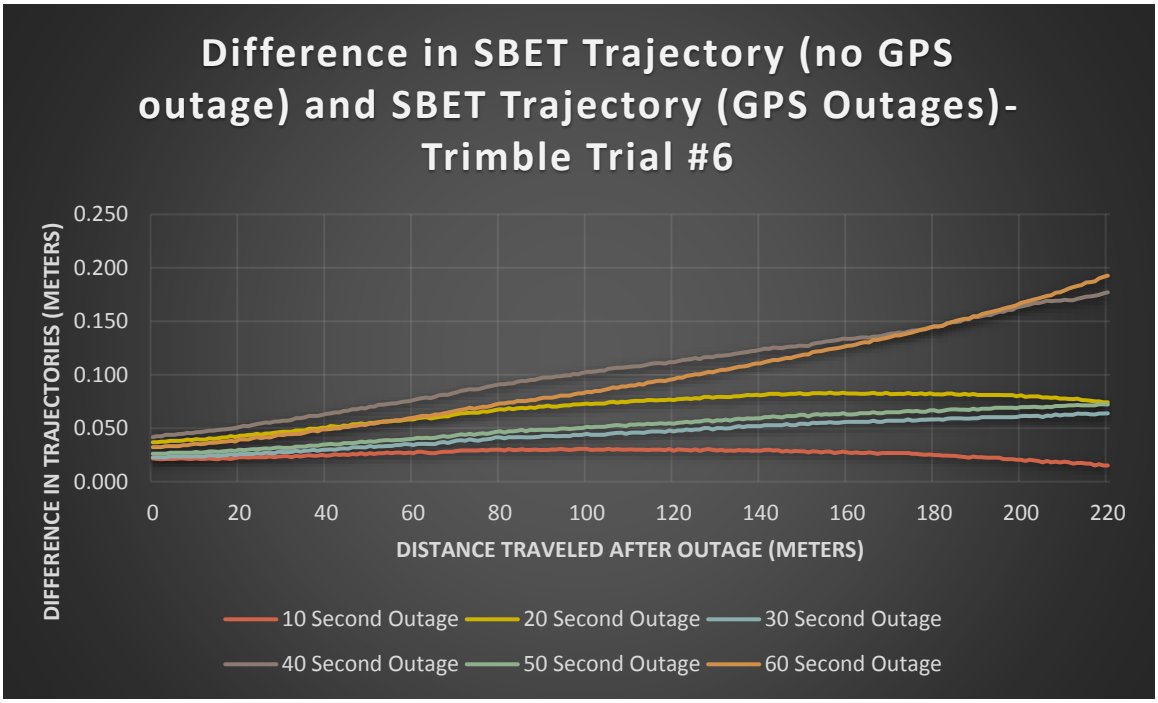
Difference in SBET Trajectory (no GPS outage) and SBET Trajectory (GPS Outages)- Trimble Trial #6
DIFFERENCE IN TRAJECTORIES (METERS)
0.250
0.200
0.150
0.100
0.050
0.000
0 20 40 60 80 100 120 140 160 180 200 220
DISTANCE TRAVELED AFTER OUTAGE (METERS)
10 Second Outage
20 Second Outage
30 Second Outage
40 Second Outage
50 Second Outage
60 Second Outage

Trial #7 – Time Stamp 408450s – 408510s

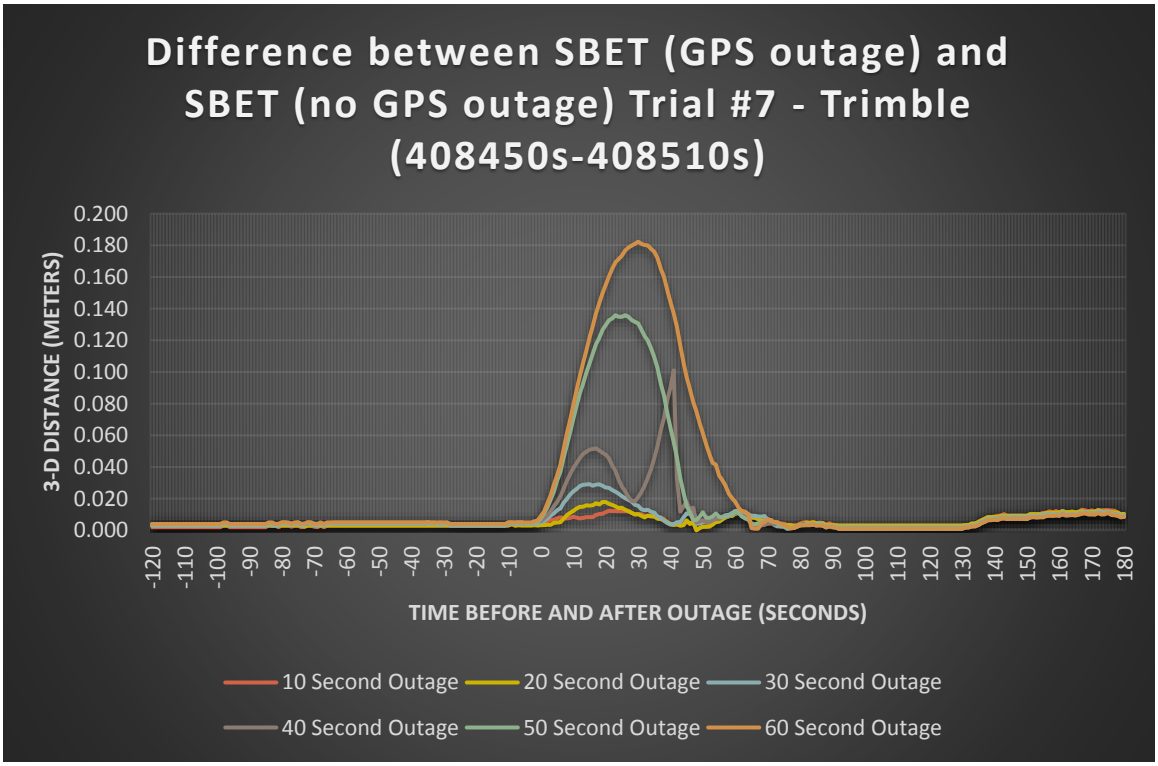

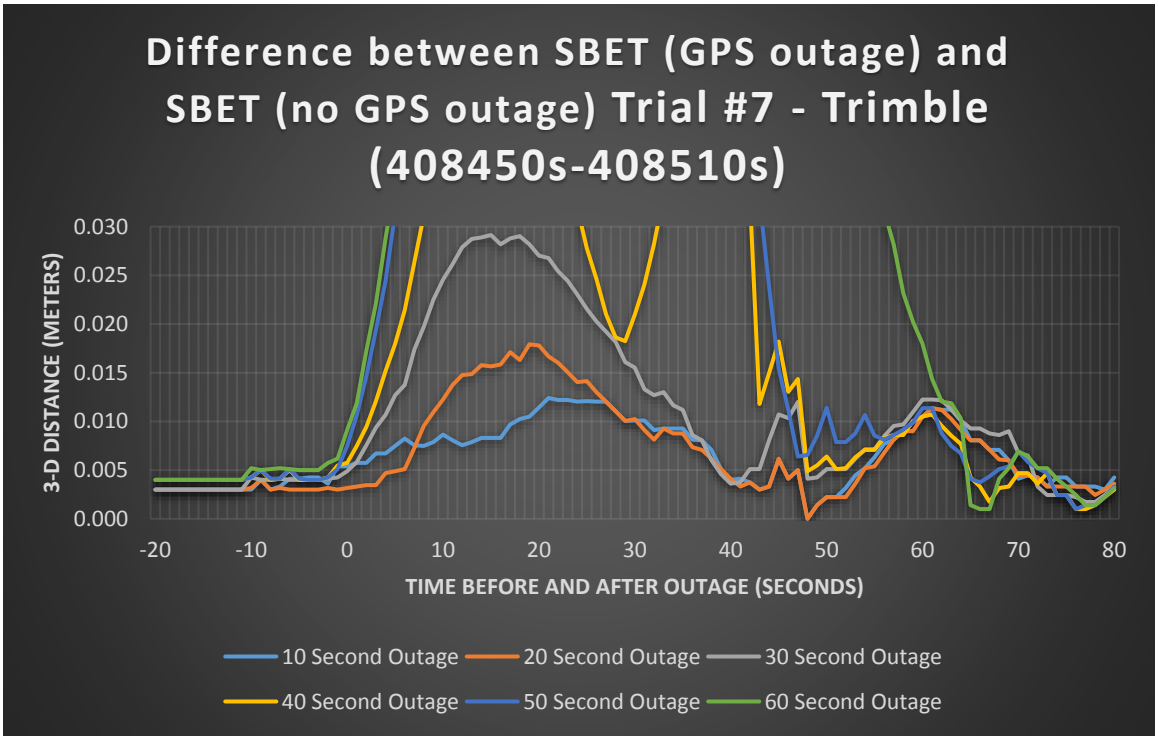

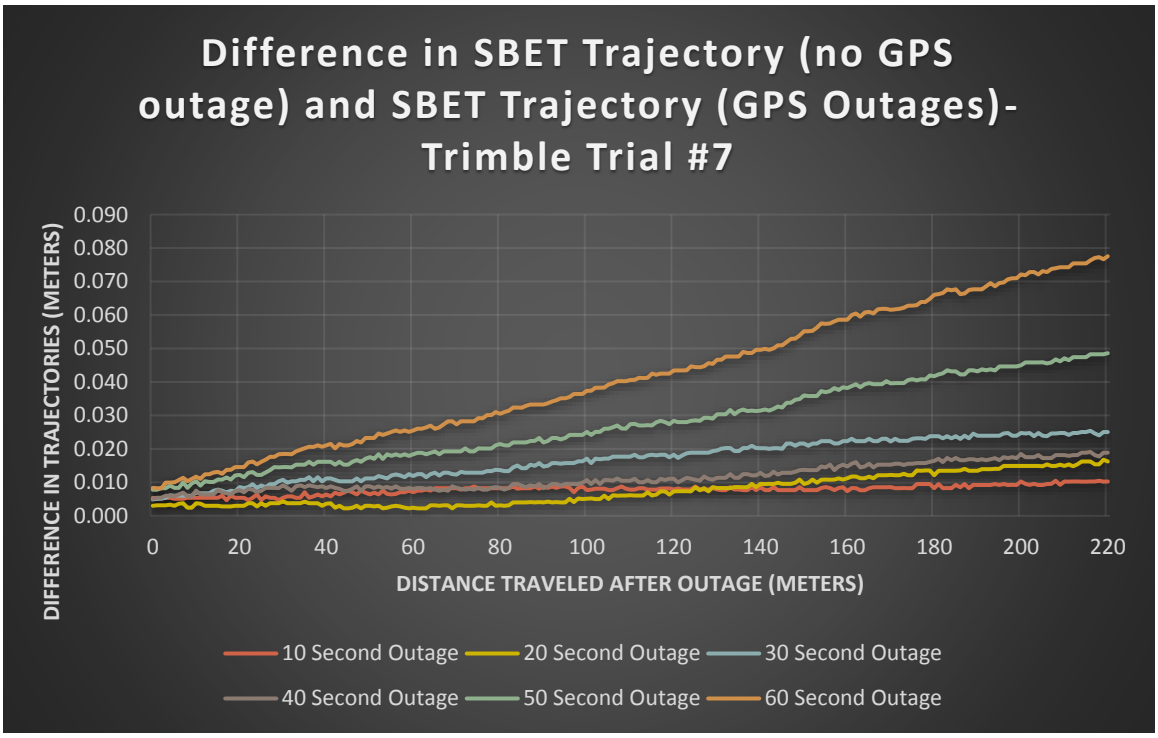
Difference in SBET Trajectory (no GPS outage) and SBET Trajectory (GPS Outages)- Trimble Trial #7
DIFFERENCE IN TRAJECTORIES (METERS)
0.090
0.080
0.070
0.060
0.050
0.040
0.030
0.020
0.010
0.000
0 20 40 60 80 100 120 140 160 180 200 220
DISTANCE TRAVELED AFTER OUTAGE (METERS)
10 Second Outage
20 Second Outage
30 Second Outage
40 Second Outage
50 Second Outage
60 Second Outage

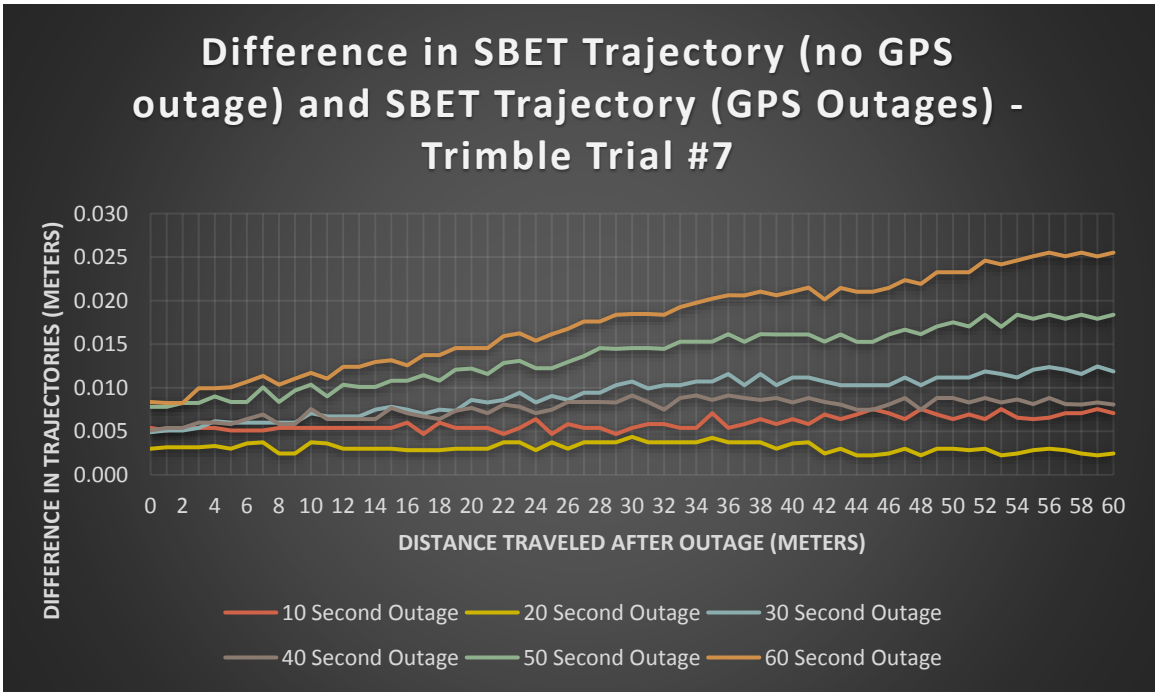
Difference in SBET Trajectory (no GPS outage) and SBET Trajectory (GPS Outages) - Trimble Trial #7
DIFFERENCE IN TRAJECTORIES (METERS)
0.030
0.025
0.020
0.015
0.010
0.005
0.000
0 2 4 6 8 10 12 14 16 18 20 22 24 26 28 30 32 34 36 38 40 42 44 46 48 50 52 54 56 58 60
DISTANCE TRAVELED AFTER OUTAGE (METERS)
10 Second Outage
20 Second Outage
30 Second Outage
40 Second Outage
50 Second Outage
60 Second Outage

Trial #8 – Time Stamp 408600s – 408660s

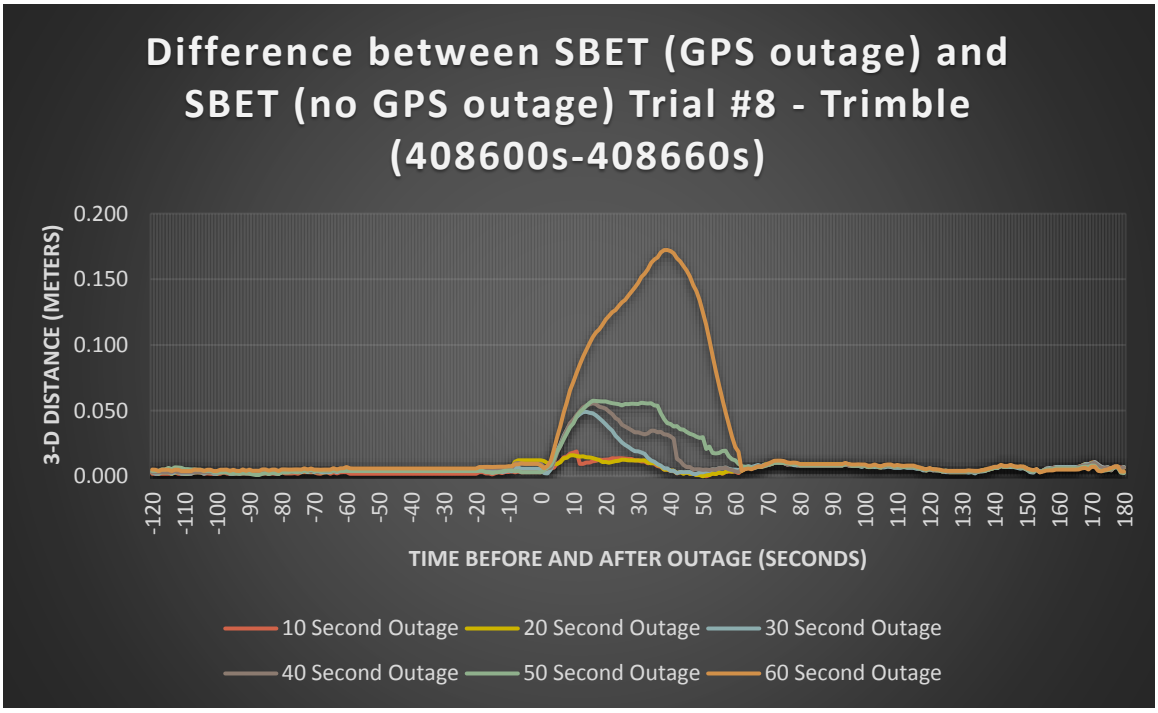

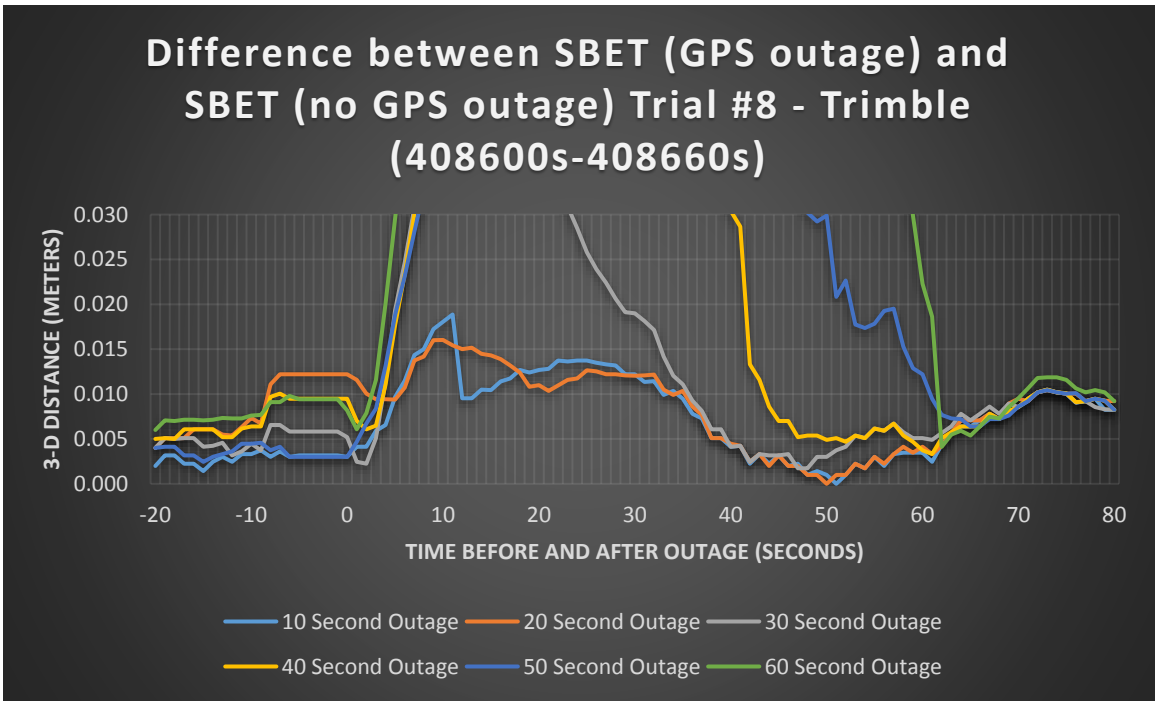

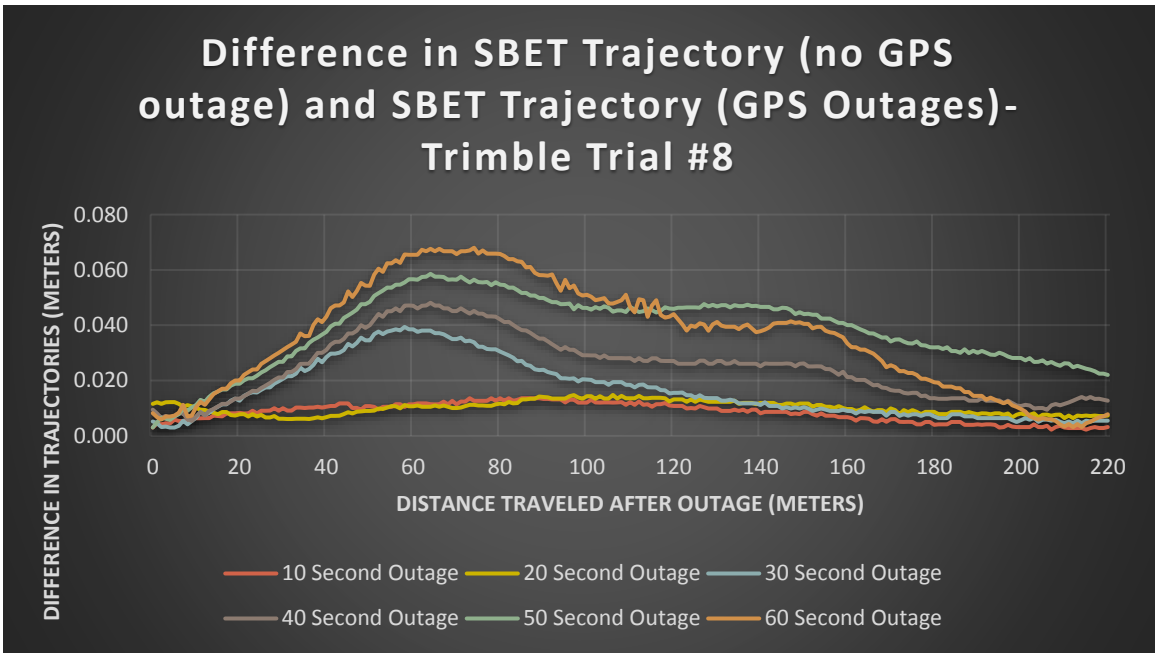
Difference in SBET Trajectory (no GPS outage) and SBET Trajectory (GPS Outages)- Trimble Trial #8
DIFFERENCE IN TRAJECTORIES (METERS)
0.080
0.060
0.040
0.020
0.000
0 20 40 60 80 100 120 140 160 180 200 220
DISTANCE TRAVELED AFTER OUTAGE (METERS)
10 Second Outage
20 Second Outage
30 Second Outage
40 Second Outage
50 Second Outage
60 Second Outage

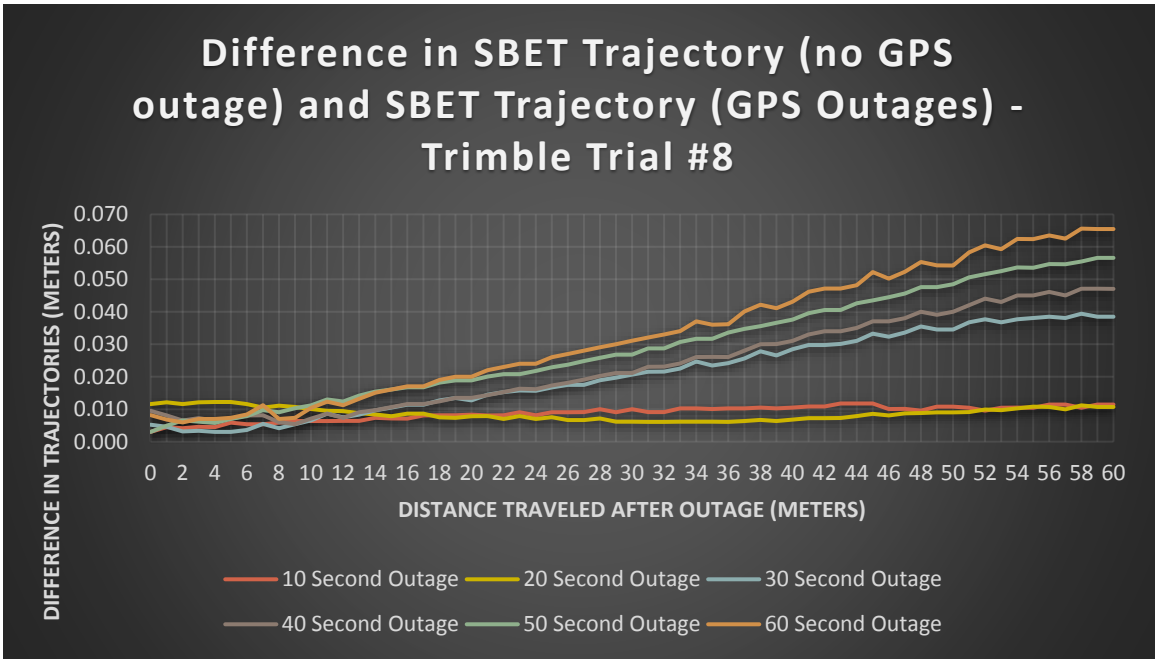
Difference in SBET Trajectory (no GPS outage) and SBET Trajectory (GPS Outages) - Trimble Trial #8
DIFFERENCE IN TRAJECTORIES (METERS)
0.070
0.060
0.050
0.040
0.030
0.020
0.010
0.000
0 2 4 6 8 10 12 14 16 18 20 22 24 26 28 30 32 34 36 38 40 42 44 46 48 50 52 54 56 58 60
DISTANCE TRAVELED AFTER OUTAGE (METERS)
10 Second Outage
20 Second Outage
30 Second Outage
40 Second Outage
50 Second Outage
60 Second Outage

Trial #9 – Time Stamp 408830s – 408890s

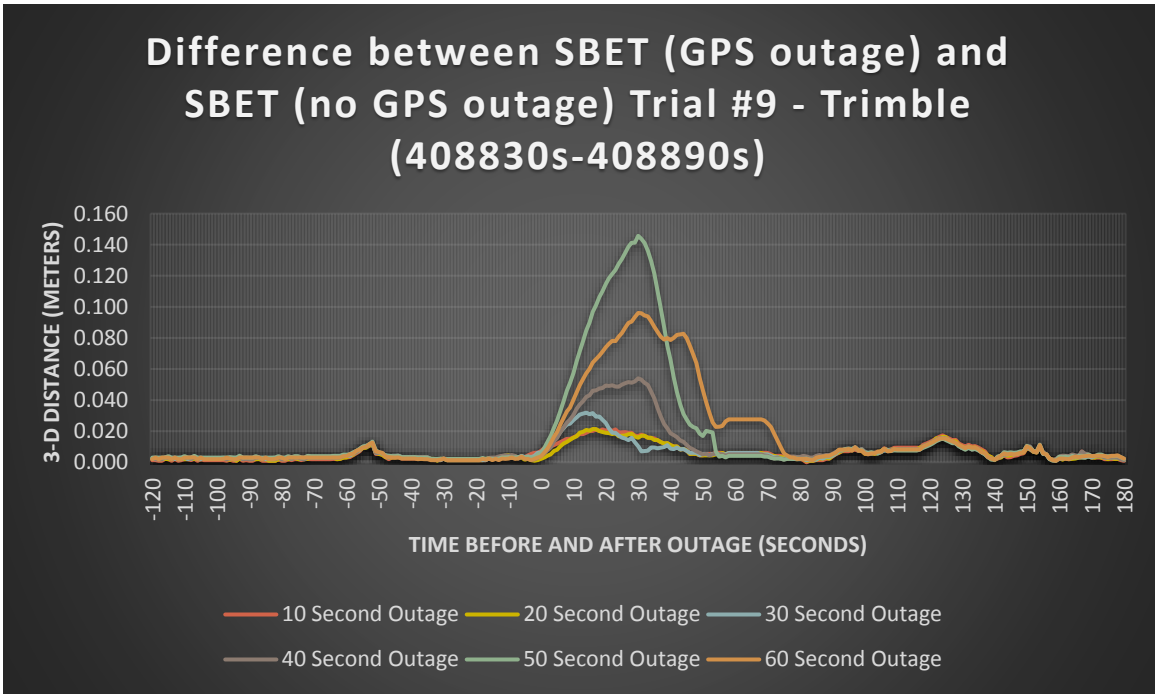

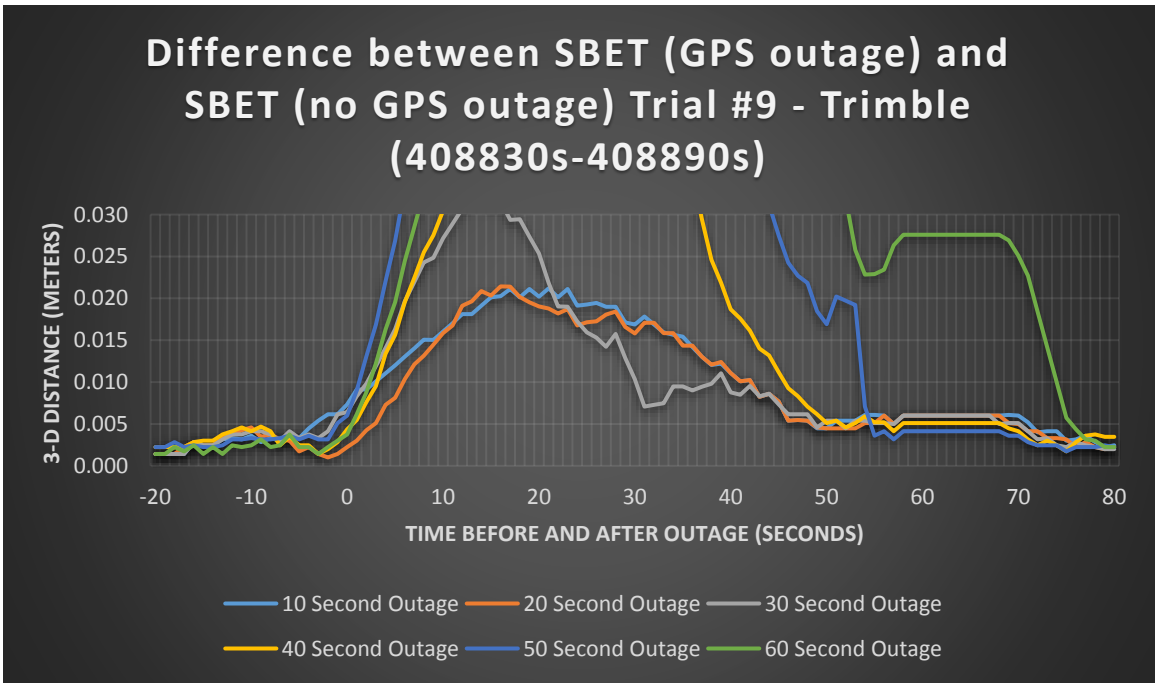

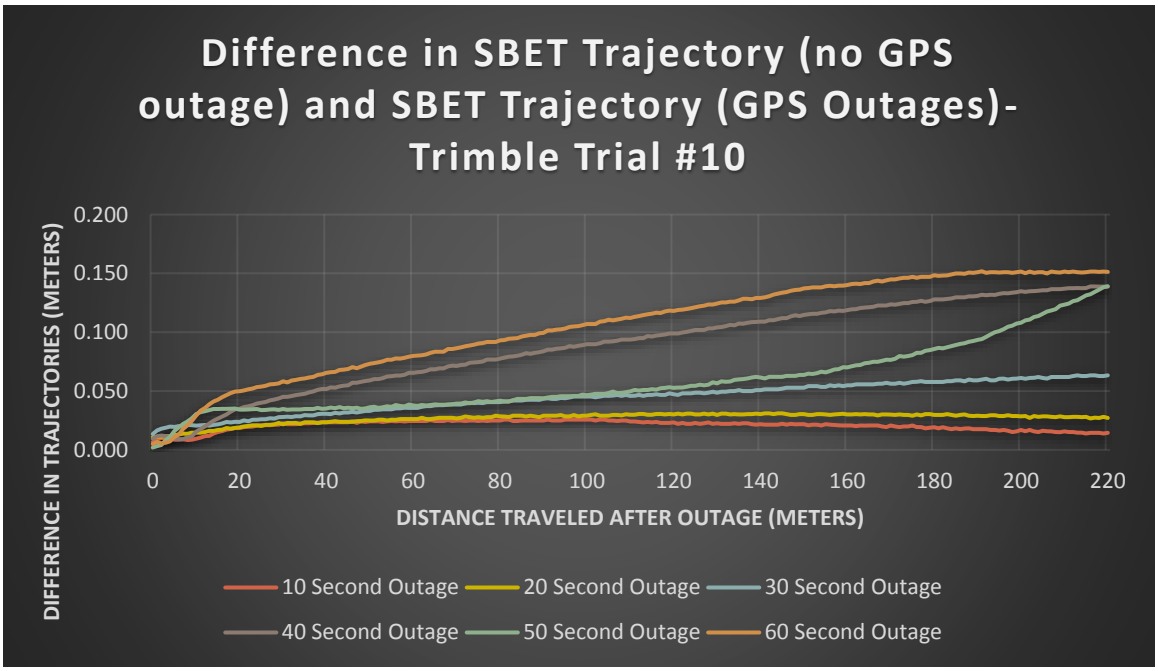
Difference in SBET Trajectory (no GPS outage) and SBET Trajectory (GPS Outages)- Trimble Trial #10
DIFFERENCE IN TRAJECTORIES (METERS)
0.200
0.150
0.100
0.050
0.000
0 20 40 60 80 100 120 140 160 180 200 220
DISTANCE TRAVELED AFTER OUTAGE (METERS)
10 Second Outage
20 Second Outage
30 Second Outage
40 Second Outage
50 Second Outage
60 Second Outage

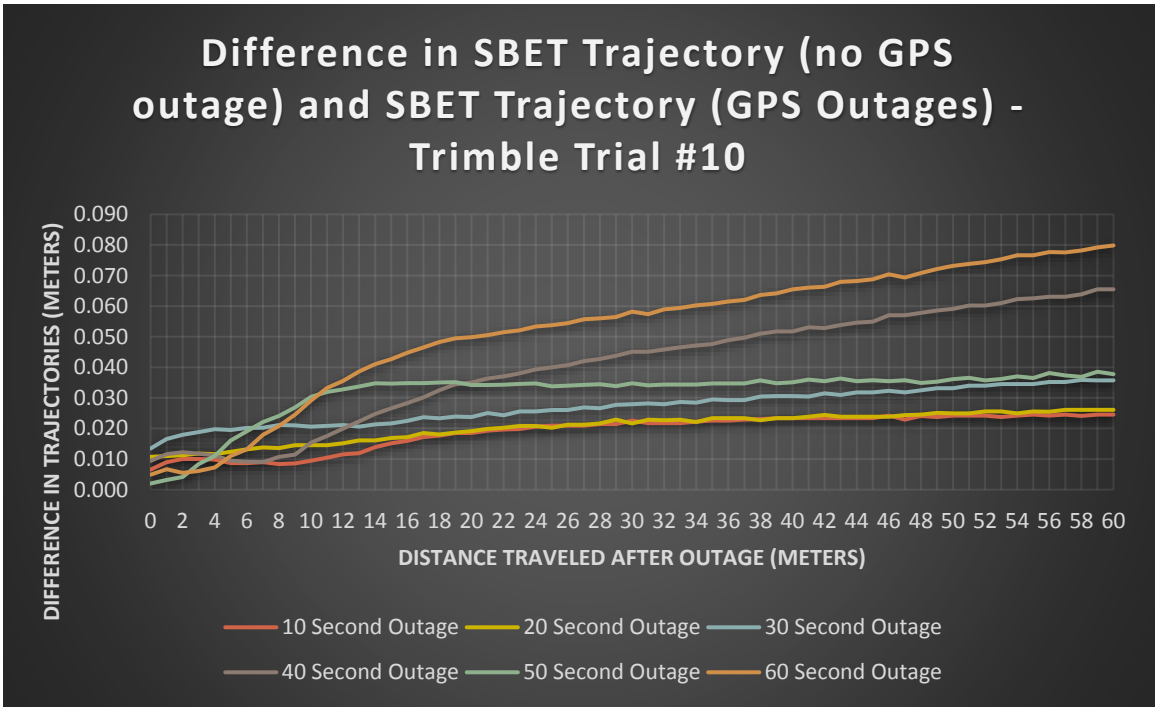
Difference in SBET Trajectory (no GPS outage) and SBET Trajectory (GPS Outages) - Trimble Trial #10
DIFFERENCE IN TRAJECTORIES (METERS)
0.090
0.080
0.070
0.060
0.050
0.040
0.030
0.020
0.010
0.000
0 2 4 6 8 10 12 14 16 18 20 22 24 26 28 30 32 34 36 38 40 42 44 46 48 50 52 54 56 58 60
DISTANCE TRAVELED AFTER OUTAGE (METERS)
10 Second Outage
20 Second Outage
30 Second Outage
40 Second Outage
50 Second Outage
60 Second Outage

REFERENCES

[1] Puente, I., Gonzalez-Jorge, H., Arias, P., & Armesto, J. (2011) Land-based mobile laser scanning systems: A Review. *Close Range Remote Sensing and Photogrammetry Group, School of Mining Engineering. Campus Lagaos-Marcosende, Vigo, Spain*

[2] Poreba, M & Goulette, F. (2012) Assessing the Accuracy of Land-Based Mobile Laser Scanning Data. *Geomatics and Environmental Engineering*, 6, No.3, 73-81).

[3] Barber, D., Mills, J., Smith-Voysey, S. (2008) Geometric Validation of a ground-based mobile laser scanning system. *ISPRS Journal of Photogrammtery and Remote Sensing*, 63, 128-141.

[4] National Cooperative Highway Research Program (NCHRP) Report 748, "Guidelines for the Use of Mobile LIDAR in Transportation Applications," 2013. [Online]. Available: http://onlinepubs.trb.org/onlinepubs/nchrp/nchrp_rpt_748.pdf [Accessed: January 9, 2014].

[5] Vosselman, G. & Maas, H.G. (2010). *Airborne and Terrestrial Laser Scanning.* Scotland, UK: Melita Press Malta.

[6] Puente, I., Gonzalez-Jorge, H., Martinez-Sanchez, J. & Arias, P. (2013) Review of mobile mapping and surveying technologies. *El Sevier*, Measurement 46, 2127-2145. Retrieved at www.elseviier.com/locate/measurement

[7] Applanix, a Trimble Company, POS LV. [Online]. Available: https://www.applanix.com/downloads/products/specs/POS_LV_Datasheet.pdf [Accessed: September 4, 2018].

[8] Riegl USA. Mobile Mapping, VZ-400 Conversion to a mobile Mapping Platform Guide. *Riegl USA*, retrieved at http://www.rieglusa.com/pdf/mobile_mapping_integration.pdf

[9] Applanix, a Trimble Company, "GPS Azimuth Measurement Subsystem (GAMS)" (2005). [Online]. Available: ftp://128.128.250.51/pub/instruments/posmv/info_from_knorr/POS_MV_GAMS_Calibration_Memo_February_2005.pdf [Accessed: January 9, 2014].

[10] California Department of Transportation. (2011). Terrestrial Laser Scanning Specifications. In *CALTRANS Survey Manual.* Retrieved from http://www.dot.ca.gov/hq/row/landsurveys/SurveysManual/15_Surveys.pdf

[11] Hiremagalur, J., K. S. Yen, K. Akin, T. Bui, T. A. Lasky, and B. Ravani (2007). Creating Standards and Specifications for the Use of Laser Scanning in Caltrans Projects. AHMCT Rept.# UCD-ARR-07-06-30-01, Davis.

[12] Ussyshkin, V. (2009). "Mobile laser scanning technology for surveying application: From data collection to end products." In *Proceedings of the FIG Working Week 2009, Surveyors Key Role in Accelerated Development,* Eilat, Israel.

[13] State of Georgia, Department of Transportation, "GDOT Automated Survey Manual," March 1, 2018. [Online]. Available: http://www.dot.ga.gov/PartnerSmart/DesignManuals/SurveyManual/SurveyManual.pdf [Accessed: September 3, 2018].

[14] S. Johnson, J. Bethel, C. Supunyachotsakul, S. Peterson, "Laser Mobile Mapping Standards and Applications in Transportation", Purdue University, Nov. 2016.

[15] Florida Department of Transportation, "Terrestrial Mobile LiDAR Surveying & Mapping Guidelines," October 7, 2013. [Online]. Available: http://www.fdot.gov/geospatial/documentsandpubs/20131007_tml_guidelines.pdf [Accessed: January 9, 2014].

[16] Mississippi Department of Transportation (MDOT), "Survey Manual," February 22, 2007. [Online]. Available: http://sp.mdot.ms.gov/RoadwayDesign/MDOT%20Survey%20Manual/2008%20Survey%20Manual.pdf [Accessed: January 9, 2014].

[17] Kaartinen, H., Hyyppa, J., Kukko, A., Jaakkola, A., Hyyppa, H. (2012) Benchmarking the Performance of Mobile Laser Scanning Systems Using a Permanent Test Field. *Sensors*, 12, 12814-12835.

[18] Lim, S., Thatcher, C.A., Brock, J.C., Kimbrow, D.R., Danielson, J.J. & Reynolds, B.J. (2013). Accuracy assessment of a mobile terrestrial lidar survey at Padre Island National Seashore. *International Journal of Remote Sensing, 34, no.18, 6355-6366.*

[19] Schwarz, K.P, Martell, H.E., El-Sheimy, N., Li, R., Chapman, M.A., Cosandier, D. (1993) *Proceedings from IEEE Vehicle Navigation and Information Systems Conference: VISAT – A mobile Highway Survey System of High Accuracy*., Ottawa, Canada.

[20] Yousif, H., J. Li, M. Chapman, and Y. Shu (2010). Accuracy Enhancement of Terestrial Mobile LIDAR Data Using Theory of Assimilation. *International Archives of Photogrammetry, Remote Sensing and Spatial Information Sciences*, Vol. 38, No. 5.

[21] B. Bailey, "A New Way to Control Mobile LiDAR Data," LiDAR News, Vol. 2, No. 6. 2012. [Online]. Available: http://lidarmag.com/wp-content/uploads/PDF/LiDARMagazine_Bailey-SurveyControl_Vol2No6.pdf [Accessed January 9, 2014].

[22] National Spatial Data Infrastructure. (1998). Geospatial Positioning Accuracy Standards Part 3: National Standard for Spatial Data Accuracy. In *Federal Geographic Data Committee.* Retrieved from https://www.fgdc.gov/standards/projects/accuracy/part3/chapter3

[23] Haala, N., Peter, M., Kremer, J., & Hunter, G. Mobile lidar mapping for 3d point cloud collection in urban areas – a performance test. *Institute for photogrammetry (ifp),* Universitaet Stuttgart, Germany.

[24] Remondino, F., Grzia Spera, M., Nocerino, E., Menna, F., Nex, F., (2014) State of the art in high density image matching. *The Photogrammetric Record,* Record 29, 144-166.

[25] Geosystems, Leica (2013). Leica ScanStation P20 System Field Manual. *Leica Geosystems,* 2.

[26] I. Puente, H. Gonzalez-Jorge, B. Riveiro, P. Arias (2012). Accuracy verification of the Lynx Mobile Mapper system. *El Sevier*, Optics and Laser Technology 45 (2013) 578-586.

VITA

Education

- **PHD Candidate –** Geomatics Engineering – Purdue University (December 2013 - Present) – expected graduation December 2017
- **Master of Science** in Geomatics Engineering – Purdue University (May 2013)
- **Certified Federal Surveyor** – (February 2012)
- **Associates in Applied Science, with a Major in Surveying** – Salt Lake Community College (May 2007)
- **B.S. in Biology** - Brigham Young University (December 2005)

Teaching

- Assistant Professor – Civil & Geomatics Engineering, Lyles College of Engineering, California State University – Fresno (Fall 2014 – Present)
- Lecturer – Earth, Physical Sciences and Engineering – Math, Science and Engineering Division – Fresno City College (Fall 2014 – Fall 2015)
    - Engineering 1A – Elementary Plane Surveying
- Purdue University, Civil Engineering/Geomatics Department
    - Introduction to Geodesy Instructor (Graduate Course) Fall 2013
    - Graduate Teaching Assistant – Principles and Practices of Geomatics, August 2011- Dec 2012

Professional Registrations

- PLS (Professional Land Surveyor) – License #6845090-2201 (UT)
- CFedS (Certified Federal Surveyor) – Certificate #1545.

Conference Presentations

- Parol Evidence, 2016 California Land Surveyors Association (CLSA) – Rohnert Park, CA, March 2016
- Coordinates, Moving Forward, 2016 Annual Geomatics Conference – Fresno, CA, January 2015
- Functional Surface Target as Control and Validation of 3D Laser Scanner Point Cloud, 38th Annual Central Research Symposium, CSU Fresno, 2017 – Ayad Ahmed project under Scott Peterson
- Functional Surface Target as Control and Validation of 3D Laser Scanner Point Cloud, 31st Annual CSU Student Research Competition, 2017 - Ayad Ahmed project under Scott Peterson

Publications

- Johnson, S.D., Bethel, J.S., Supunyachotsakul, C., & Peterson, S. (2016). *Laser mobile mapping standards and applications in transportation* (Joint Transportation Research Program Publication No. FHWA/IN/JTRP-2016/01). West Lafayette, IN: Purdue University. http://dx.doi.org/10.5703/1288284316164

Research Grants

- "FID Flow Measurement Device Project", Scott Peterson – Co PI, October 2018 – December 2019, $50,000 funded
- "Photogrammetry-based Bridge Dynamic Deformation Monitoring – California State University Transportation Consortium (CSUTC), Fresno State Transportation Institute (FSTI), Yushin Ahn – PI, Scott Peterson – Co PI, Maryam Nazari – Co PI, June 2018 – December 2018, $39,938 funded
- "Small UAV Standards" – CALTRANS – Riadh Munjy – PI, Scott Peterson – Co PI, Mustafa Berber – Co PI, June 2016 – June 2019, $450,000 funded
- "Low Cost Terrestrial Mobile Laser Scanner Concept Development" – Scott Peterson – Co PI, Riadh Munjy – Co PI, Mustafa Berber Co PI, $6,000 funded
- "Relative comparison of drone Photogrammetry and LiDAR 3D Point Cloud" – CSU Fresno Undergraduate Research Grant, 2017 – 2018, $1000 funded
- "Vertical Network Creation with a Robotic Total Station" – CSU Fresno Undergraduate Research Grant, 2016-2017, granted

Professional involvement

• Member California Land Surveying Association (CLSA)	1/2015 – Present
• Education Committee Chair San Joaquin Valley Chapter (CLSA)	1/2015 - Present
• Member Geomatics Advisory Council	8/2014 – Present
• History Committee Chairman for Utah Council of Land Surveyors	1/2010 – 8/2011
• Timpanogos Chapter Vice President UCLS	2/2010 – 2/2011
• State Executive Board Member UCLS	2/2009 – 2/2010
• Legislative Committee Liaison UCLS	2/2009 – 2/2010
• Timpanogos Chapter President UCLS	2/2009 – 2/2010
• Legislative Committee UCLS	2/2008 – 8/2011
• Member UCLS	2003 – 8/2011